AN ANALYTICAL STUDY OF PROJECTILE PENETRATION INTO ROCK

Dwain K. Butler

Army Engineer Waterways Experiment Station

Prepared for:

Defense Nuclear Agency

June 1975

TECHNICAL REPORT S-75-7

AN ANALYTICAL STUDY OF PROJECTILE PENETRATION INTO ROCK

by

Dwain K. Butler

Soils and Pavements Laboratory
U. S. Army Engineer Waterways Experiment Station
P. O. Box 631, Vicksburg, Miss. 39180

June 1975
Final Report

Prepared for Defense Nuclear Agency
Washington, D. C. 20305

Under Subtask SB211, Work Unit 04,
"Earth Penetrator Calculation Studies
and Comparative Analyses with Field Measurements"

Unclassified

SECURITY CLASSIFICATION OF THIS PAGE (When Data Entered)

REPORT DOCUMENTATION PAGE		READ INSTRUCTIONS BEFORE COMPLETING FORM
1. REPORT NUMBER Technical Report S-75-7	2. GOVT ACCESSION NO.	3. RECIPIENT'S CATALOG NUMBER
4. TITLE (and Subtitle) AN ANALYTICAL STUDY OF PROJECTILE PENETRATION INTO ROCK		5. TYPE OF REPORT & PERIOD COVERED Final report 6. PERFORMING ORG. REPORT NUMBER
7. AUTHOR(s) Dwain K. Butler		8. CONTRACT OR GRANT NUMBER(s)
9. PERFORMING ORGANIZATION NAME AND ADDRESS U. S. Army Engineer Waterways Experiment Station Soils and Pavements Laboratory P. O. Box 631, Vicksburg, Miss. 39180		10. PROGRAM ELEMENT, PROJECT, TASK AREA & WORK UNIT NUMBERS Subtask SB211, Work Unit 04
11. CONTROLLING OFFICE NAME AND ADDRESS Defense Nuclear Agency Washington, D. C. 20305		12. REPORT DATE June 1975 13. NUMBER OF PAGES 91
14. MONITORING AGENCY NAME & ADDRESS(if different from Controlling Office)		15. SECURITY CLASS. (of this report) Unclassified 15a. DECLASSIFICATION/DOWNGRADING SCHEDULE

16. DISTRIBUTION STATEMENT (of this Report)

Approved for public release; distribution unlimited.

17. DISTRIBUTION STATEMENT (of the abstract entered in Block 20, if different from Report)

18. SUPPLEMENTARY NOTES

19. KEY WORDS (Continue on reverse side if necessary and identify by block number)

Projectile penetration
Rock masses
Rock properties

20. ABSTRACT (Continue on reverse side if necessary and identify by block number)

This report presents the results of a parameter study of projectile penetration into rock using a computer code based on U. S. Army Engineer Waterways Experiment Station modifications and extensions of the Ross-Hanagud penetration theory, which in turn is based on the dynamic cavity expansion theory of Goodier. The theory treats the projectile as a rigid body and the target as an elastic-plastic locking material. The objectives were to gain (1) a qualitative and quantitative understanding of the factors of importance in

(Continued)

DD FORM 1 JAN 73 1473 EDITION OF 1 NOV 65 IS OBSOLETE

Unclassified

SECURITY CLASSIFICATION OF THIS PAGE (When Data Entered)

20. ABSTRACT (Continued).

rock penetration, (2) a feel for the depths of penetration which may be attainable, and (3) an appreciation for the complexities and uncertainties involved. Such an understanding is essential for the design of penetrating weapons for use against targets in rock or in situations in which, because of incomplete target intelligence, the possibility of encountering rock cannot be eliminated. Three rock targets were selected for the parameter study, with properties typical of the low-, medium-, and high-strength rock classifications in Deere and Miller's engineering rock classification scheme. The projectiles considered have ogive noses, a weight range of 250-1000 pounds, a diameter range of 5-10 inches, a caliber radius head range of 2-10, a sectional pressure range of 10-15 psi, and impact velocities of 1000-3000 fps. Using the penetration computer code, five actual field penetration tests into rock targets classified by Deere and Miller's method were simulated. The agreement between the predicted penetration depths and the actual measured depths is quite good. Based on this agreement, it is proposed that the penetration depth for a particular rock target can be bounded given only the engineering classification of the rock. The computer code was also used to calculate rigid body motion-time histories for two rock penetration events for comparison with the published finite difference code calculations of the same events. Good agreement between projectile time histories determined by the two procedures was obtained.

Destroy this report when no longer needed. Do not return it to the originator.

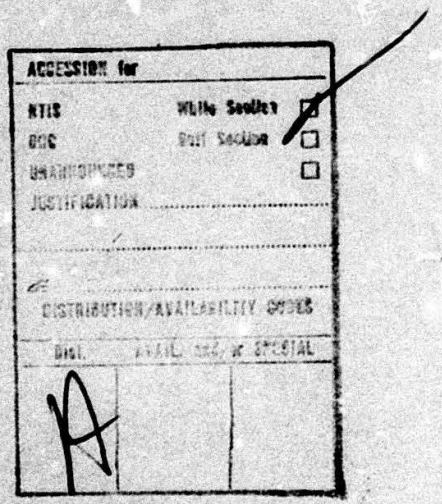

PREFACE

The investigation reported herein was conducted by personnel of the Soil Dynamics Division (SDD), Soils and Pavements Laboratory (S&PL), U. S. Army Engineer Waterways Experiment Station (WES), during the period November 1973-June 1974. The research was sponsored by the Defense Nuclear Agency (DNA) under NWED Subtask SB211, Work Unit 04, "Earth Penetrator Calculation Studies and Comparative Analyses with Field Measurements." MAJ Todd D. Stong, CE, was the DNA Project Officer for Subtask SB211.

This study was conducted and the report prepared by Mr. D. K. Butler, SDD. Technical consultation and direction were provided by Dr. B. Rohani, SDD Research Team Leader, and Dr. P. F. Hadala, Program Manager for DNA-sponsored work within SDD. SP4 D. C. Creighton assisted Mr. Butler with the computer calculations.

The work was performed under the general supervision of Messrs. J. P. Sale and R. G. Ahlvin, Chief and Assistant Chief, respectively, S&PL, and Dr. J. G. Jackson, Jr., Chief, SDD. COL G. H. Hilt, CE, was Director of WES during the investigation and the publication of this report. Mr. F. R. Brown was Technical Director.

CONTENTS

TABLES

FIGURES

CONVERSION FACTORS, U. S. CUSTOMARY TO METRIC (SI) UNITS OF MEASUREMENT

U. S. customary units of measurement used in this report can be converted to metric (SI) units as follows:

Multiply	By	To Obtain
inches	2.54	centimeters
feet	0.3048	meters
square inches	6.4516	square centimeters
pounds (mass)	0.45359237	kilograms
pounds (mass) per cubic foot	16.0185	kilograms per cubic meter
slugs per cubic foot	515.3788	kilograms per cubic meter
pounds (force) per square inch	6894.757	pascals
pounds (force) per square foot	47.88026	pascals
feet per second	0.3048	meters per second

AN ANALYTICAL STUDY OF PROJECTILE PENETRATION INTO ROCK

CHAPTER 1

INTRODUCTION

1.1 SETTING THE STAGE

Penetration of projectiles into earth media is a subject of great interest due to the increasing number of potential applications. With respect to military applications, in which the projectiles may range from small-caliber munitions and shell fragments to bombs and missiles or specially designed earth penetrating weapons (EPW),[1] interest arises from both offensive and defensive considerations. Typical applications include:

1. Destruction of underground targets by penetrating bombs or missiles which explode near or within the target.

2. Destruction or disablement of surface targets due to the cratering, ejecta, or direct-induced ground shock phenomena associated with a nuclear or high explosive detonation buried nearby at a shallow-to-optimum depth.

3. Implantation of mines and sensors.

4. Design and construction of underground protective structures to resist penetrating weapons effects.

McNeill (Reference 1) describes the potential use of instrumented penetrators for rapid mapping of soil and rock profiles. Typical situations might be the investigation of alternate construction sites and alternate routes for trenches, canals, and tunnels and the study of inaccessible and remote areas.

This report presents the results of a parametric study of projectile penetration into rock. Rock penetration has not been investigated in laboratory and in situ test programs as extensively as has

---

[1] For convenience, symbols and unusual abbreviations are listed and defined in the Notation (Appendix A).

penetration into soils. As military penetration interest extends to increasingly greater depths of penetration, the probability of encountering rock increases rapidly; also, there is a significant percentage of the earth's surface with exposed rock or rock covered by only a thin mantle of soil. Thus penetration into rocks must at least be considered in the "trade-off" studies involved in many penetrating weapon system designs.

In order to effect penetration into rock, design structurally sound penetrators for use in rock, and predict depth of penetration, it is important that rock penetration be more thoroughly investigated. Reference 2 describes a continuing program, initiated in 1966 by Sandia Laboratories, on the penetration of in situ rock; it is concluded in this reference that it is possible to design, construct, and instrument projectiles which can survive the environment of impact and penetration into low- and medium-strength rock. A brief history of rock penetration studies is given in Reference 2, and Reference 3 is a comprehensive state-of-the-art report on the subject. From the literature it is evident that the number of carefully documented, full-scale, in situ penetration tests is very small. Thus the empirical data base available is not yet sufficient to provide an adequate empirical basis for determining the effects of independent variables on the rock penetration process. If a theory could be found which would even approximately replicate the limited data on rock penetration, it could be used for parameter studies of the effects of its independent variables, and the results of this study would then be relevant to the performance of penetrating weapons impacting rock. By conducting a systematic parameter study using an analytical penetration model which does not rely on empirical "constants" and which has been successfully used in predicting depth of penetration for a number of shallow penetration events[2] into a variety of materials, including rock and concrete, it is hoped that this report will allow the reader to gain a qualitative understanding of the factors of importance in rock penetration, a feel for the depths of penetration

---

[2] See Chapter 4.

which may be attainable, and an appreciation of the complexities and uncertainties involved.

1.2 PURPOSE

The purposes of this report are (1) to demonstrate that a rigid body penetration theory developed from the cavity expansion theory (References 4 through 6) can approximately predict the results of shallow penetration tests in hard media and (2) to parametrically investigate the effects of variations in rock properties, nose shape, sectional pressure, and impact velocity on penetration depth and deceleration-time histories over a range which is of potential interest in connection with the design of EPW's.

1.3 PENETRATION PARAMETERS

Penetration of a projectile into rock (or actually any material) is a function of parameters describing the impact geometry, projectile shape and material properties, and rock material properties. The following paragraphs describe the parameters involved in the general penetration problem and then discuss the assumptions and specializations used in this report.

1.3.1 Impact Geometry. The geometry for a general impact situation is shown in Figure 1.1a and involves specification of an angle of obliquity and an angle of attack (also called angle of yaw); note that the projectile axis of symmetry does not necessarily lie in the plane of incidence, and the projectile may or may not be spinning about its axis at impact. Treatment of this general impact geometry is beyond the state of the art, and this report considers the case of normal impact of a nonspinning projectile (Figure 1.1b) with the trajectory coincident with the projectile axis of symmetry. Figure 1.1c defines the depth of penetration as used in this report.

1.3.2 Projectile Shape and Material Properties. In general, projectiles of interest may be considered to be cylindrical, having a body length ℓ, diameter D, and nose section which may be blunt (right-circular cylinder), hemispherical, conical, ogival, or some

combination of these shapes. The projectiles considered in this report have ogival nose shapes, with the nose length and "sharpness" determined by the Caliber Radius Head (CRH) and the body diameter D as illustrated in Figure 1.2. For the normal penetration case considered in this report, the projectile body length ℓ is not an explicit parameter. Also, the projectiles are considered to be rigid bodies; hence internal structure and material properties are not explicitly considered (body length, internal structure, and material density enter as implicit parameters in the determination of projectile mass m).

1.4 SCOPE

The penetration model used for the work reported herein is presented in Chapter 2. A discussion of a general rock classification scheme, which will later be shown to be useful for predicting penetration into rock, is presented in Chapter 3, and the parameters necessary for use in the penetration model are selected. In Chapter 4, studies performed to demonstrate that the penetration model can qualitatively simulate many aspects of actual penetration tests into rock are presented. In Chapter 5, a systematic parameter study of the independent variables over the range of interest in rock penetration is presented. Depths of penetration are computed for a range of impact velocities for projectiles with various weights, diameters, and CRH values.

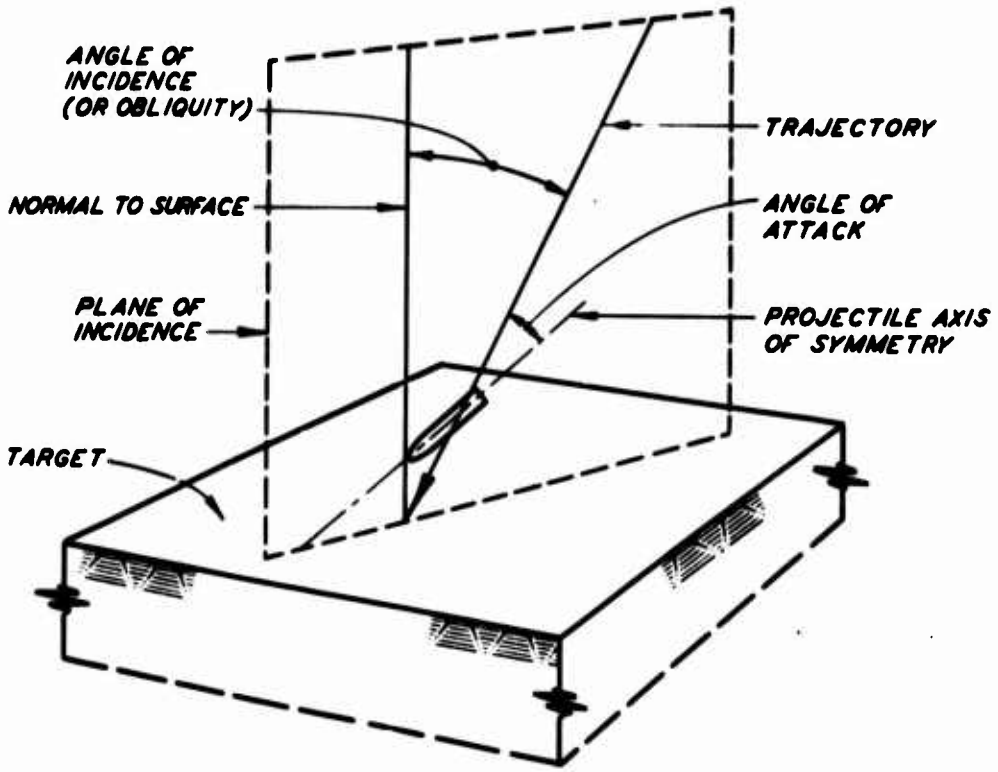

a. Geometry of generalized impact problem.

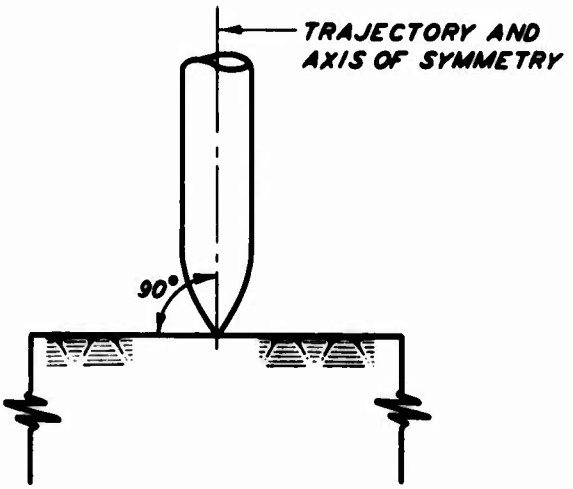

b. Normal impact.

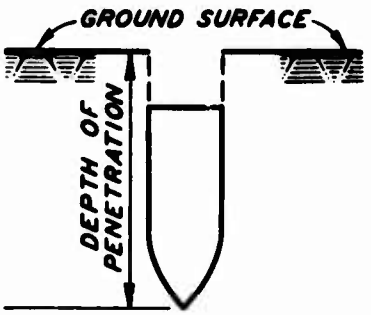

c. Definition of depth of penetration.

Figure 1.1 Projectile impact geometry.

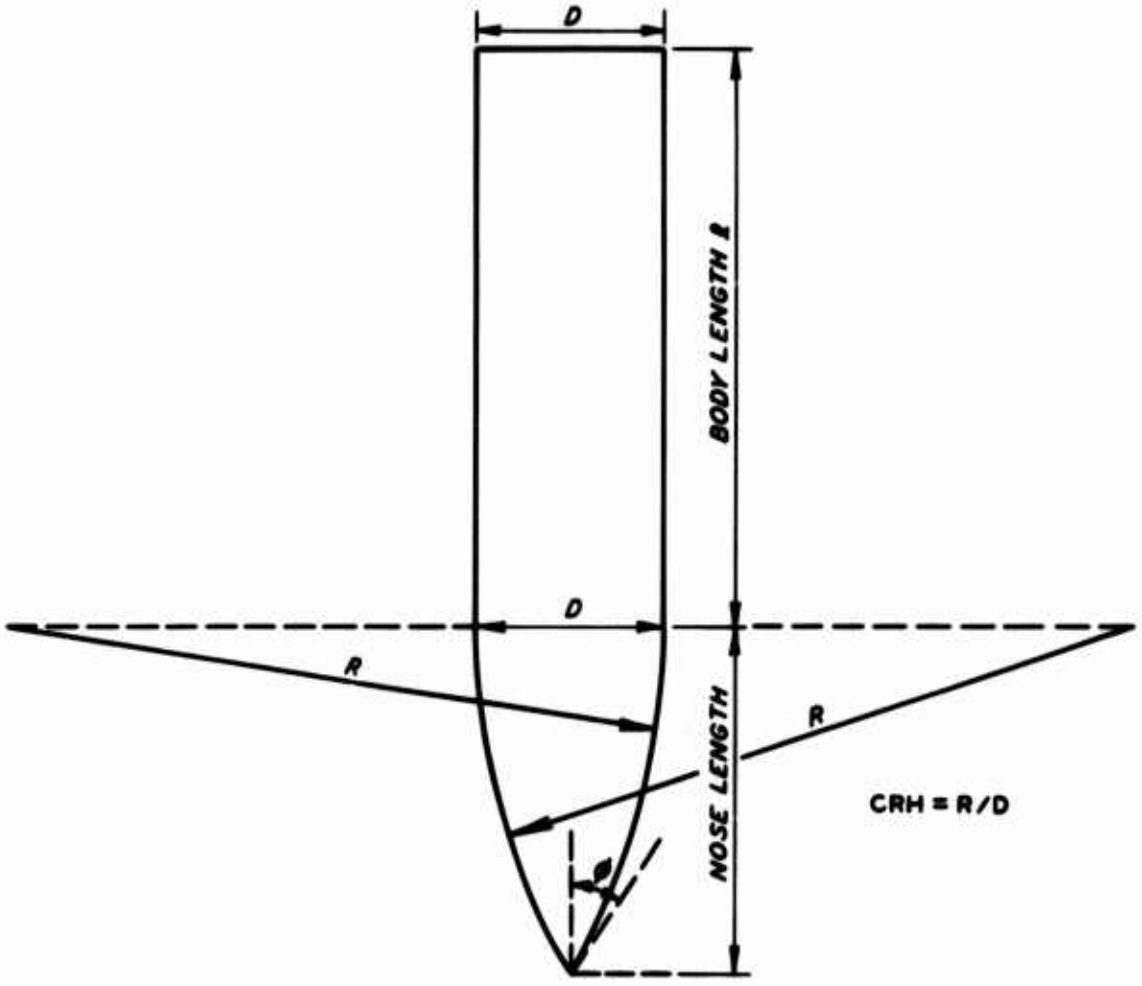

Figure 1.2 Definition of CRH .

CHAPTER 2

PENETRATION MODEL

2.1 FORCE LAWS AND EMPIRICAL RELATIONS

References 1 and 4 present histories of the attempts to develop equations for predicting the depth of projectile penetration into earth materials. The prevalent procedures have been to develop purely empirical equations relating the measured depths of penetration for a set of experimental tests to various test parameters or to assume that the penetration event is governed by a particular form of force law. Using initial and end conditions, the equation of motion (based on the assumed force law) may be integrated to yield time histories and an equation relating final depth of penetration to initial velocity. The resulting equation will contain one or more constants which must be determined from actual penetration data by curve-fitting techniques.

The basic deficiency of both the purely empirical approach and the force law method is that they both contain coefficients not uniquely defined in terms of the physical properties of the target materials and the geometry of the projectile. Also, since the coefficients must be evaluated from penetration test results for a given velocity range, projectile geometry, and target type, the penetration equations cannot be used reliably outside the range of test conditions used in fitting the equations.

2.2 THEORETICAL PENETRATION MODEL

2.2.1 Original Formulation. A theory of penetration of rigid projectiles into incompressible elastic-plastic targets was developed by Goodier (Reference 5). The theory was extended by Ross and Hanagud (Reference 6) to include the compressibility of the target and has been used successfully in studies of penetration of ice, frozen soil, sand, and clay (References 4, 6, and 7). The theory has also been used to predict mine penetration into a variety of earth targets (Reference 8) and

bomb penetration into concrete (Reference 9).[1] Treatment of penetration into a multilayered medium is presented in Reference 10.

The penetration theory is based on the theory of dynamic cavity expansion in locking elastic-plastic materials whose behavior can be idealized by the compressibility and shear behavior illustrated in Figure 2.1, in which e_i is the volumetric strain related to the jump from zero to finite stress (elastic region), e_p is the volumetric strain related to the jump from the elastic to the plastic region of the stress-strain curve, E_t is the strain-hardening modulus corresponding to the locked plastic region, G_t is the strain-hardening shear modulus, E is Young's modulus of elasticity corresponding to the locked elastic region, and G is the elastic shear modulus. The resulting penetration equation is the solution of the equation of motion of a rigid body subjected to a distributed normal stress on its nose. The local normal stress is determined from the theory of dynamic cavity expansion for an assumed velocity field in the media adjacent to the projectile. The normal stress or cavity pressure is obtained from the solution of a boundary-value problem and is expressed in terms of parameters defined explicitly in terms of measurable material properties of the target and the mass and geometry of the projectile.

2.2.2 WES Extensions of the Penetration Model.[2] In the original formulation, Ross and Hanagud assumed a hemispherical-nosed projectile and normal impact. WES is currently involved in theoretical efforts to extend the penetration model to apply to oblique impact conditions as well as to conical and ogival nose geometries and layered targets. Since this report considers ogival projectiles, the penetration equation as modified to apply to ogives is used. The relevant equations are listed without derivation, since the derivations and documentation of

---

[1] In this reference, results of application of this theory are shown to be in very good agreement with empirically based concrete penetration formulas within the range of the parameters for which the formulas are considered accurate.

[2] The expression "penetration model" is used in the remainder of this report to refer to the Ross-Hanagud penetration theory and any WES modifications and extensions to the basic theory.

the model will be the subject of a future WES technical report.

The equation of motion for a rigid projectile of mass m and diameter D penetrating in the z-direction (origin at ground surface, positive downward) is given by the following:

$$m \frac{d^2z}{dt^2} + \frac{\pi D^2}{4} \left\{ p_s + f(\epsilon)\rho_p \left[B_1 \frac{D}{2} \frac{d^2z}{dt^2} + B_2 \left(\frac{dz}{dt} \right)^2 \right] \right\} = 0 \qquad (2.1)$$

The parameters in Equation 2.1 are given in terms of the target material properties by the following:

$$B_1 = 1 - \delta^{1/3} \qquad (2.2)$$

$$B_2 = \frac{3}{2} - (1 + \alpha_p)\, \delta^{1/3} + \frac{1}{2} \delta^{4/3} \qquad (2.3)$$

$$p_s = \frac{4}{9} E \left[1 - \exp(-3\beta) \right] - \frac{2}{3} Y \ln \delta + \frac{2}{27} \pi^2 E_t - \frac{4}{9} E_t \eta \qquad (2.4)$$

$$\delta = 1 - \frac{\rho_o}{\rho_p} \exp(-3\beta) \qquad (2.5)$$

$$\alpha_p = 1 - \frac{\rho_o}{\rho_p} \qquad (2.6)$$

$$\eta = \sum_{n=1}^{\infty} \frac{\delta^n}{n^2} \qquad (2.7)$$

$$\beta = \frac{Y}{2E} - \frac{e_i}{3} \qquad (2.8)$$

$$\rho_p = \rho_o \exp(e_p) \qquad (2.9)$$

where

ρ_o = initial density of target material, slugs/cu ft^3

Y = yield strength of target material (shown in Figure 2.1), psf

E = Young's modulus of elasticity, corresponding to locked elastic

region in Figure 2.1, psf = 3G (G = elastic shear modulus)

E_t = strain-hardening modulus, corresponding to locked plastic region in Figure 2.1, psf = $3G_t$ (G_t = strain-hardening shear modulus)

e_i = volumetric strain related to the jump from zero to finite stress (elastic region) in the stress-strain curves in Figure 2.1

e_p = volumetric strain related to the jump from the elastic to the plastic region of the uniaxial stress (i.e., unconfined compression) stress-strain curve in Figure 2.1b

The function $f(\varepsilon)$ is the ogive nose factor:[4]

$$f(\varepsilon) = \frac{2}{\varepsilon^2} \int_0^{\phi(\varepsilon)} \left[\sin^2 \psi + \frac{\sin^3 \psi \cos^2 \psi}{1 - (1 - \varepsilon) \cos \psi} \right] (\cos \psi - 1 + \varepsilon)\, d\psi \qquad (2.10)$$

where

$$\varepsilon = \frac{1}{2\ CRH} \qquad (2.11)$$

$$\cos \phi = 1 - \varepsilon \text{ , or}$$

$$\phi(\varepsilon) = \tan^{-1} \left(\frac{2\varepsilon - \varepsilon^2}{1 - \varepsilon} \right) \qquad (2.12)$$

CRH is defined in Figure 1.2 and ϕ is the limiting cone half-angle. A plot of $f(\varepsilon)$ versus CRH is given in Figure 2.2.

The target material is defined by six material parameters (e_i , e_p or ρ_p , ρ_o , E , E_t , and Y) and the projectile by three parameters (m , CRH , and D). The parameters e_i and e_p can be obtained from a hydrostatic compression test on undisturbed specimens of target material conducted at strain rates and carried to peak stress levels generally anticipated during the penetration event. The parameters E ,

---

[3] A table of factors for converting U. S. customary units of measurement to metric (SI) units is presented on page 5.

[4] R. S. Bernard, private communication, January 1974. Equation 2.10 represents a first attempt at incorporating nose shape effects into the model.

E_t , and Y can be determined from an undrained dynamic uniaxial stress test (unconfined compression) or from a dynamic triaxial test at a confining pressure simulating the in situ stress state.

The constitutive model assumed in the cavity expansion theory is a relatively simple one. Strength is independent of stress level, volume change can occur only at the initiation of stress or at the onset of plastic behavior, and dilatation in shear is not possible in the model. Such simplifications are at variance with the observed behavior of real soil and rock. Thus, it should be noted that the material properties used provide only a crude description of the stress-strain behavior of the material; and as with any analytical technique, it is within the realm of possibility to obtain "good results" from a fortuitous selection of parameters, even though individually the parameters might not be the correct choice for the particular event.[5] Their use (as well as the use of the theory itself) can only be justified on the basis of agreement of the analytical results with available penetration data. Such agreement will be demonstrated later in this report for a number of cases within the range of variables of relevance to EPW rock penetration.

Equation 2.1 is easily amenable to an incremental solution in terms of velocity by using the initial and end conditions.

$$\frac{dz}{dt} = V_o \ , \quad \text{when} \quad z = 0$$
$$\frac{dz}{dt} = 0 \ , \quad \text{when} \quad z = P \tag{2.13}$$

where V_o is the impact velocity and P is the final depth of penetration. After n time steps Δt , the velocity V is given by

---

[5] The penetration event, for example, may produce a distinctive stress field in the target which in itself would establish the appropriate confining pressure for laboratory property determination (rather than the natural in situ stress field).

$$V(n\Delta t) = V_o - \sum_{k=1}^{n} \Delta V_k \qquad (2.14)$$

where ΔV_k is the incremental velocity change in the k^{th} time step as computed from Equation 2.1. The acceleration during the k^{th} time step is $\Delta V_k/\Delta t$, and the distance penetrated during the k^{th} time step is computed as

$$\Delta z_k = \frac{V(k\Delta t) + V[(k-1)\Delta t]}{2} \Delta t \qquad (2.15)$$

A number of small computer codes have been used to solve Equation 2.1 in the manner described. Although it can be solved in closed form to give a final depth of penetration in a homogeneous half space, solving the equation incrementally has a number of advantages. During the early phase of penetration, until the ogival nose is completely embedded, the effective cross-sectional area of the projectile varies; and by letting the diameter vary with penetration in Equation 2.1, as required to reflect the effective cross-sectional area, the embedding process is included in the model. Also the incremental solution allows the material properties of the target to be changed at any time step, which in turn allows layered targets to be considered. The computer codes may be accessed from time sharing terminals and are easy and inexpensive to operate. On-line plotters can be used to produce parameter plots.

One additional WES modification to the theory was to allow ρ_p to be changed with time in the incremental method as the cavity pressure drops, i.e., the complete target pressure-volumetric strain curve may be used instead of the locking approximation.

a. Behavior in hydrostatic compression.

b. Behavior in unconfined compression.

Figure 2.1 Idealized stress-strain curves for a locking elastic-plastic material.

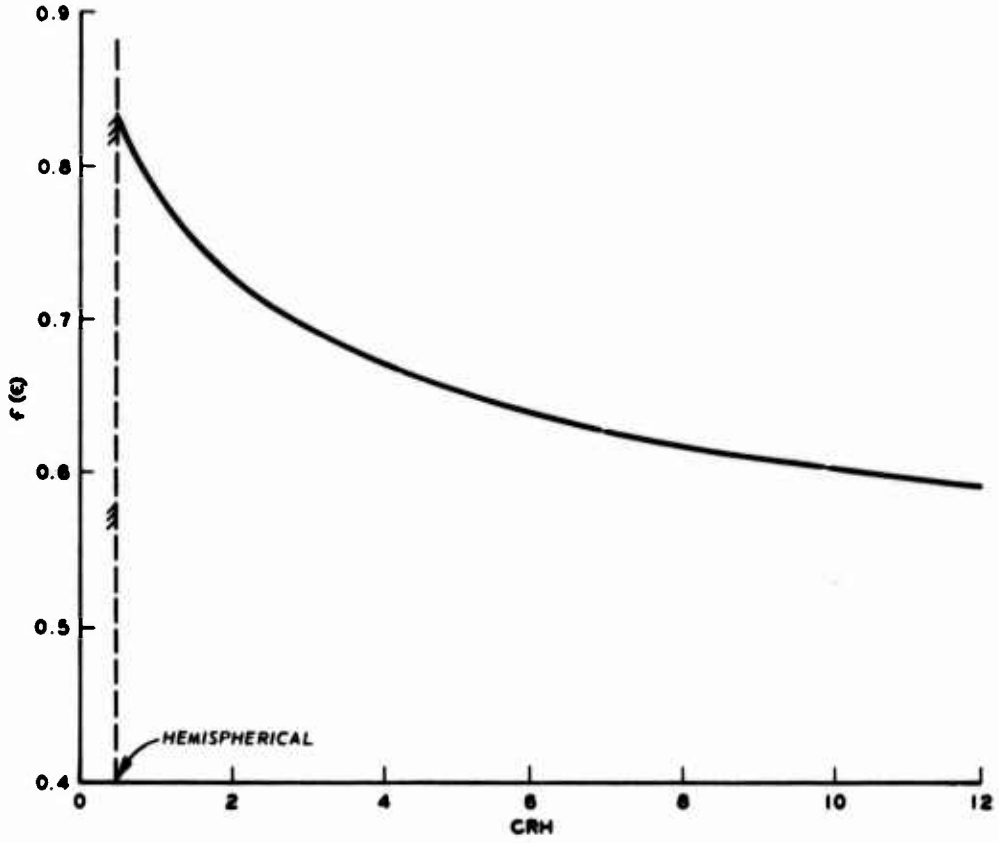

Figure 2.2 Ogive nose factor.

CHAPTER 3

SELECTION OF TARGET PARAMETERS

3.1 INTACT AND IN SITU ROCK PROPERTIES: AN OVERVIEW

Rock is properly described as a nonlinear, hysteretic material and in its in situ state is nonhomogeneous, anisotropic, and discontinuous. Even the most sophisticated finite difference or finite element computer code cannot treat the intrinsic and discontinuum properties of the in situ rock mass in all their complexity. Rock mechanics, being a relatively new formal discipline, does not benefit from a large repertoire of carefully documented cases of engineering successes and failures. Also, unlike soil mechanics, rock mechanics has not enjoyed much success in using laboratory test results to design and predict the behavior of structures in and on rock. In a fundamental sense, the reasons for the problems encountered in rock mechanics might be reduced to a problem in probability and statistics (Reference 11),[1] although such an approach may prove to be of limited utility, since it is difficult to conceive how probability density functions, for example, could be constructed for general cases.

Rock contains not only small-scale defects such as cracks, flaws, inclusions, grain boundaries, etc., but also large-scale inhomogeneities, such as layers, joints, faults, fractures, folds, etc., with scales ranging from centimeters to hundreds of meters. Also the rock surfaces involved in these geologic structures may be weathered or may be characterized as being completely random with regard to asperities or as having undulating asperities with characteristic "wave lengths" and "amplitudes" ranging from centimeters to hundreds of meters. Thus the reasons for the existence of a "size effect" problem in the determination of constitutive properties become apparent. Not only are there variations in strength and deformability of intact rock specimens in

---

[1] This reference contains a discussion of reducing rock mechanics problems to a problem in probability and statistics and also a comprehensive bibliography.

the laboratory as size increases (References 11 and 12), but also the mode of failure may change (brittle to ductile, for example). The "size effect" problem becomes even more significant when it is desired to extrapolate laboratory data for properties in situ. In situ tests have been a tremendous aid to engineers, but the obvious problem still arises, as emphasized by Heuze in Reference 13, that the size of the in situ test should be representative of the size of the in situ prototype.

Since in situ rock mass strength and deformability depend on both the intact properties and the discontinuum properties, considerable effort has been expended in recent years to understand the mechanics of jointed rock (References 13 through 15, for example). Also, progress has been extensive in developing engineering oriented classifications and index properties for intact and in situ rock (References 16 through 18). The result of these efforts is the recognition of correlations between certain laboratory test results, between certain in situ test results, between laboratory and in situ test results, and importantly between discontinuum index descriptors and laboratory and in situ test results.

Obviously, the penetration model is intended to apply to a homogeneous isotropic continuum. Thus, if it is to be used successfully in rock penetration, a methodology must be developed for selecting equivalent continuum properties for the rock target such that the theory gives answers which correlate with real tests on the discontinuum. A methodology for this purpose is described in this chapter.

3.2 USE OF IN SITU AND INTACT ROCK CLASSIFICATION SCHEMES TO ESTIMATE RANGES OF CONSTITUTIVE PROPERTIES

Reference 17 presents a classification scheme for intact rock based on two properties of engineering significance (strength and deformability). Table 3.1, which summarizes the classification scheme developed by Deere and Miller (Reference 17), evolved from numerous laboratory tests on many different rock types. Use of the modulus ratio concept results from an observed correlation between uniaxial compressive strength and tangent modulus of elasticity; Figure 3.1 (from Reference 17) illustrates the classification concept. Rocks can be classified under this scheme from a knowledge of the values of strength

and modulus determined in laboratory tests. As illustrated in Figure 3.1 for the particular case of igneous rocks, rocks of a given type tend to cluster in a restricted region of the space. The limiting values for the average modulus ratio band were chosen to encompass the majority of the data for rocks with interlocking textures. Thus some of the power and utility of the classification scheme can be realized. In many cases, knowledge of rock type and texture may enable an "educated estimate" of engineering properties to be made; and if rock type and either strength or modulus are known, then the other property can be predicted with a much higher degree of confidence.

Other important correlations exist between the engineering properties and various quantitative rock index properties, such as Schmidt hardness, Shore hardness, and dry unit weight. The importance of these correlations is that the index tests can be performed easily, quickly, and economically on rock cores in the field. Nomograms based on the observed correlations, such as Figures 3.2 and 3.3, can then be used to estimate strength and modulus. Thus rocks can be classified according to Table 3.1 based solely on simple index tests.

Reference 18 presents a systematic classification scheme for the quality of in situ rock (i.e., the degree to which the rock represents a continuum). The in situ classification scheme is based on a quantitative core logging procedure proposed by Deere in 1964. The in situ nature of the rock mass is described by its Rock Quality Designation (RQD), which is obtained by measuring the total length of all unweathered pieces of core greater than or equal to 4 inches and then dividing by the total length of core run. RQD has been shown to correlate with other qualitative descriptions of rock quality such as fracture frequency and velocity ratio $(V_f/V_L)^2$, where V_f is the in situ and V_L the laboratory (intact) compressional wave velocity. The RQD is expressed as a percentage, with an RQD of 100 percent corresponding to a fracture frequency of 0 and a velocity index of 1. Table 3.2 summarizes the classification system.

On the basis of extensive in situ testing to determine apparent elastic moduli, such as plate jack tests, radial jack tests, borehole

deformation tests, etc., various important correlations between RQD and the ratio of intact to in situ constitutive properties have been determined (References 18 and 19). Correlations have been established between the ratio of apparent Young's moduli (E_{insitu}) and the intact specimen Young's modulus (E_{intact}) and RQD . Figure 3.4 shows one of the correlations as given in Reference 20. The general trend of E_{insitu}/E_{intact} versus RQD has been confirmed by other investigators in field tests, model studies, and finite element studies, although a straight line correlation should not be expected and it is probable that the ratio approaches a value of 0.1-0.15 at low values of RQD . This suggests that an estimate of in situ modulus of elasticity can be easily obtained from a knowledge of RQD , Schmidt hardness, and dry unit weight by using correlations such as those shown in Figures 3.3 and 3.4. If the intact modulus is known, only an estimate of RQD is needed in order to estimate the in situ modulus.

In many instances rock masses may be described as being laminated or tri-orthogonally jointed. For these conditions, Duncan and Goodman (Reference 21) derive an expression relating in situ modulus of deformation E_{insitu} to the intact modulus E_{intact} , normal joint stiffness K_n , and fracture spacing s :

$$E_{insitu} = \frac{1}{\frac{1}{E_{intact}} + \frac{1}{K_n s}} \tag{3.1}$$

By using a correlation by Deere (Reference 20) between RQD and fracture frequency f , where

$$f \equiv \frac{1}{s} = 6\left(1 - \frac{RQD}{100}\right) \tag{3.2}$$

it is possible to determine K_n in terms of E_{intact} if it is assumed that the ratio E_{insitu}/E_{intact} approaches 0.1-0.15 at $RQD = 0$ as suggested previously. Figure 3.5 shows the relation for the ratio values 0.1 and 0.15 at $RQD = 0$.

The discussion thus far has not referred to in situ strength, and

indeed "handy" correlations such as those shown in Figure 3.5 for the relation of in situ and intact unconfined compressive strengths do not exist. Thus it is in general not possible to deduce in situ strength from a knowledge of RQD and intact strength, for example, as it was for the modulus values (Figure 3.5). Much of the problem arises from misconceptions regarding the nature of rock strength; as stated by Hudson (Reference 22), properties such as tensile and compressive strengths are experimental, not intrinsic, properties. Thus laboratory strength values depend on the method of testing and size of the test specimen. Despite these concepts, properties such as tensile and compressive strengths, yield strength, ultimate strength, crushing strength, etc., are still used and needed for many types of engineering analyses. Therefore, caution is required in specifying strength values and in describing the test method. Speaking in terms of a statistically significant number of tests for a given type of strength test, several "values of strength" may be observed as the size of the test specimen is increased, because in some cases failure occurs due to flaws or discontinuities (References 11, 12, and 22) and the scale dimensions of the various types of discontinuities vary by several orders of magnitude (grain boundaries, cracks, layer boundaries, joint block boundaries, faults, etc.). Thus it is important that strength data or estimates apply to the size scale of interest.

In order to discuss in situ strength for projectile penetration calculations, it is necessary then to specify both the type of experimental strength value and the scale of the test. For the depths of interest in projectile penetration (<200 feet), confining pressures will probably not exceed 150 psi. Thus triaxial tests with very low confining pressures or unconfined tests will suffice. The maximum projectile body diameter considered in this report is 10 inches, which can be considered as a representative size scale for a large class of earth penetrators (Reference 23). Nearly all earth penetrators have a sharply pointed nose section (the projectiles considered in this report are all ogives). Compressive failure of the rock occurs in the region surrounding the tip of the nose, and failure is envisioned to progress radially

outward from the initial region of failure as the nose penetrates; thus the size scale of interest for strength value considerations is of the order of or smaller than the body diameter. Based on these considerations, it is postulated that strength values determined from typical laboratory-size test specimens are adequate for penetration calculations and that corrections for the differences between the appropriate scale in situ test and the laboratory strength test are not necessary.

3.3 BASIC CRITERIA FOR THE SELECTION OF ROCK TARGET CONSTITUTIVE PROPERTIES

In Section 2.2.2, a penetration model requiring six constitutive parameters for the target is presented. The appropriate in situ Young's modulus E can be estimated from a value for the intact (laboratory) modulus and the in situ rock quality RQD by the methodology presented in Section 3.2. It is fortunate, for calculational purposes, that most rocks at low confining pressures (<1000 psi) exhibit brittle failure or at least little or no strain hardening (References 24 and 25). For these rocks, the yield strength, ultimate strength, compressive strength, and crushing strength can all be considered the same in unconfined or triaxial compression tests at low confining pressure. Thus the strain-hardening Young's modulus E_t can be set equal to zero, and the value for the strength Y can be determined from unconfined compression tests on laboratory-size specimens. For finely jointed and weathered rock (low RQD), it may be necessary to apply reduction factors to the intact (laboratory) value for Y, using results such as those presented in References 14, 15, 26, and 27 as guides.

The concept of locking material behavior is discussed in Reference 6. While the plastic locking strain or density concept might be a valid one for rocks, it is felt that the actual locked plastic density is not the appropriate value to use for ρ_p in Equation 2.1. The locked plastic density may be approached in the material surrounding the point of impact, but the density increase will be much less during the remainder of the penetration event. The pressure-relative density behavior of several rock types is shown in Figure 3.6. For soils, the "lock-up" density or volumetric strain can be estimated as being equal

to the porosity. However, due to the strength of the rock matrix itself, the porosity of rocks is not such a controlling factor, although it obviously affects the total compressibility. The porosity of rocks ranges from essentially zero to as much as 30 percent. If the impact pressure, average pressure in the media during penetration, existing cavity pressure, etc., can be estimated or approximated and the initial density ρ_o is known, then a value for ρ_p can be obtained from a pressure-relative density relation (such as Figure 3.6).

The parameter e_i has been shown not to be a sensitive parameter in maximum penetration predictions (Reference 4). It is postulated that setting e_i equal to zero for rocks is an appropriate assumption.

3.4 SELECTION OF GENERAL TARGET MATERIAL PROPERTIES

3.4.1 Selection of Strength and Modulus Values for Representative Rock Groups. It was desired to keep the parameter study in this report very general with respect to the rock target parameters. Using the intack rock classification scheme presented in Section 3.2 as a guide, low-strength (6000 psi), medium-strength (12,000 psi), and high-strength (24,000 psi) rock targets were selected, with the strength values representing the median values for Classes D, C, and B, respectively (Table 3.1). The targets were characterized as being in the average modulus ratio Class M with modulus ratio of 350. Thus the three targets would be classified as BM, CM, and DM. The strain-hardening modulus E_t is set equal to zero based on the arguments presented in Section 3.2.

3.4.2 Selection of Initial Densities and Methods for Estimating the Compressibilities. The remaining three parameters needed for the three rock targets as input to the penetration model are the initial densities ρ_o, locked elastic volumetric strains e_i, and locked plastic volumetric strains e_p or plastic densities ρ_p. While it is not true in general that rocks with higher densities have higher strengths, it is true in many cases and correlations exist to this effect (Reference 16). Thus initial densities were selected which were thought to be representative of the three strength classes in an increasing

fashion: 2.1, 2.6, and 2.9 g/cm^3 for low-, medium-, and high-strength targets, respectively. The locked elastic volumetric strain e_i was set equal to zero for all three rock targets.

The procedure used to estimate ρ_p for the three rock targets was to estimate first the peak stress at impact by graphical impedance matching[2] (for the maximum impact velocity of 3000 fps considered in this report) in pressure versus particle velocity space (Figure 3.7) and then the compressibilities at the peak stresses from the relations in pressure versus ρ_o/ρ space (Figure 3.8). The value of ρ_p for use in Equation 2.1 is then estimated from the compressibility at a stress level approximately one-half the peak stress for each rock type. Neither the method used here nor the actual curves in Figures 3.7 and 3.8 are intended to be rigorous or strictly representative of particular rocks. The curves are intended to be representative of rocks in the three strength categories and are composites of data, such as those presented in Figure 3.6 and References 28, 30, 33, and 34. Discussion of the graphical impedance matching techniques and the equations connecting the various parameters of interest can be found in many sources (see References 34 through 37 for examples). Table 3.3 summarizes the assumed rock properties for DM, CM, and BM rocks.

---

[2] Plane wave assumption.

TABLE 3.1 ENGINEERING CLASSIFICATION FOR INTACT ROCK

I. On basis of strength

Class	Description	Uniaxial Compressive Strength psi	Uniaxial Compressive Strength kbar $= \left(10^9 \frac{\text{dynes}}{\text{cm}^2}\right)$
A	Very high strength	Over 32,000	2.2
B	High strength	16,000-32,000	1.1-2.2
C	Medium strength	8,000-16,000	0.55-1.1
D	Low strength	4,000-8,000	0.28-0.55
E	Very low strength	Less than 4,000	0.28

II. On basis of modulus ratio

Class	Description	Modulus Ratio[a]
H	High modulus ratio	Over 500
M	Average modulus ratio	200-500
L	Low modulus ratio	Less than 200

Classify rock as BM, BH, BL, etc.

[a] Modulus ratio = E_{t50}/σ_a .

where

E_{t50} = tangent modulus at 50% ultimate strength;

σ_a = uniaxial compressive strength.

TABLE 3.2 ENGINEERING CLASSIFICATION FOR IN SITU ROCK

RQD, %	Velocity Index	Fracture Frequency No./ft	Description
0-25	0-0.2	6-4.5	Very poor
25-50	0.2-0.4	4.5-3	Poor
50-75	0.4-0.6	3-1.5	Fair
75-90	0.6-0.8	1.5-0.75	Good
90-100	0.8-1.0	0.75-0	Excellent

TABLE 3.3 ROCK PROPERTIES

Rock Type	E^a, psi	E_t	Y, psi	ρ_o, slugs/ft^3	ρ_p, slugs/ft^3	e_i
Low strength	2.1×10^6	0	6,000	4.07	4.95	0
"DM"	(0.14 Mbar)		(0.414 kbar)	(sp gr = 2.1)	(sp gr = 2.55)	
Medium strength	4.2×10^6	0	12,000	5.04	5.72	0
"CM"	(0.29 Mbar)		(0.828 kbar)	(sp gr = 2.6)	(sp gr = 2.95)	
High strength	8.4×10^6	0	24,000	5.63	6.3	0
"BM"	(0.58 Mbar)		(1.65 kbar)	(sp gr = 2.9)	(sp gr = 3.25)	

[a] Average modulus ratio, i.e., E/Y, = 350 for all three rock types.

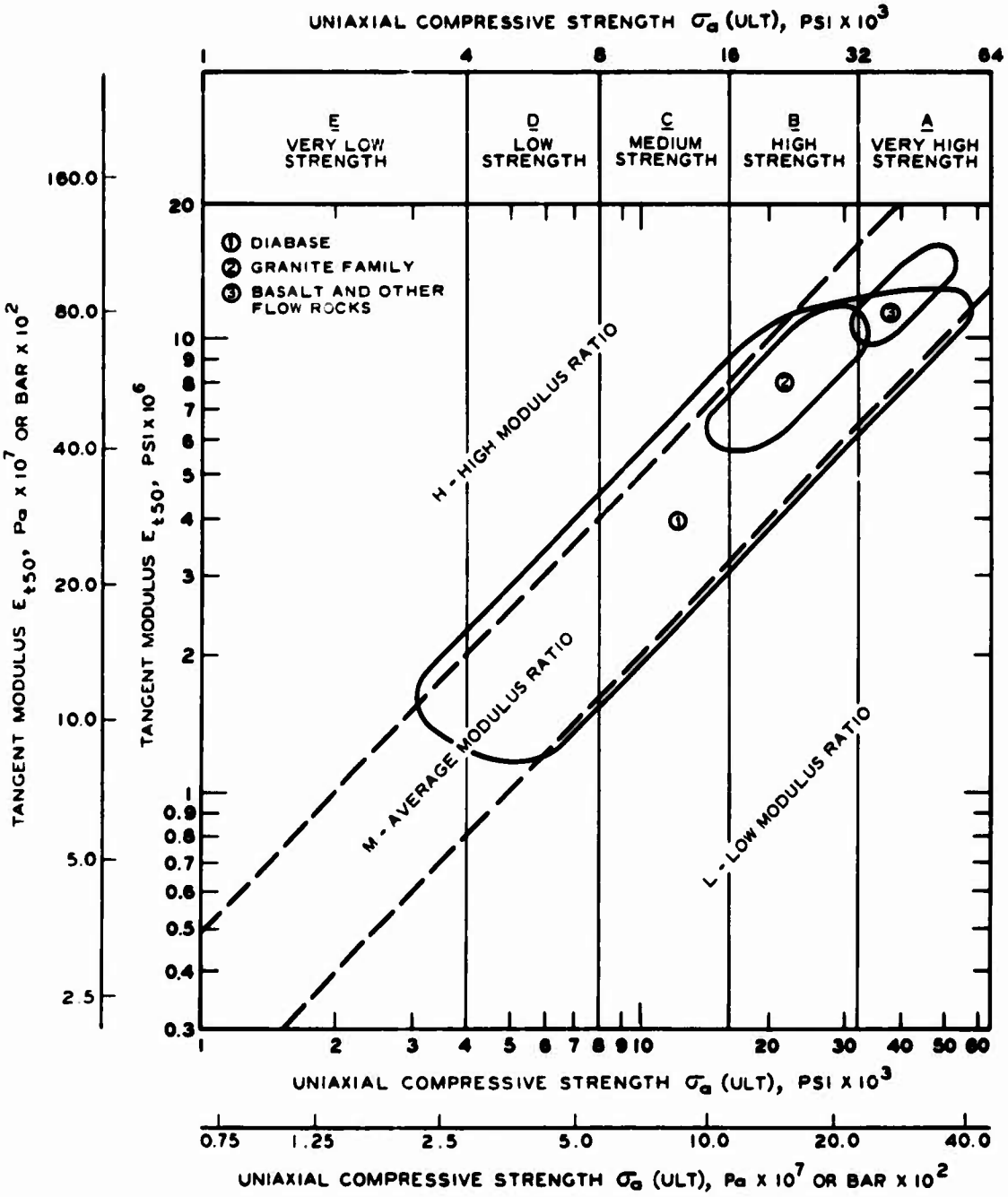

Figure 3.1 Engineering classification for intact rock; summary plot for igneous rocks (176 specimens, 75 percent of points) (Reference 17).

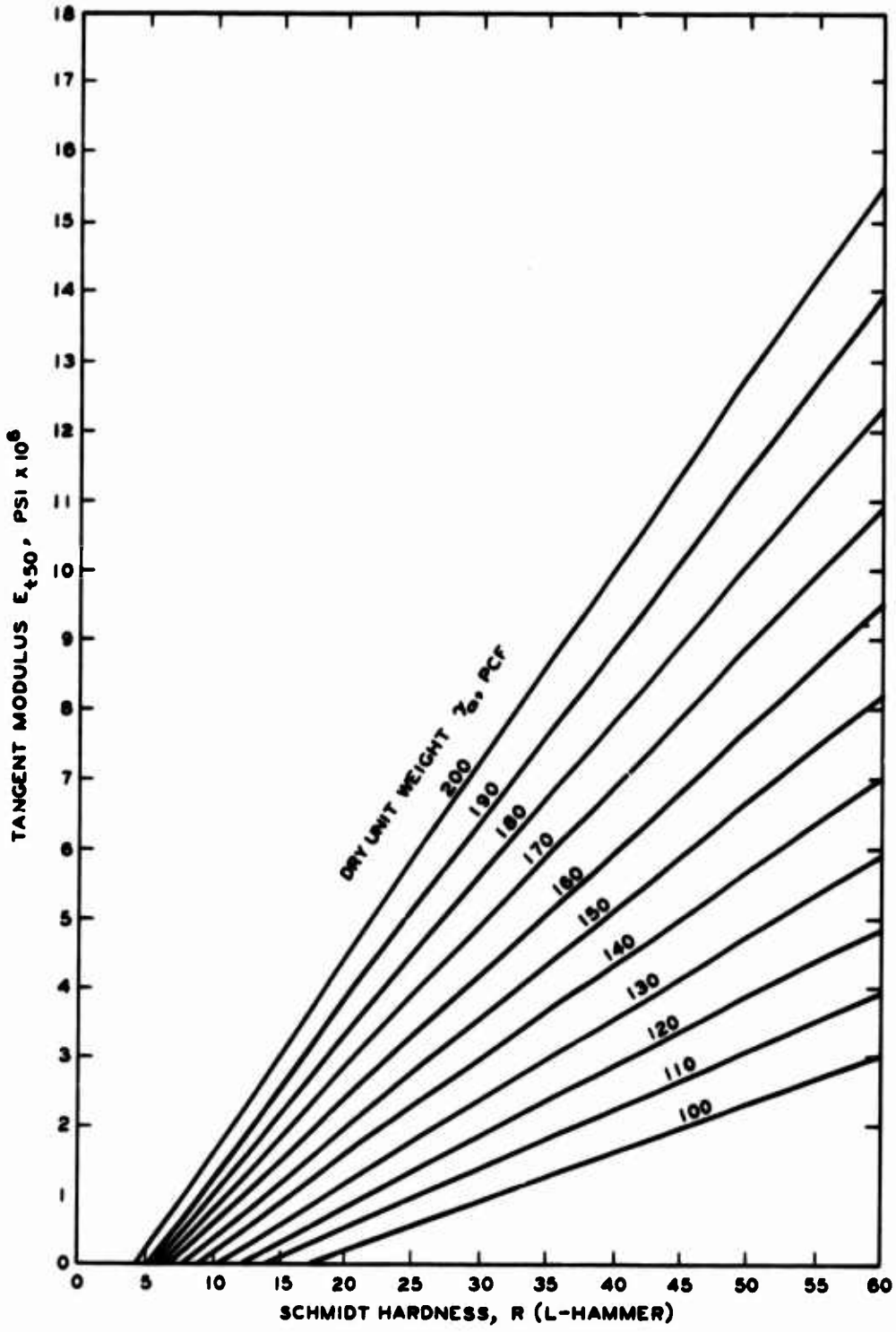

Figure 3.2 Rock modulus chart based on Schmidt hardness (Reference 16).

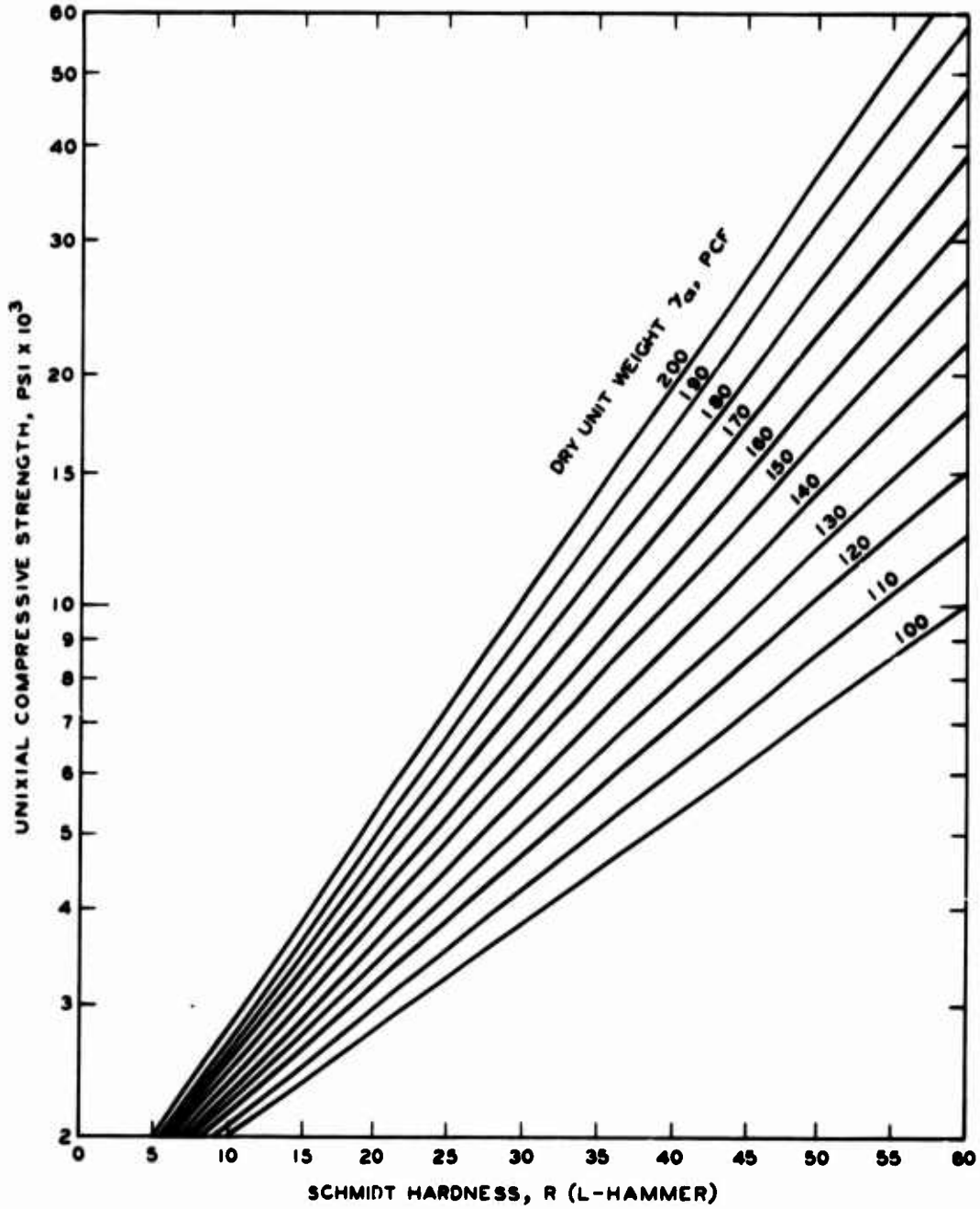

Figure 3.3 Rock strength based on Schmidt hardness (Reference 16).

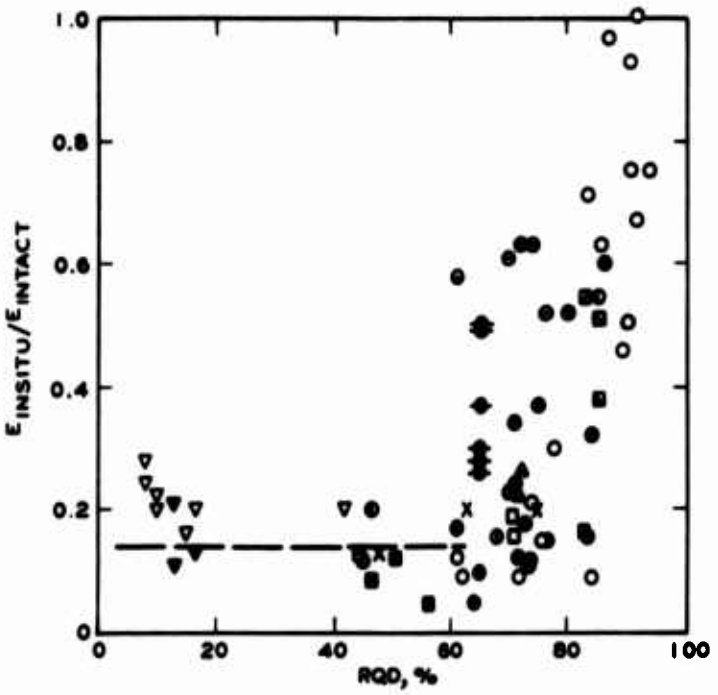

Figure 3.4 Variation of modulus ratio E_{insitu}/E_{intact} with RQD (Reference 20).

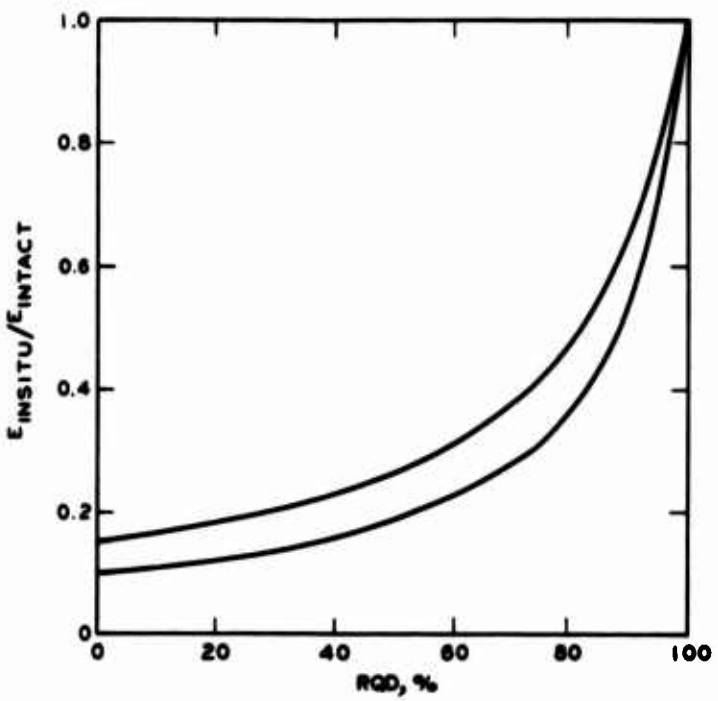

Figure 3.5 Behavior of E_{insitu}/E_{intact} versus RQD for two limiting values.

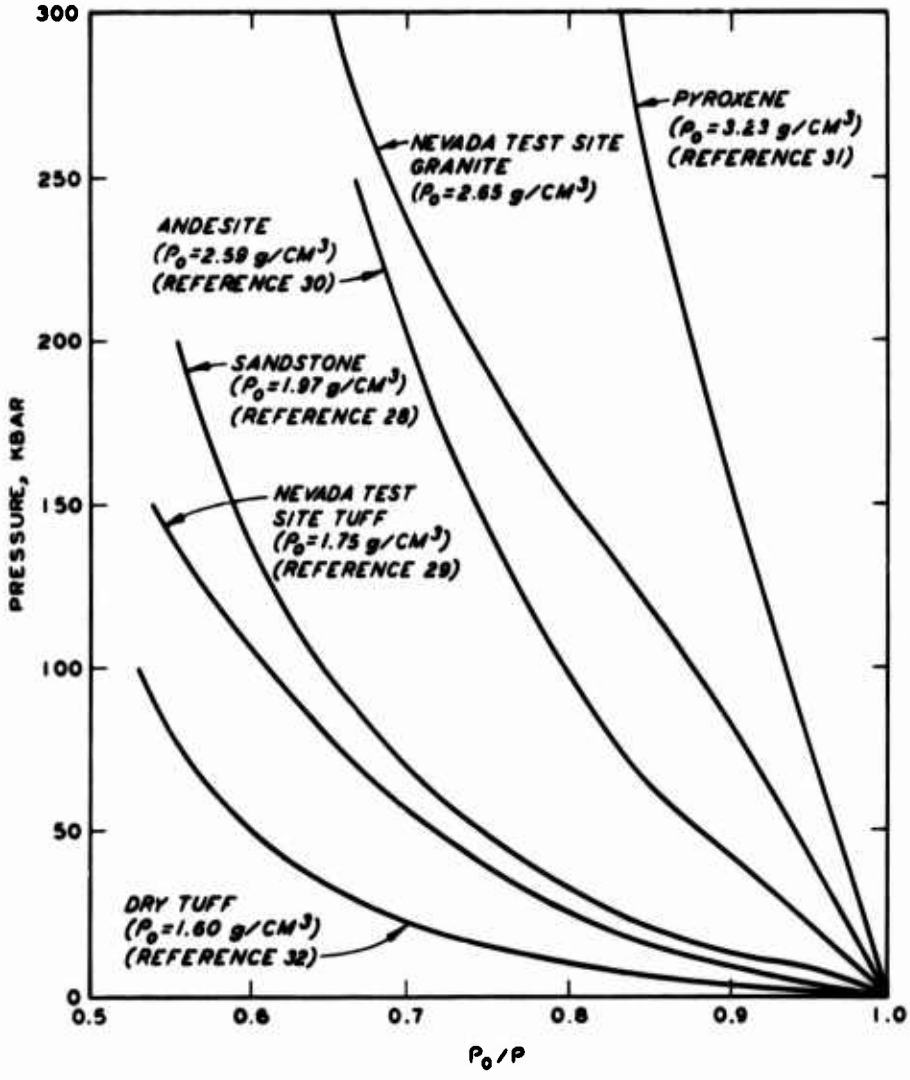

Figure 3.6 Presure-relative density relations for several rock types.

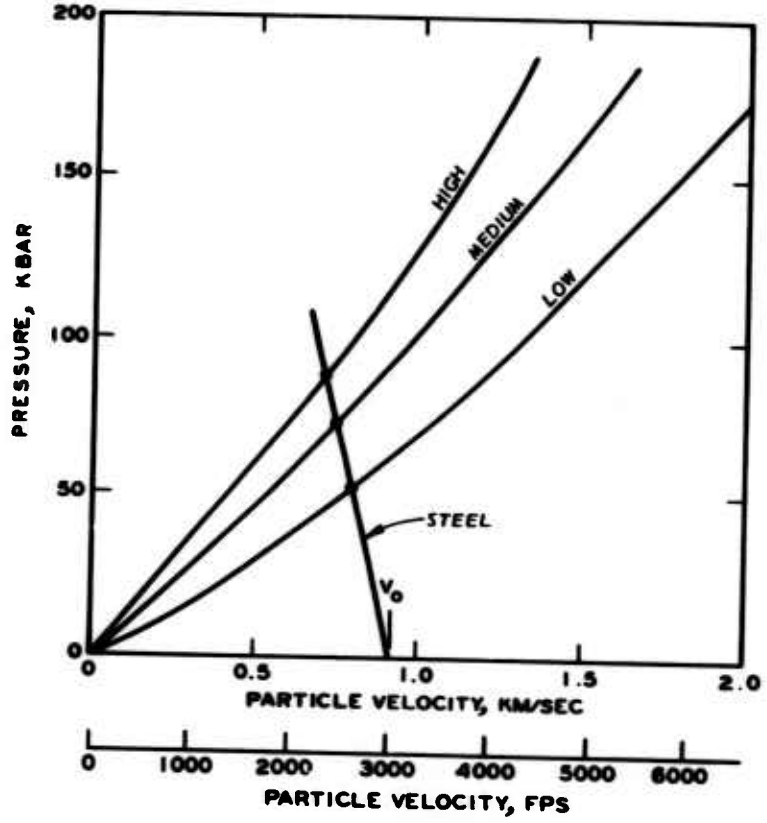

Figure 3.7 Impedance matching to obtain estimate of impact pressures for three rock targets at impact velocity V_o of 3000 fps and assuming a steel projectile.

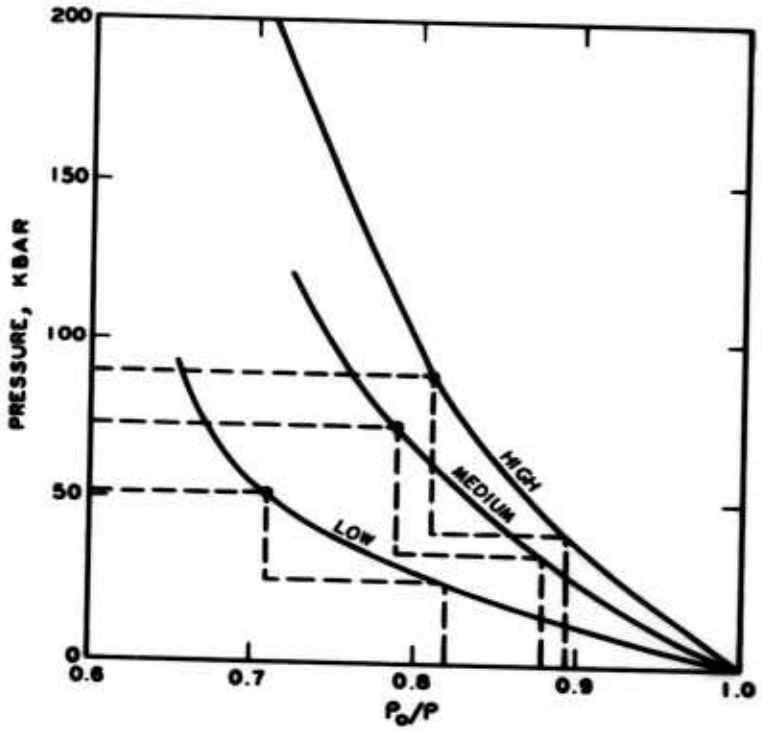

Figure 3.8 Estimation of compressibilities of the rock targets at the impact pressures indicated in Figure 3.7.

CHAPTER 4

COMPARISON OF PENETRATION MODEL PREDICTIONS WITH EXPERIMENTAL RESULTS

4.1 COMPARISON OF PENETRATION MODEL PREDICTIONS USING GENERAL ROCK PROPERTIES WITH EXPERIMENTAL RESULTS

In an effort to gain insight concerning the reliability of the penetration model for predicting actual dynamic penetration into rock, five field tests were modeled and penetration predictions obtained. The tests were selected from those reported in Reference 2. The author of the reference reported RQD values for the targets and classified the rock according to the scheme presented in Table 3.1. Based on the classification of the targets, the general rock properties listed in Table 3.3 were used as presented, except that if the target was listed as having a high modulus ratio, the value 500 was used in conjunction with the Y value to obtain E; likewise, for low modulus ratio classifications, a value of 200 was used. Table 4.1 presents the projectile characteristics and target properties used in the penetration model and compares the predicted and measured depths of penetration. The projectile type and test numbers refer to identification numbers used in Reference 2. The agreement between the predicted and measured penetration depths is very good in most cases. It is emphasized again that the rock properties used were those of Table 3.3 for low-, medium-, and high-strength rock and that actual stress-strain and strength data were not available. The fact that adequate simulation could be obtained from such limited rock property information is fortunate, since the military targeteer rarely has detailed material property data for specific targets available to him.

The worst agreement was obtained for Test No. 120-127, for which the prediction is 36 percent lower than the measured value for penetration into Madera limestone. For this case the RQD at the site was not reported. For Test No. 120-106, the initial prediction was about 25 percent too low. Based on judgment, it was felt that the low value of RQD (32 percent) for the weathered granite at the test site was due

to vertical as well as to horizontal fractures (contrasted to a sedimentary rock, for which a low value of RQD might be due entirely to horizontal fractures). Since vertical fractures would obviously enhance penetration and reduce strength, a second calculation was attempted with the value of Y lowered to 4000 psi, which is the lower limit for low-strength rocks in Table 3.1. This attempt yielded results which agreed much better with those obtained in the experiment (second entry for Test No. 120-106 in Table 4.1). In similar fashion, a second calculation for Test No. 120-127 with Y lowered to 8000 psi (the lower limit of CH rocks) yielded much better agreement with the experimental result (second entry for Test No. 120-127).

For the limited number of comparison cases, the good agreement shown in Table 4.1 could be due to fortuitous combinations of material parameters. Thus it is profitable to obtain upper and lower limit penetration predictions for each case and then compare these with the measured penetration depths. This comparison is shown in Figure 4.1, in which predicted upper and lower limit depths of penetration are plotted versus measured depth of penetration (the perfect correlation line is shown for reference). The upper and lower limits of penetration for each case were calculated using the lower and upper limits, respectively, of the compressive strength for a given intact rock classification (i.e., a factor of two variation in strength). Furthermore, since the compressibility characteristics of the target materials were not known, it was assumed that the upper limits of compressive strengths correspond to 1 percent and the lower limits to 20 percent compressibility. Any other reasonable combinations of material properties will result in penetration depths which fall within these limits. As shown in Figure 4.1, the use of the rather extreme range of properties still produces ranges of predicted penetration depths which are acceptable for many practical applications.

4.2 TARGET PARAMETER STUDY OF SANDIA TEST NO. 120-106

In order to determine if the success achieved by changing the yield strength of the target (E adjusted to keep modulus ratio at 500) and

keeping other target properties constant was accidental, a parameter study of Sandia Test No. 120-106 was conducted to illustrate the sensitivity of penetration predictions to all the target properties. The projectile parameters were not varied: weight W = 613 pounds, diameter D = 8 inches, sectional pressure W/A = 12.2 psi, and CRH = 9.25 . Figure 4.2 illustrates the effect of varying Y within the range 4000-8000 psi, using E , ρ_o , and ρ_p from Table 3.3 for a low-strength rock. The penetration data in Figure 4.2 are replotted in Figure 4.3 for selected velocities as a function of modulus ratio, where in this case the modulus ratio varies due only to Y since E is held constant. In Figure 4.4, E is varied by a factor of 20, and the effect on penetration is seen to be very small (less than 5 percent over the entire velocity range). Thus, for a factor of two change in Y , the effect on predicted penetration depth for a given velocity will be of the order of 40 percent, while E has a minimal effect (at least for a factor of 10 change in E).

The effect of rock target density and compressibility on penetration is investigated in Figures 4.5 through 4.7 for constant values of E and Y . A constant value of the quantity ρ_p/ρ_o is maintained in Figure 4.5 while varying both ρ_o and ρ_p ; the effect on penetration is seen to be minimal at low velocities and approaches a spread of only 7 percent about the median penetration depth at 1900 fps. The effect of varying the compressibility while keeping ρ_o constant is shown in Figure 4.6, and Figure 4.7 shows the effect of varying compressibility while keeping ρ_p constant. While it is obviously important to choose realistic values for ρ_o and ρ_p , it is the ratio ρ_p/ρ_o which appears to have a more significant effect on predicted depth of penetration (for a given Y). As shown in Figure 4.6, in the upper range of compressibility (for example, $1.11 \leq \rho_p/\rho_o \leq 1.35$), a variation of 10 percent in ρ_p/ρ_o affects the predicted depth of penetration by the order of 10 percent. For the relatively incompressible range (for example, $1.00 \leq \rho_p/\rho_o \leq 1.01$), a variation of only 1 percent affects the predicted de[illegible] of penetration by the order of 15 percent. For the range of velocity of 1000-3000 fps, the value of ρ_p/ρ_o should be

in the range $1.01 \leq \rho_p/\rho_o \leq 1.20$ for most rocks. Considering Figure 3.8, a reasonable maximum variation of the estimate of ρ_p/ρ_o should be ± 5 percent. For the above range of ρ_p/ρ_o, this variation in ρ_p/ρ_o would produce maximum variations in the predicted depth of penetration of the order of ± 10 percent.

For Test No. 120-106, the RQD in situ is given as 32 percent; using the general parameter value (Table 3.2) for low-strength rock of 2.1×10^6 psi as the intact modulus, the in situ modulus can be estimated using Figure 3.6 (upper curve) to be 0.4×10^6 psi. Reference to Figure 4.4 indicates that this reduction in E will probably have negligible effect on penetration at the impact velocity of 860 fps. Thus, it is seen that, for this case, a reasonable range of variation in Y has a much more significant influence than does a reasonable range of variation of any other parameter in the theory. It is expected that this same statement will hold true for each of the other four rock penetration tests simulated.

4.3 TENTATIVE PROCEDURE FOR BOUNDING PENETRATION DEPTH IN ROCK

It is proposed that reasonable upper and lower bounds for penetration predictions into rock within the range of interest for EPW's can be obtained if a strength classification such as "DH" for the intact target material is known or can be inferred (e.g., from comparison with similar rocks, from aerial photos, geologic maps, or literature, etc.) by using the ρ_o, ρ_p, and E values from Table 3.3 and varying Y between the limits indicated for the particular strength classification in Figure 3.1. If in addition the RQD is known or can be estimated, the E value can be lowered by use of Figure 3.5 as previously shown. This concept is illustrated in Figure 4.8 for Test No. 120-106. For badly weathered or fractured rock, this procedure may not be valid, and more work is needed on correlations between RQD, for example, and in situ strength. The measured penetration depth for Test No. 120-106 lies at the upper bound of Figure 4.8 (RQD = 32 percent). The cutoff for the validity of this method may be in the range of RQD = 30-40 percent, although as discussed in Chapter 3, the type of rock may influence the

limit of validity of the method. While the procedure proposed here needs further verification, it is in general agreement with all known relevant data and is based on a rational theory whose assumptions and limitations are defined.

4.4 EXTENSION OF PENETRATION MODEL TO TREAT THE COMPLETE TARGET PRESSURE-DENSITY CURVE

In Chapter 3, for simplicity and generality, a single value of locked plastic density was estimated for each hypothetical rock target and used in the penetration model for the entire velocity range considered. The effect of target compressibility on depth of penetration predictions has been discussed previously in this report. The effect of compressibility on deceleration-time histories will be discussed in this section. A better way of treating the compressibility, which is still within the framework of the constant locked plastic density concept, would be to input a value for ρ_p, estimated as in Section 3.3.2, for example, for each impact velocity. The idea of using a value for compressibility at a stress equal to one-half the impact stress at the maximum velocity of interest was arbitrary and a representation of the fact that the stress in the target media drops very rapidly following impact and in fact is probably much below one-half the peak stress value for most of the penetration event. To improve the treatment of compressibility in the penetration model, a logical and desirable extension is to input the correct ρ_p for the existing cavity pressure at each integration cycle, i.e., the complete target pressure versus density curve should be an input to the model. Since the cavity pressure is available from the calculations in the computer codes, the extension to treat the complete target pressure-density relation was not difficult and was carried out as part of this study.

4.5 EVALUATION OF EFFECT OF PRESSURE-DENSITY CURVE MODIFICATION

The improvements made are expected to have their greatest influence on the deceleration-time history. Regrettably, no deceleration records were available for the five events simulated earlier in this chapter. However, Reference 38 presents calculated deceleration-time histories

for particular points in deformable projectiles as part of the results of numerical solutions to projectile penetration into two rock types. These numerical solutions were obtained by using a large, multipurpose, two-dimensional, Lagrangian finite difference computer code. The two rock types were welded tuff (low-strength rock) and Madera limestone (medium-strength rock). The results of these two calculations are used to test the penetration model as presented in this report and as modified to treat the complete target pressure-density relation using projectile and target properties presented in Reference 38. The target hydrostats are modeled in Reference 38 using the Mie-Grüneisen equation of state:

$$p = \frac{\rho_o c_o^2 \eta}{(1 - q\eta)^2}\left[1 + \frac{\gamma_o}{2}\eta(1 - \eta)\right] + \gamma_o \rho_o E_i \qquad (4.1)$$

where

ρ_o = initial density

c_o = initial velocity of sound

$\eta = 1 - \rho_o/\rho$

q = material constant relating shock velocity to sound and particle velocities

γ_o = Grüneisen constant

E_i = internal energy

ρ = density

Table 4.2 (data taken from Reference 38) summarizes the target and projectile properties for the two penetration events. In the finite difference code calculation, very large yield strengths were input to assure that no plastic deformations took place in the projectile. Body forces, heat conduction, and energy sources were also neglected. In the present penetration model, a rigid projectile is assumed and the other factors are not considered. Figures 4.9 and 4.10 are pressure versus density relations obtained from Equation 4.1, using the data in Table 4.2; Figure 4.11 is a higher pressure extension of Figure 4.9.

Figure 4.12 is a reproduction of a plot from Reference 38 showing the finite difference code computed deceleration versus time response for the welded tuff penetration calculation of a particle located at

the tip of the projectile nose. Superimposed on this is the rigid body prediction from the penetration model calculation (dashed line). In Figure 4.13 the penetration model deceleration-, velocity-, and displacement-time histories (dashed lines) are superimposed on the time histories calculated by the finite difference code for a particle located on the centerline of the projectile at a distance equal to the nose length from the tip. As can be seen in these figures, the penetration model deceleration-time histories are quite similar to the lower frequency portion obtained from the deformable body finite difference calculations. These high-frequency oscillations represent particle accelerations and decelerations due to stress wave propagation in the projectile, which of course cannot be simulated with a rigid body penetration model. As shown in Figure 4.13, the effect of differences in the acceleration curves has a negligible effect on velocity- and displacement-time histories from the two calculational methods. It is interesting to note that the observed final penetration depth for the test simulated in Figure 4.13 was 4.95 feet. This value is in close agreement with the calculated results.

As discussed in Reference 38, although the peak decelerations in Figures 4.12 and 4.13 for the finite difference calculation are drastically different, the decelerations for both curves should oscillate about the common "rigid body deceleration" of the projectile; and it is evident that the agreement of the penetration model prediction of the rigid body motion with that predicted from the finite difference code results is excellent in terms of general shapes of the time histories, magnitudes, and duration of the event.

Figure 4.14 presents the time histories for the limestone penetration calculated with the penetration model superimposed on the finite difference code generated time histories (base figure reproduced from Reference 38). For this case, the time histories are for a particle on the projectile centerline at a distance of 2 feet from the nose tip. Again the penetration model predictions are in excellent agreement with the finite difference results. The maximum depth of penetration observed in the event simulated here was 3.6 feet. Again

both calculations are in reasonably good agreement with this value. Also, both the penetration theory and the finite difference deceleration-time results are in qualitative agreement with the experimental deceleration-time history shown in Figure 4.14 (this represents the only available complete deceleration-time record for projectile penetration into a nonlayered rock target).

To illustrate the importance of the details of target compressibility on the prediction of deceleration-time histories, a parameter study was conducted. The results are shown in Figures 4.15 and 4.16. Figure 4.15 shows the effect on penetration versus time plots of using the constant locked plastic density model with various compressibility estimates for the welded tuff case. The plot for 0.5 percent compressibility agrees approximately in final penetration depth and event duration with the prediction based on the complete pressure-density curve as shown in Figure 4.13. Figure 4.16 shows deceleration versus time plots for the 5.3 and the 0.5 percent compressibilities along with the deceleration-time curve from Figure 4.13. The concept begins to emerge that if the "right" constant locked plastic density value could be selected, then the simple constant locked plastic density model could be used to obtain results in good agreement with those obtained when the complete pressure-density relation is known and used.

If the <u>details</u> of the deceleration-time history of rock penetration events are of interest, it is clearly important to choose the "right" ρ_p. How should one go about estimating a "right" constant locked plastic density for a particular penetration problem? Another estimate of target compressibility can be obtained by considering the contribution to the dynamic cavity pressure expressed by the term $f(\varepsilon)\rho_p B_2 V^2$, where V is the velocity (see Equation 2.1). By using the impact velocity V_o in this term, an estimate is obtained of the peak dynamic cavity pressure contribution from this term. For impact and penetration into the medium-strength rock of Chapter 3 at a velocity of 1000 fps, with $CRH = 6$, $W = 750$ pounds, and $D = 8$ inches, the calculated peak dynamic cavity pressure is about 2 kbar. Following the procedure of estimating the compressibility at half of this peak stress, which was

proposed in connection with Figure 3.8, yields approximately 1 percent compressibility compared to (1) the 5 percent compressibility estimated from the same procedure but using peak stresses at impact estimated from impedance matching for V_o = 1000 fps and (2) the 13 percent compressibility used in Table 3.2 (based on impedance matching for the upper limit of V_o = 3000 fps). Figure 4.17 shows the time histories for this case for a 1 percent compressibility and for the case in which the entire hydrostat of Figure 3.8 was used. The event duration, depth of penetration, and peak deceleration agree very closely. The general effect of using the model with constant locked plastic density with a compressibility which is too large is to overestimate the depth of penetration and the event duration and to underestimate the peak deceleration. A compressibility of 0.5 percent (shown in Figure 4.16) is too small, at least for the early part of the event, and the peak deceleration is slightly overpredicted compared with the plot for the complete pressure-density relation calculation.

It is emphasized that if only the final depth of penetration is of interest, then the need to select the "right" ρ_p is not of overriding importance, and a simple method such as the impedance matching procedure will be adequate. Based on these considerations, the original rock property values given in Table 3.3 were used in the parameter study in Chapter 5, since penetration depth was the primary dependent variable of interest. However, the penetration predictions to be presented in Chapter 5 should be viewed as upper bound estimates, particularly at the lower impact velocities, since the compressibilities are somewhat high.

TABLE 4.1 COMPARISON OF PENETRATION MODEL PREDICTIONS WITH FIELD PENETRATION TEST RESULTS

Sandia Test No. (Reference 2)	Projectile Velocity Type	Rock Type	Code Input	Penetration Predicted	Penetration Measured
120-112	Type III	Sandstone	ρ_o = 4.07	126 in	122 in
	CRH = 9.25; D = 10.188 in	DH	ρ_p = 4.95		
	W/A = 14.3 psi	RQD = 37%	E = 3 × 10^6 psi		
	V_o = 825 fps		Y = 6000 psi		
339-16	Type IV	TTR[a] welded tuff	ρ_o = 4.07	99 in	110 in
	CRH = 6.0; D = 9 in		ρ_p = 4.95		
	W/A = 16.0 psi	DL			
		RQD = 80%	E = 1.2 × 10^6 psi		
	V_o = 650 fps		Y = 6000 psi		
120-77	Type I	TTR welded	ρ_o = 4.07	161 in	156 in
	CRH = 9.25; D = 9 in	agglomerate	ρ_p = 4.95		
	W/A = 13.5 psi	DM			
		RQD = 60%	E = 2.1 × 10^6 psi		
	V_o = 1065 fps		Y = 6000 psi		
120-106	Type II	Weathered granite	ρ_o = 4.07	113 in	150 in
	CRH = 9.25; D = 8 in		ρ_p = 4.95		
	W/A = 12.2 psi	DH			
		RQD = 32%	E = 3 × 10^6 psi		
	V_o = 860 fps		Y = 6000 psi		
120-106			ρ_o = 4.07	144 in	150 in
			ρ_p = 4.95		
			E = 2 × 10^6 psi		
			Y = 4000 psi		
120-127	Type V	Madera limestone	ρ_o = 5.04	79 in	124 in
	CRH = 9.25; D = 8 in	CH	ρ_p = 5.72		
	W/A = 13.4 psi		E = 6 × 10^6 psi		
	V_o = 950 fps		Y = 12,000 psi		
120-127			ρ_o = 5.04	101 in	124 in
			ρ_p = 5.72		
			E = 4 × 10^6 psi		
			Y = 8000 psi		

[a] Tonopah Test Range.

TABLE 4.2 PROPERTIES FOR PROJECTILE PENETRATION INTO TUFF AND LIMESTONE

Welded Tuff Penetration	
Tuff Properties	**Projectile Properties**
ρ_o = 1.85 g/cm^3 = 115 pcf	D = 22.86 cm = 9 in
Poisson's ratio = 0.1	W = 4.55 × 10^5 g = 1000 lb
Y = 3.8 × 10^8 dynes/cm^2 = 5510 psi	W/A = 15.76 psi
c_o = 2.05 × 10^5 cm/sec = 6725 fps	Nose CRH = 6
γ_o = 2.00	V_o = 21,184 cm/sec = 695 fps
q = 1.49	

Madera Limestone Penetration	
Limestone Properties	**Projectile Properties**
ρ_o = 2.69 g/cm^3 = 168 pcf	D = 20.32 cm = 8 in
Poisson's ratio = 0.32	W = 3.055 × 10^5 g = 673.6 lb
Y = 9.44 × 10^8 dynes/cm^2 = 13,690 psi	W/A = 13.4 psi
c_o = 3.4 × 10^5 cm/sec = 11,150 fps	Nose CRH = 9.25
γ_o = 2.00	V_o = 17,374 cm/sec = 570 fps
q = 1.27	

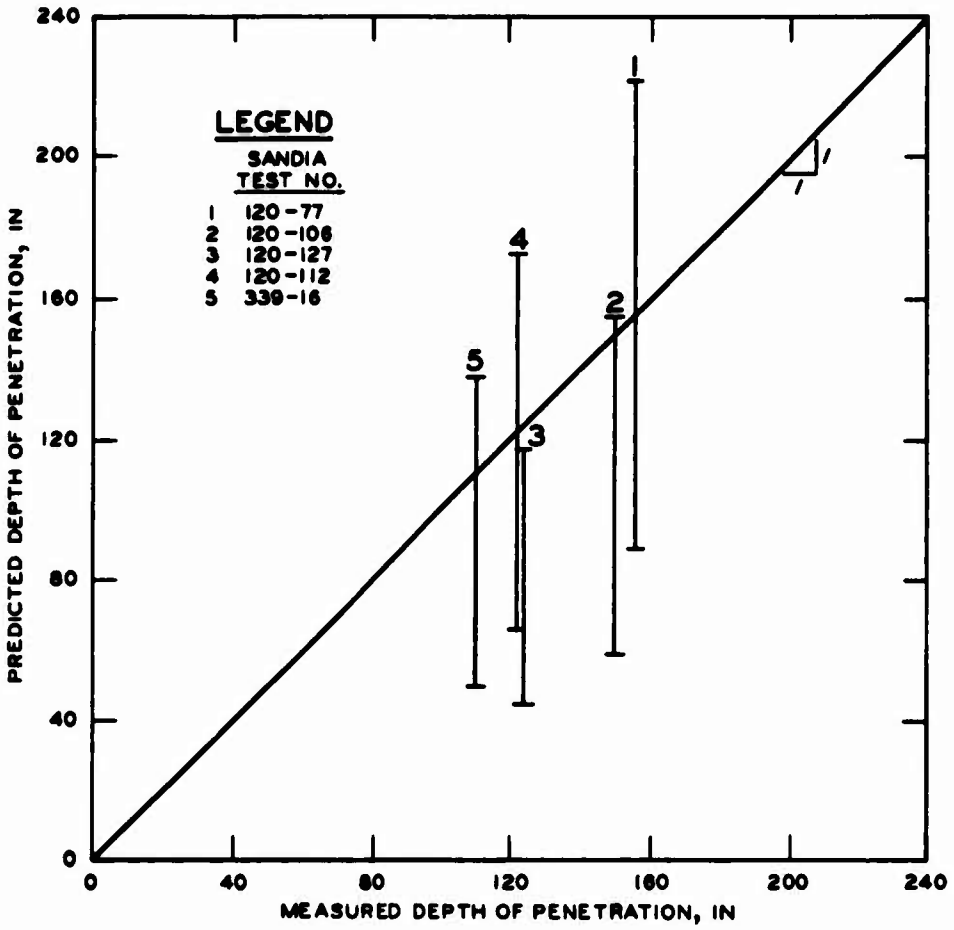

Figure 4.1 Measured versus predicted depth of penetration into rock targets.

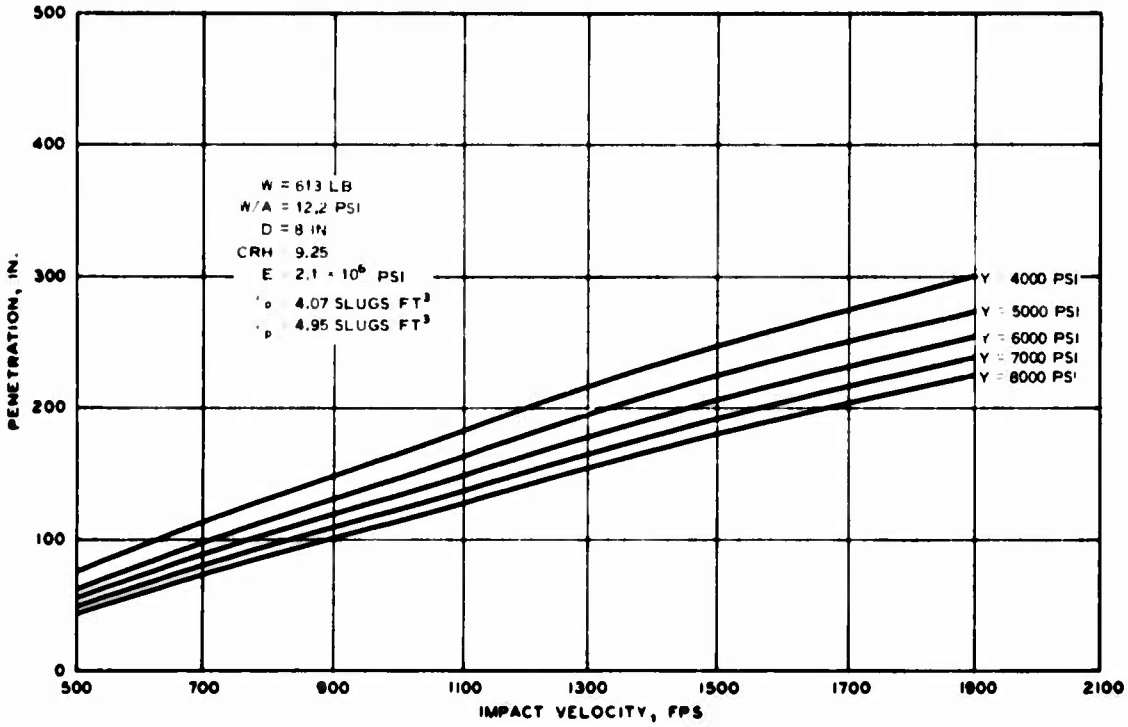

Figure 4.2 Effect of varying Y on penetration versus impact velocity plot (Test No. 120-106).

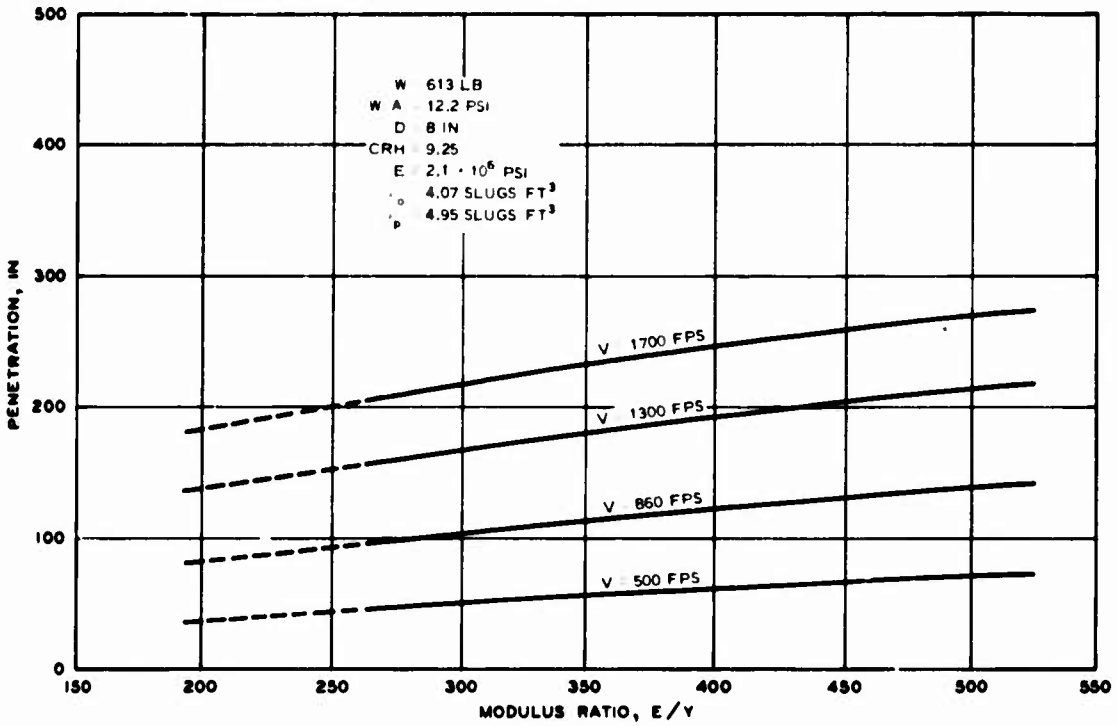

Figure 4.3 Penetration versus modulus ratio for constant E.

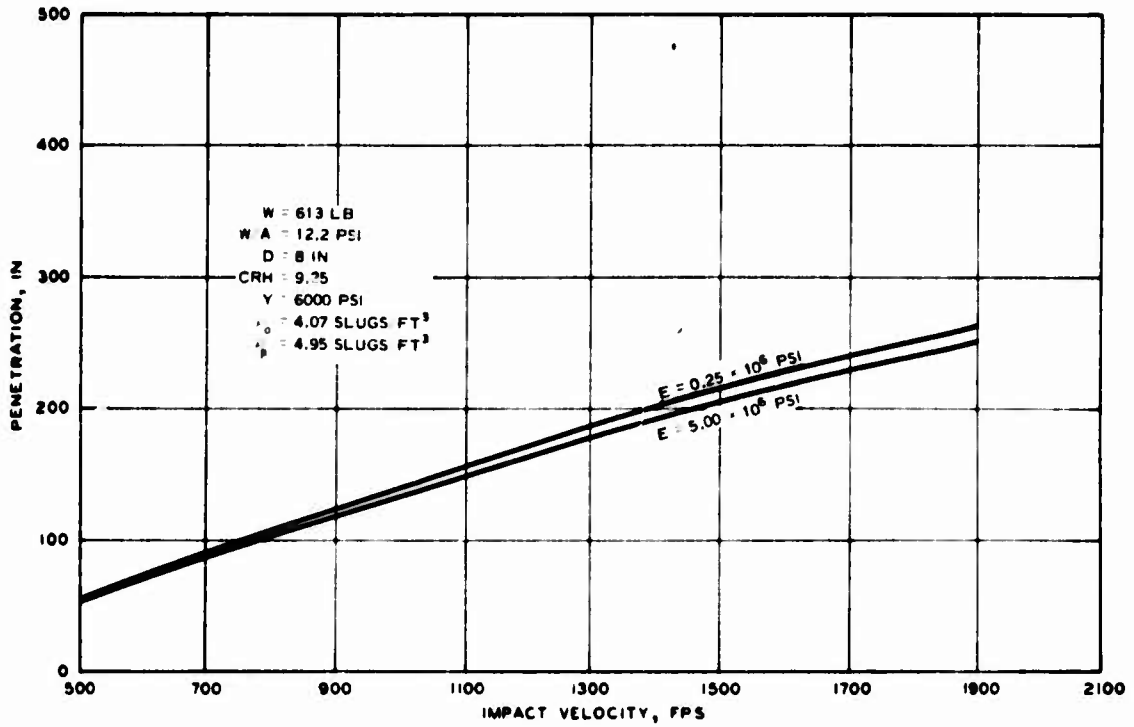

Figure 4.4 Effect of modulus on penetration.

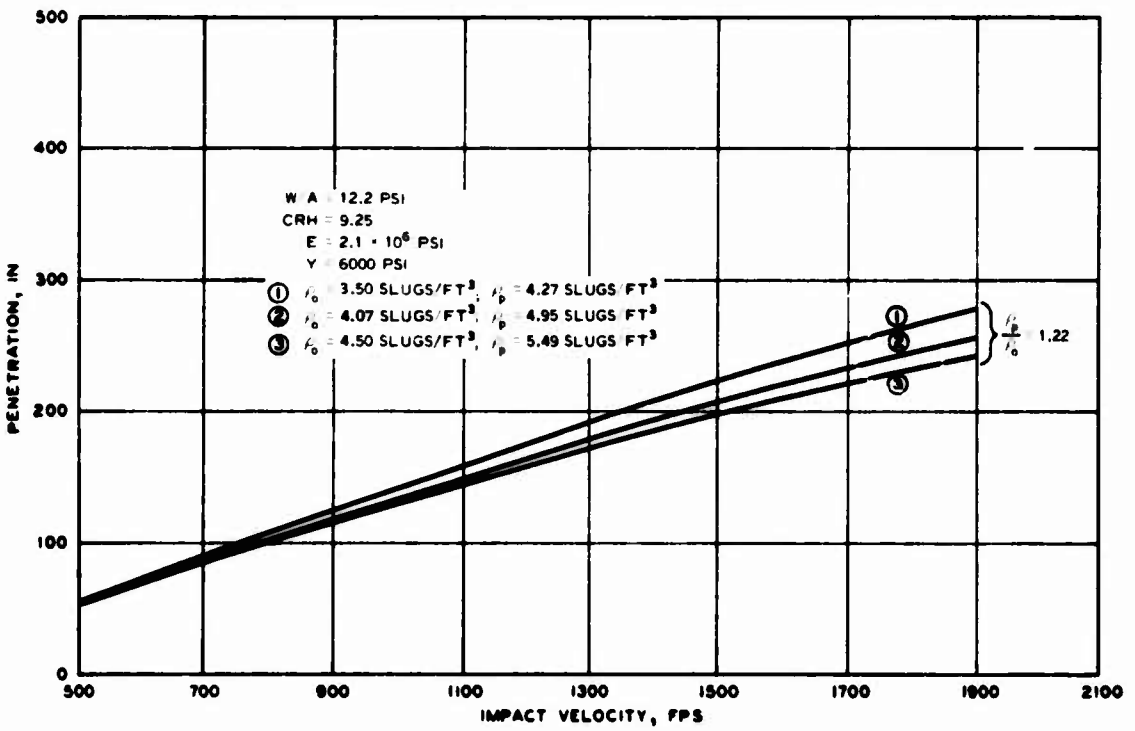

Figure 4.5 Effect of ρ_o and ρ_p on penetration while maintaining ρ_p/ρ_o constant.

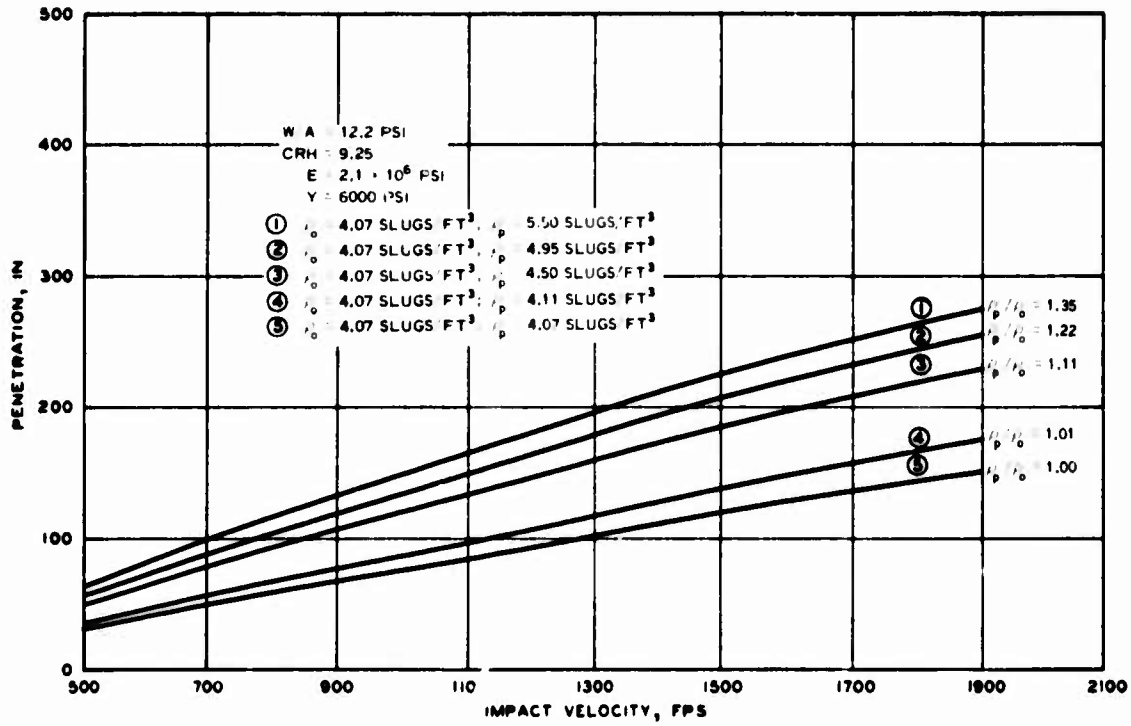

Figure 4.6 Effect of ρ_p/ρ_o on penetration while maintaining ρ_o constant.

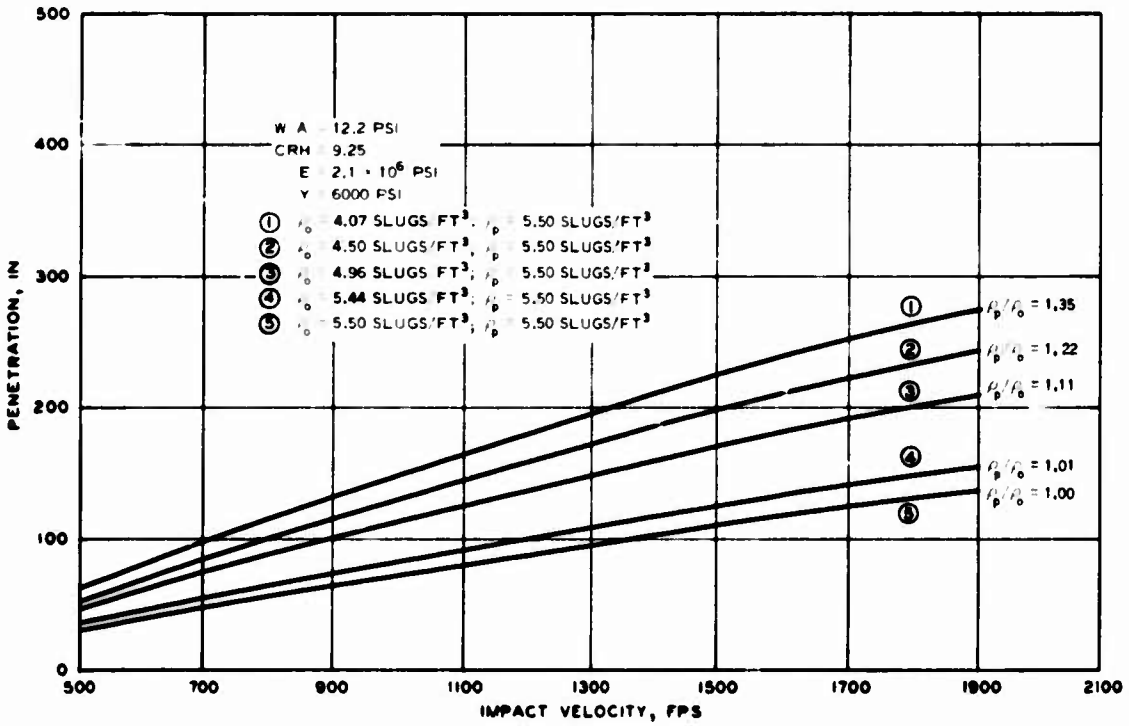

Figure 4.7 Effect of ρ_p/ρ_o on penetration while keeping ρ_p constant.

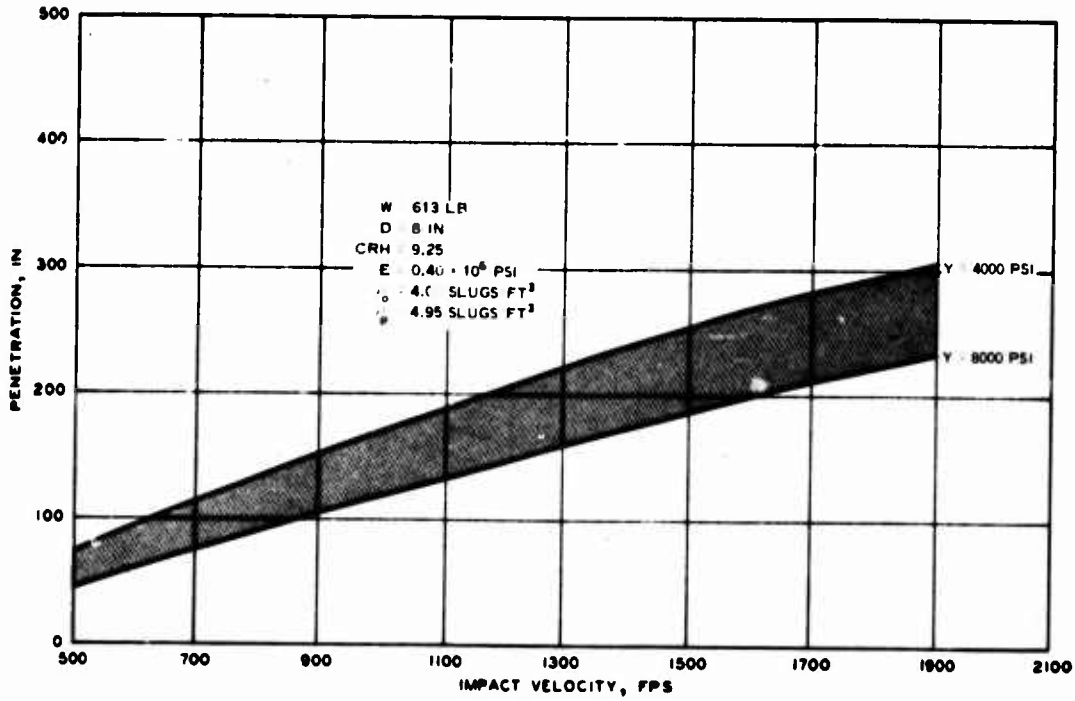

Figure 4.8 Establishment of upper and lower bounds for Test No. 120-106.

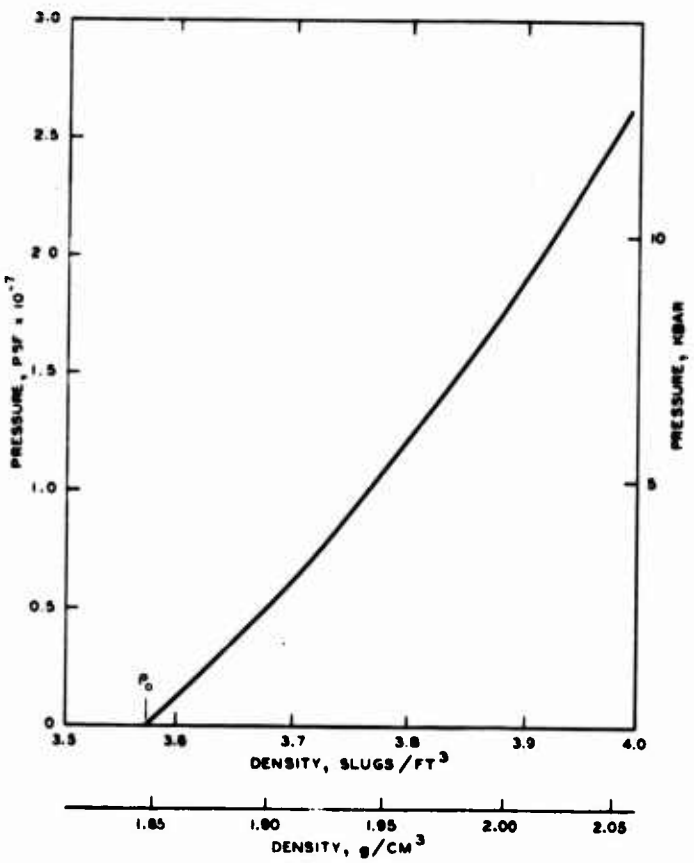

Figure 4.9 Pressure-density relation for welded tuff based on Equation 4.1.

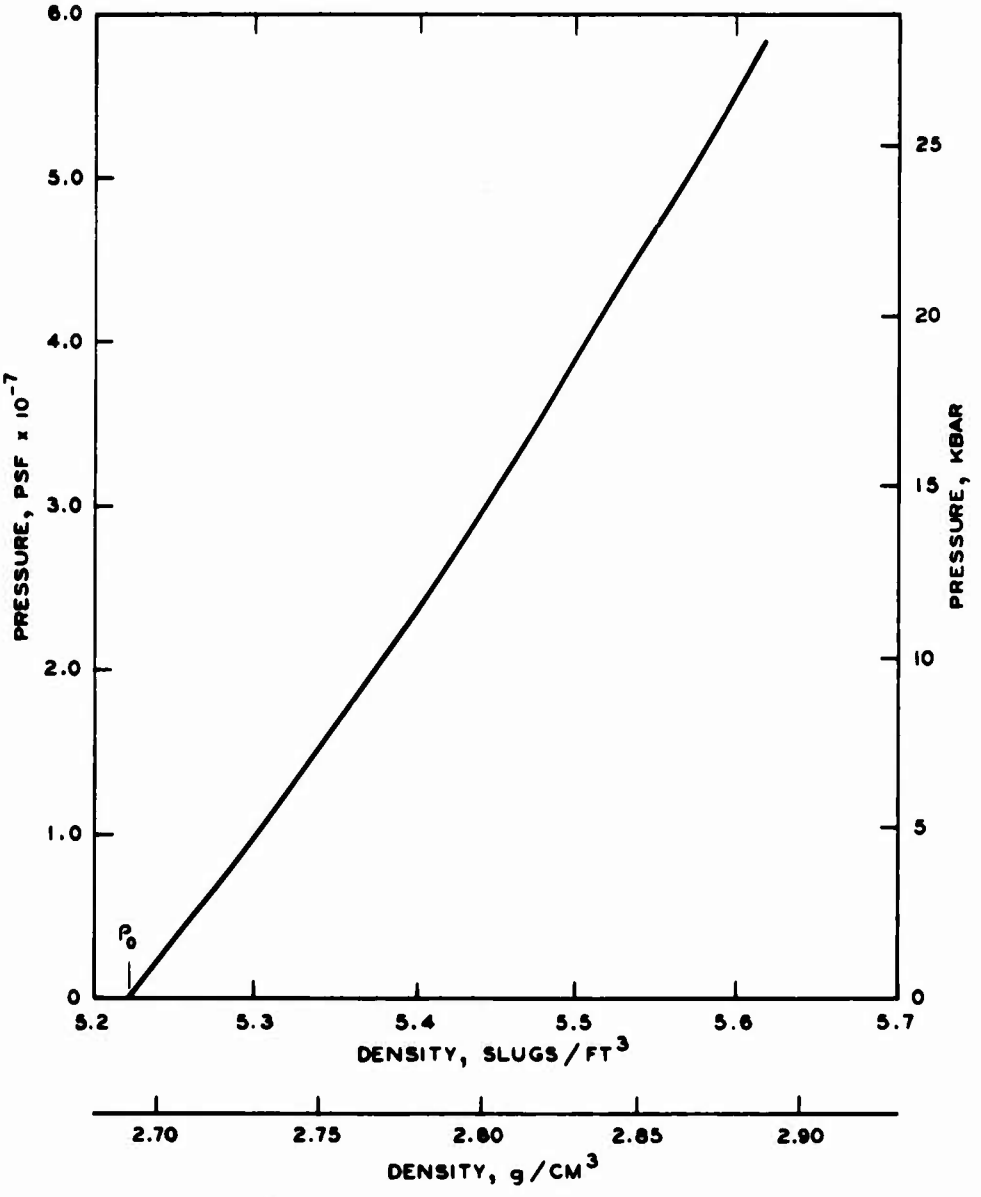

Figure 4.10 Pressure-density relation for Madera limestone based on Equation 4.1.

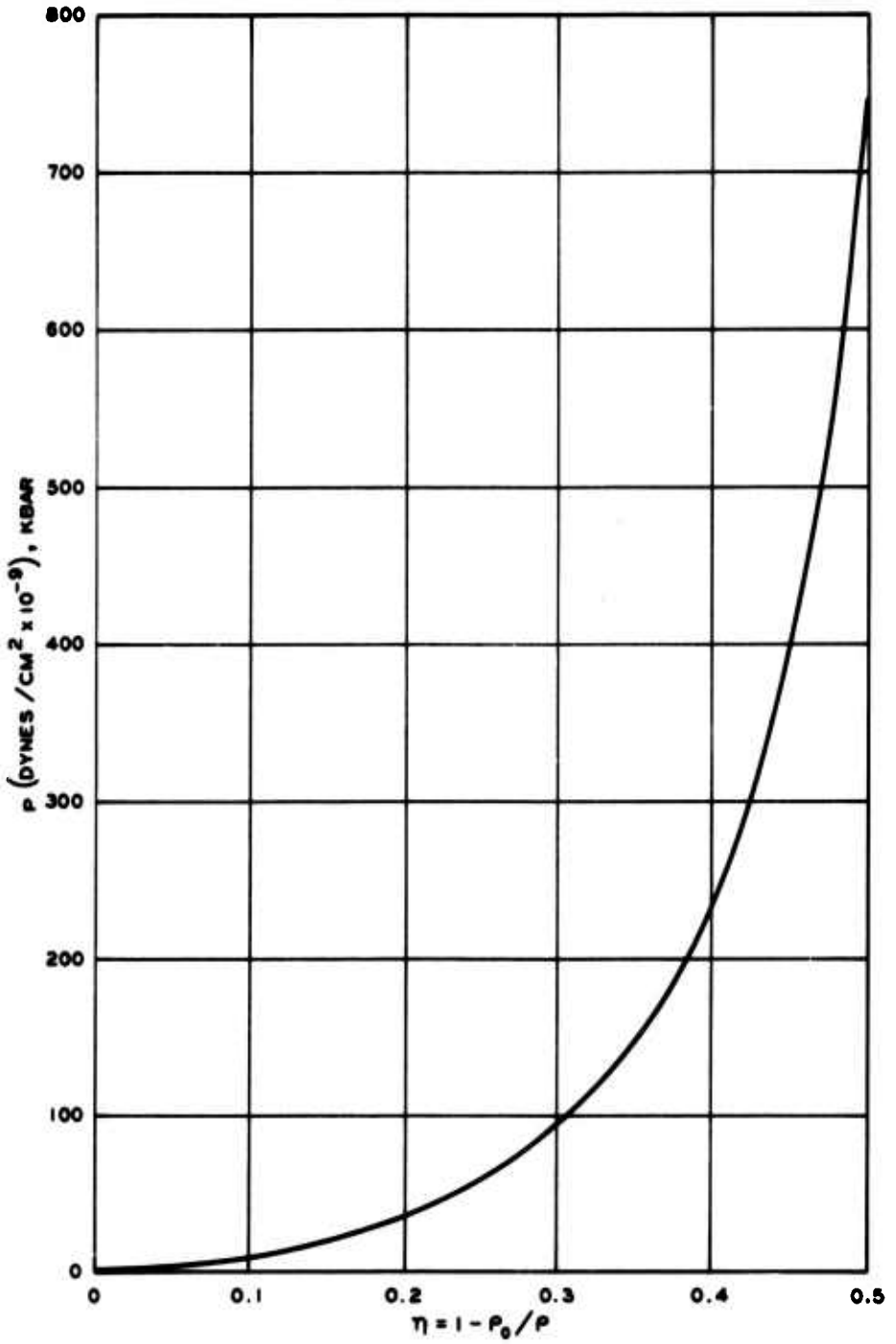

Figure 4.11 Plot of p versus η for welded tuff.

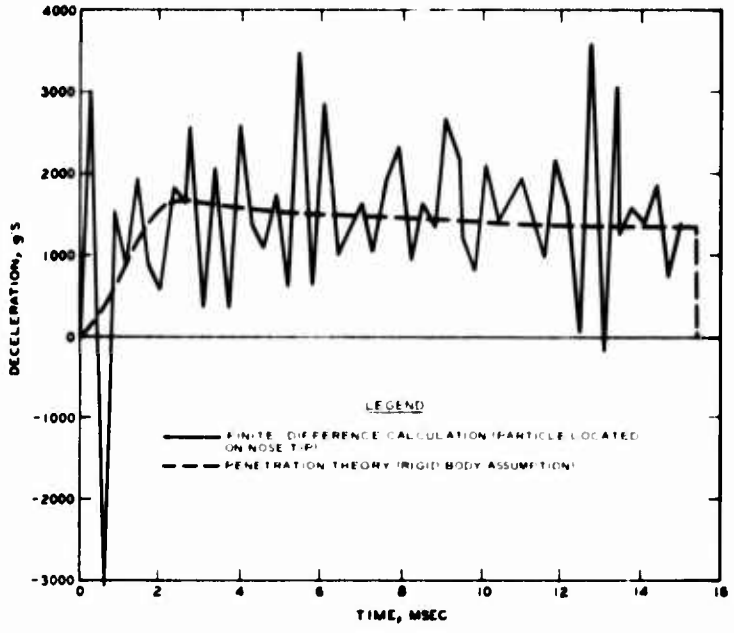

Figure 4.12 WES rigid body acceleration versus time prediction superimposed on the Sandia finite difference results for particle located on nose tip of projectile; tuff penetration.

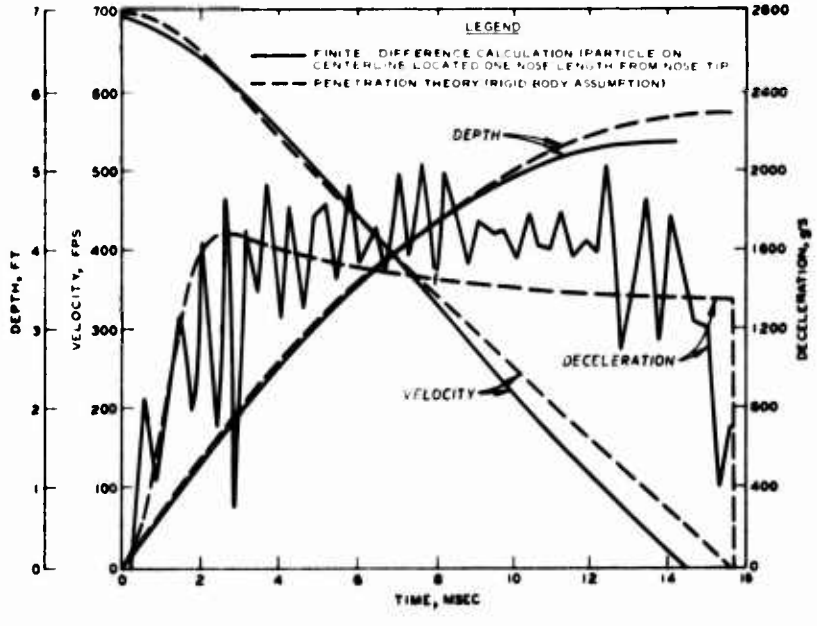

Figure 4.13 WES rigid body model time histories superimposed on the finite difference time histories for particle on centerline located one nose length from nose tip; tuff penetration.

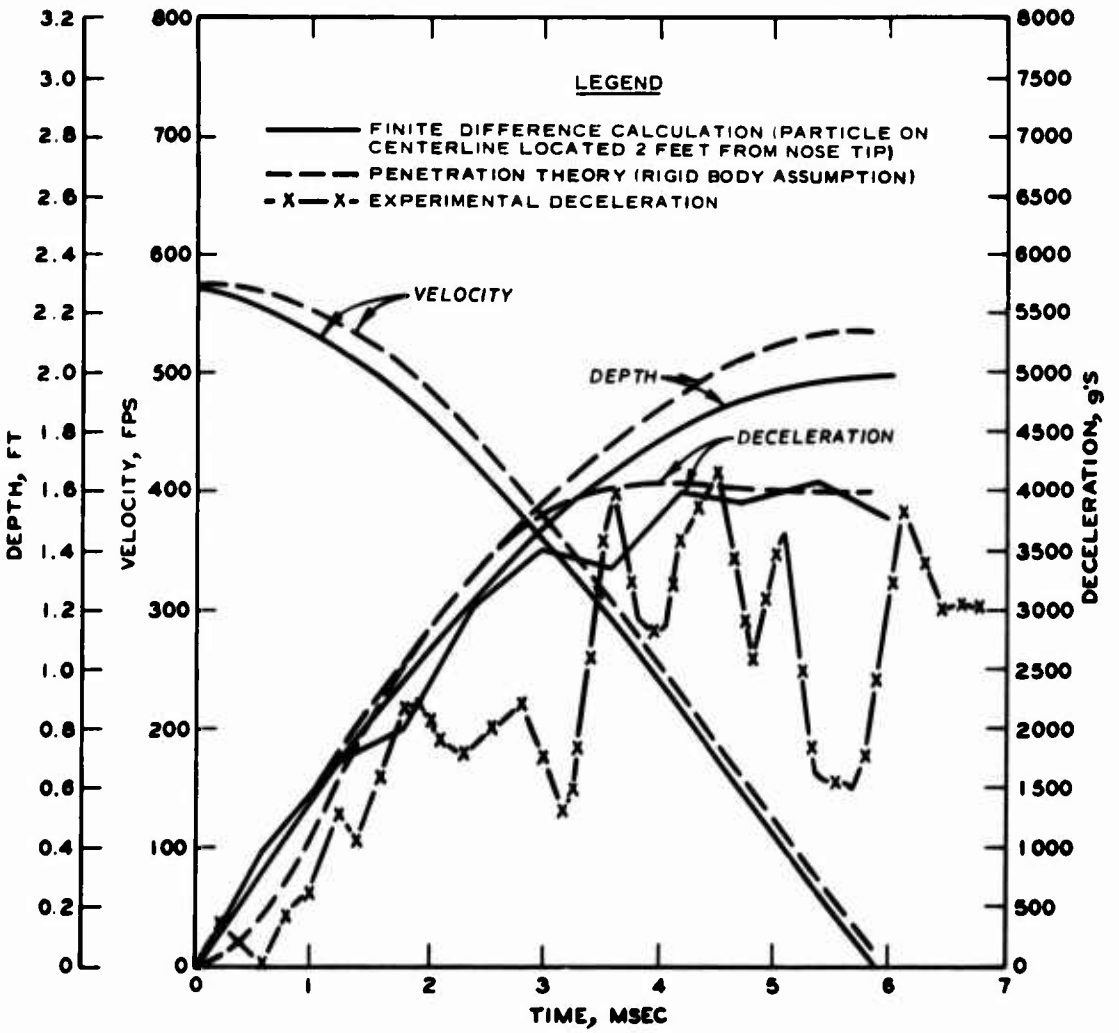

Figure 4.14 WES rigid body model time histories superimposed on the finite difference time histories for a particle on centerline located 2 feet from nose tip; limestone penetration.

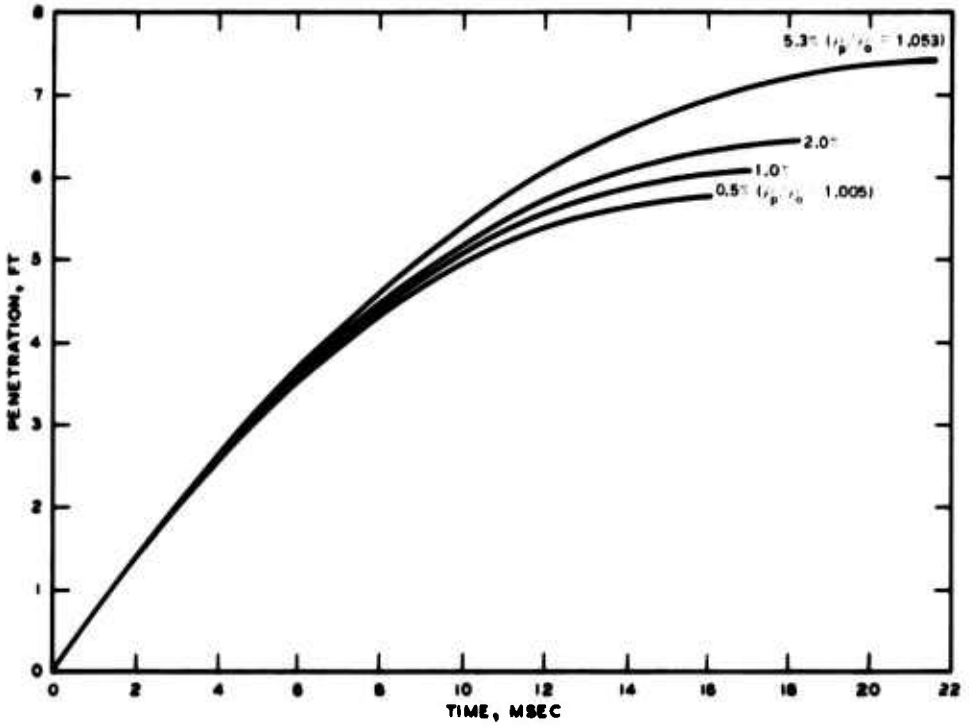

Figure 4.15 Constant locked plastic density model predictions for various compressibilities; tuff penetration.

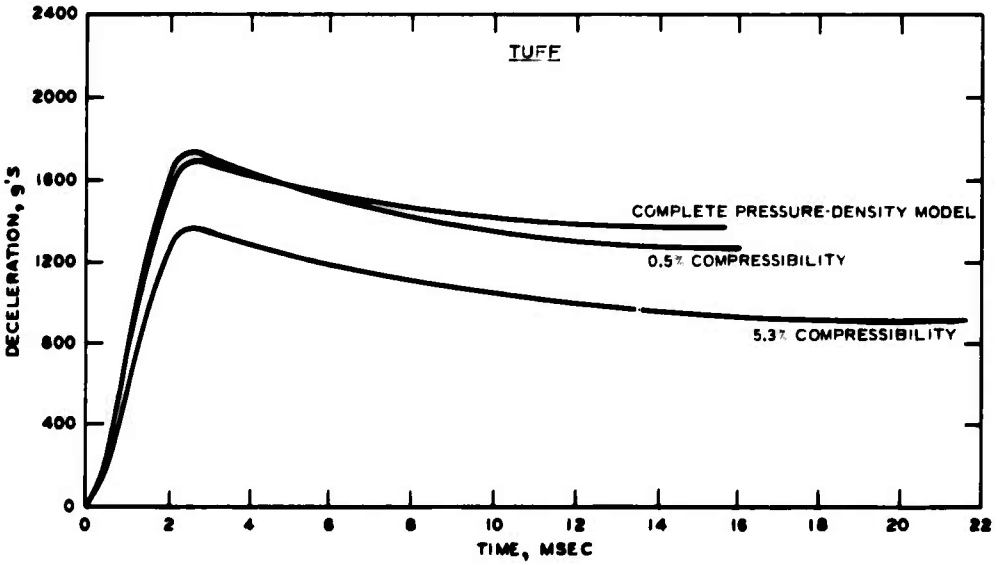

Figure 4.16 Comparison of complete target pressure-density model with two constant locked plastic density model predictions of deceleration versus time.

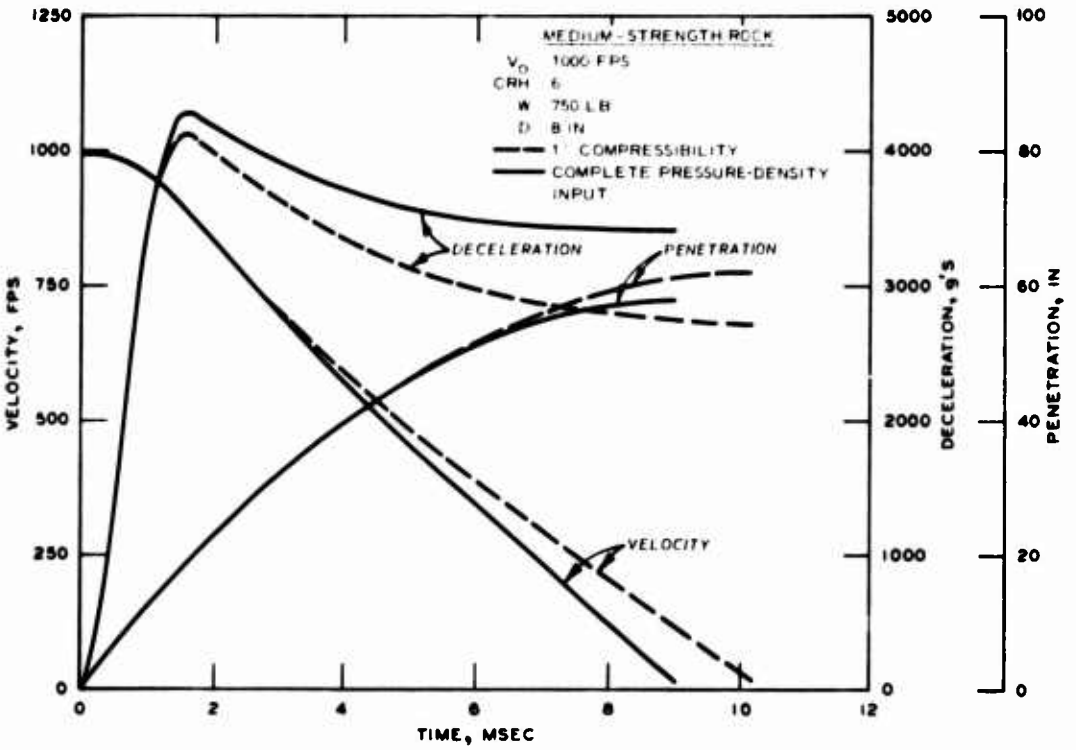

Figure 4.17 Comparison of penetration model time histories for 1 percent compressibility and the complete target Hugoniot.

CHAPTER 5

GENERAL ROCK PENETRATION PARAMETER STUDY

5.1 SYSTEMATICS OF PARAMETER STUDY

The rock properties used in the rock penetration parameter study to be discussed in this chapter were summarized in Table 3.3. In the remainder of this report, the three rock parameter groups will be indicated by L (low strength), M (medium strength), and H (high strength). Table 5.1 summarizes the ranges of projectile parameters to be considered. Obviously, it was unnecessary and impractical to consider all possible combinations of rock and projectile parameters; only those combinations of projectile weight and diameter which give values of W/A in the range of 10-15 psi are considered, as this is probably the reasonable range to be expected for EPW's. Table 5.2 summarizes some of the combinations considered.

The systematics followed during the general parameter study are outlined in Table 5.3. In each case, the final depth of penetration was calculated using the penetration model presented in Chapter 2 for initial velocities ranging from 1000 to 3000 fps in increments of 250 fps. It must be emphasized that the projectiles are considered as rigid bodies, and hence the range of velocities may not seem realistic, since it is known that structural failure of the projectile may occur at velocities considerably below 3000 fps and that the critical velocity for failure depends, of course, on target strength. However, as the state of the art in projectile design advances and as more exotic materials become available for use, the upper bound of survivable velocities for impact and penetration into rock may reasonably be expected to increase. The next three sections present the results of the parameter study, with a discussion of the results given in Section 5.5.

5.2 TIME HISTORIES

Since the penetration equation presented in Chapter 2 (Equation 2.1) is a differential equation, the model can be used to produce time

histories of penetration, velocity, and deceleration[1] for the projectiles as well as final depth of penetration. In order to illustrate the kinematics predicted by the model, typical complete time histories are presented for Cases IB1 and IIIB3 at an impact velocity of 2000 fps in Figures 5.1a and 5.2, respectively. Figure 5.1b compares the deceleration versus time plots for the three rock strengths of Cases IB1 through IB3.

5.3 PENETRATION VERSUS IMPACT VELOCITY PLOTS

Figures 5.3 through 5.14 are final depth of penetration versus impact velocity plots for Cases I through IV of Table 5.3; each figure contains plots for the three rock strength groups with other parameters held constant.

5.4 ADDITIONAL PARAMETER STUDY PLOTS

Using the data from Figures 5.3 through 5.14 and the results of other cases as required, further plots were made illustrating the effects of various parameters on predicted penetration. Figure 5.15 illustrates the effect of projectile diameter and hence sectional pressure W/A on the penetration versus impact velocity plot for medium-strength rock and a given CRH and W, i.e., W/A varies due only to a varying projectile diameter. The effect of CRH on penetration is shown in Figures 5.16a and 5.16b for low- and medium-strength rock, respectively, and for a given projectile W/A at three impact velocities. Figure 5.16c shows the effect of CRH on predicted penetration for the three rock types at a given impact velocity. Figures 5.17a through 5.17f all show the effect of W/A on predicted penetration for various combinations of impact velocity and rock type.

5.5 DISCUSSION OF RESULTS

5.5.1 Time Histories. The time histories in Figures 5.1 and 5.2

---

[1] The term deceleration is used to refer to a negative acceleration. Since the projectiles are treated as rigid bodies (i.e., no wave motions considered in the projectile) with the positive z-axis downward, all accelerations will be negative.

illustrate the kinematics of the penetration model using a constant value for the locked plastic density. Figure 5.1b illustrates the concept of increasing peak deceleration and decreasing duration of the penetration event with increasing rock strength such that the area under the deceleration versus time plots remains constant for a given impact velocity. It is important to realize that although the penetration predictions given by using the constant value for locked plastic density have been shown to agree closely with experimental results (see References 4, 6, 7, and 9 and also Chapter 4 of this report), the deceleration versus time predictions (rigid body) do not in many cases reproduce experimentally measured records. Deceleration versus time records from actual penetration tests generally do not exhibit the sharp acceleration peak followed by a rapid drop to a much lower value which is typical of the deceleration-time curves calculated by the penetration model using a constant ρ_p . Rather the experimental records show a rise to a peak (as the nose imbeds) followed by a much smaller decrease during the remainder of the penetration event. Indeed, the experimental records in many cases resemble a step pulse of magnitude equal to the average deceleration $\bar{A}$ during the event (determined from energy-work equality) of duration $\bar{t}$; this is shown as a dashed line in Figure 5.2, where

$$\bar{A} = \frac{V_o^2}{2gP} \text{ (g's)}$$
$$\bar{t} = \frac{2P}{V_o} \text{ (sec)} \qquad (5.1)$$

and V_o , g , and P are the impact velocity, acceleration of gravity, and maximum depth of penetration, respectively. In cases where the actual deceleration versus time history can be approximated by a step pulse, the peak and average decelerations may not differ by more than a factor of two (Reference 7). Deceleration versus time predictions were discussed in Chapter 4, where it was shown that using a realistic nonlinear hydrostat instead of a constant locked plastic density provides more realistic deceleration-time histories. However, since this

parameter study was conceived primarily to study the effects of independent variables on the maximum depth of penetration, and since P is not seriously changed by using a constant ρ_p instead of the actual hydrostat, the simple approach used in this study is adequate.

5.5.2 Penetration Versus Impact Velocity Plots. The first and perhaps most obvious comment regarding Figures 5.3-5.14 is that for a given velocity, penetration decreases with increasing target strength and modulus (maintaining E/Y = 350 constant). For all three target strengths, penetration increases with increasing velocity as expected, although the curves tend to flatten with increasing velocity. The curves for the three rock targets are seen not to be parallel for any of the cases considered, i.e., the numerical difference between the penetration into low-strength rock P_L and into medium-strength rock P_M does not remain constant with increasing velocity, and the same is true for the difference between the medium-strength P_M and high-strength P_H penetration versus velocity curves. Nor does the percentage decrease in penetration remain constant, but is seen to be a slowly decreasing function of velocity.

Figure 5.18 is a summary plot showing the percent decrease in penetration versus impact velocity for all the cases considered in this report (CRH range 2-10 and W/A range 10-15 psi). This figure is significant in that it illustrates qualitatively the effect of target strength on final depth of penetration predictions. Thus the relative, qualitative effect shown in Figure 5.18 is reasonable and may be more believable than the quantitative depth predictions. Three well-defined bands are identified, with the upper band representing the percent decrease in penetration between the low- and high-strength rocks $\left[(P_L - P_H)/P_L\right] \times 100$, the middle band representing the percent decrease in penetration between the low- and medium-strength rocks $\left[(P_L - P_M)/P_L\right] \times 100$, and the lower band representing the percent decrease in penetration between the medium- and high-strength rocks $\left[(P_M - P_H)/P_M\right] \times 100$. Figure 5.18 illustrates in summary fashion that the relative effect of increasing rock strength on decreasing the depth of penetration at a given velocity is not strongly sensitive to

variations in CRH or W/A . However, this is only a relative effect and does not imply that for a given rock strength, penetration depth is unaffected by CRH or W/A . As an example of the practical value of this information, it is only necessary to have an experimental penetration depth for one rock target for a given projectile in order to estimate penetration depths for that projectile into other rock targets.

5.5.3 Effects of W/A and CRH . Figures 5.15-5.17 examine in detail the effects of CRH and W/A on final depth of penetration for varying impact velocities and rock strengths. The effect of varying the projectile diameter for penetration into a medium-strength rock while maintaining W and CRH constant is illustrated in Figure 5.15; W/A varies from 10 to 17.7 psi. The increase in penetration over the velocity range considered is about 70 percent for a decrease in diameter from 8 to 6 inches. Thus, it is seen that for a W/A of 10 psi at an impact velocity of 1000 fps, increasing the W/A from 10 to 17.7 psi produces approximately the same increase in penetration as does increasing the impact velocity from 1000 to 1500 fps and maintaining W/A at 10 psi. Considerations such as this should be of great value in providing guidance for penetrator designers.

The effect of varying CRH is illustrated in Figure 5.16 for the three rock targets and at three impact velocities. CRH is seen to have little effect on depth of penetration for a given impact velocity and rock strength; the effect is greatest for high impact velocity and low rock strength. The curve for V_o = 1000 fps in Figures 5.16a and 5.16b is seen to be virtually flat over the range of CRH values (2-10). Likewise, the curve in Figure 5.16c for high-strength rock at V_o = 2000 fps shows virtually no change in penetration with variation in CRH . Thus, within the limits of parameters considered in this study, the penetration model indicates that the choice of projectile nose shape can be based solely on structural integrity and terradynamic stability considerations and not desired depth of penetration considerations. The slight coupling between CRH and impact velocity and rock strength does not appear to be significant.

Figure 5.17 demonstrates the effect of W/A on depth of penetration of a projectile with a given nose shape (CRH = 6) into the three rock targets at three impact velocities. For a given rock strength, sensitivity of depth of penetration to W/A is seen to increase as impact velocity increases, and for a given impact velocity, the sensitivity to W/A decreases as rock strength increases. It is interesting to note that the penetration versus W/A relations shown in Figures 5.17a through 5.17c for all three rock strengths appear to be linear and pass between the two predicted penetration depths for W/A = 12.7 psi (the two points for each rock strength are for projectiles with the same W/A but different weights and diameters). However, these points are separated from each other by less than 10 inches (3-20 percent) for all rock strengths and impact velocities; thus the effect is small enough to ignore in most cases.

The effect of projectile W/A on penetration varies somewhat with impact velocity and rock target being considered; however, for the range of impact velocities and rock strengths considered, the penetration model is relatively insensitive to variations in projectile CRH . For a medium-strength rock at impact velocities of 1000, 2000, and 3000 fps and CRH = 6 , the percent increase in penetration produced by a change in W/A from 10 to 15 psi is 43, 46, and 50 percent, respectively. Changing CRH from 2 to 10 for penetration into a medium-strength rock produces an average increase of only about 16 percent for the three impact velocities.

TABLE 5.1 PROJECTILE PARAMETER RANGES

Projectile Parameter	Range
Impact velocity	1000 to 3000 fps
W	250 to 1000 lb
D	5 to 10 in
W/A	10 to 15 psi
Nose caliber (CRH)	2 to 10

TABLE 5.2 W/A COMBINATIONS

W/A No.	W, lb	D, in	Area in^2	W/A psi
1	250	5	14.64	12.73
2	500	7.5	44.18	11.32
3	500	7	38.48	12.99
4	500	8	50.27	9.95
5	750	9	64.51	11.63
6	750	8	50.27	14.92
7	1000	10	78.54	12.73

TABLE 5.3 PARAMETER STUDY SYSTEMATICS

Case Identification No.	W/A No.	CRH	Rock Type
IA1	6	2	L
2			M
3			H
IB1	6	6	L
2			M
3			H
IC1	6	10	L
2			M
3			H
IIA1	7	2	L
2			M
3			H
IIB1	7	6	L
2			M
3			H
IIC1	7	10	L
2			M
3			H
IIIA1	1	2	L
2			M
3			H
IIIB1	1	6	L
2			M
3			H
IIIC1	1	10	L
2			M
3			H
IVA1	2	2	L
2			M
3			H
IVB1	2	6	L
2			M
3			H
IVC1	2	10	L
2			M
3			H
VA1	3	6	M
2	4		M
3	5		M
4	D = 6.5 in, W = 500 lb		L
5	D = 6 in, W = 500 lb		L
VIA1	2	4	M
2		8	M
3		4	L
4		8	L

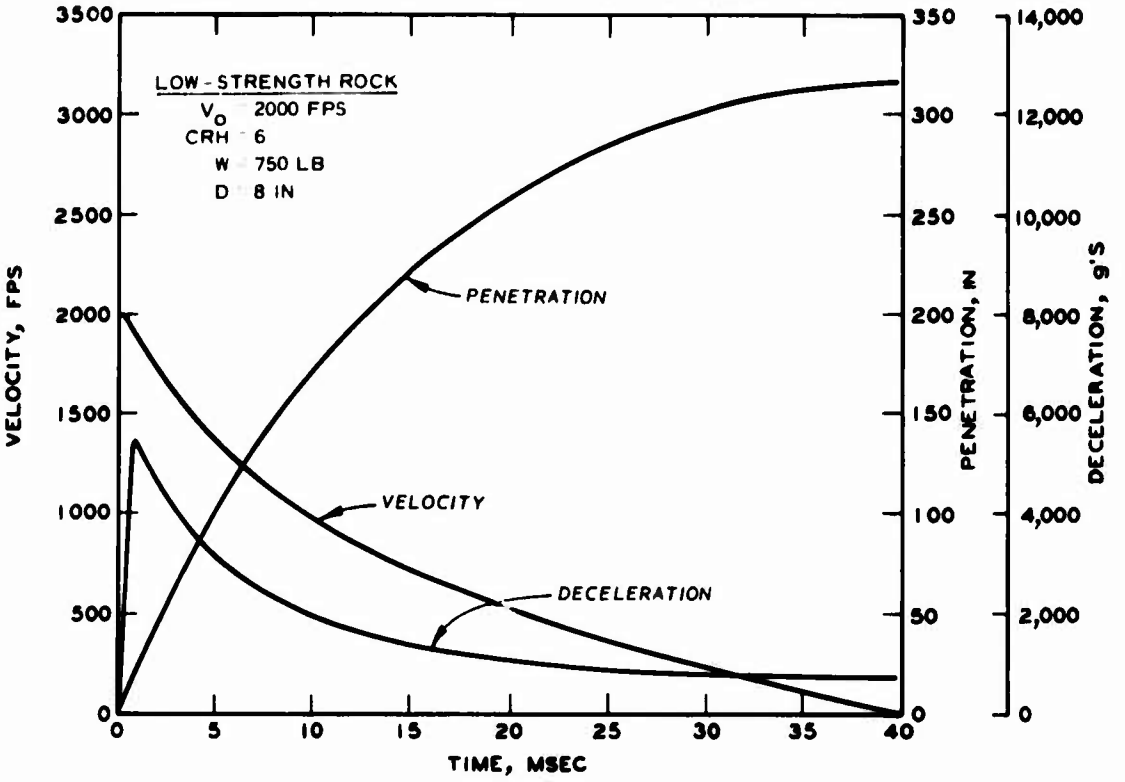

a. Case IB1.

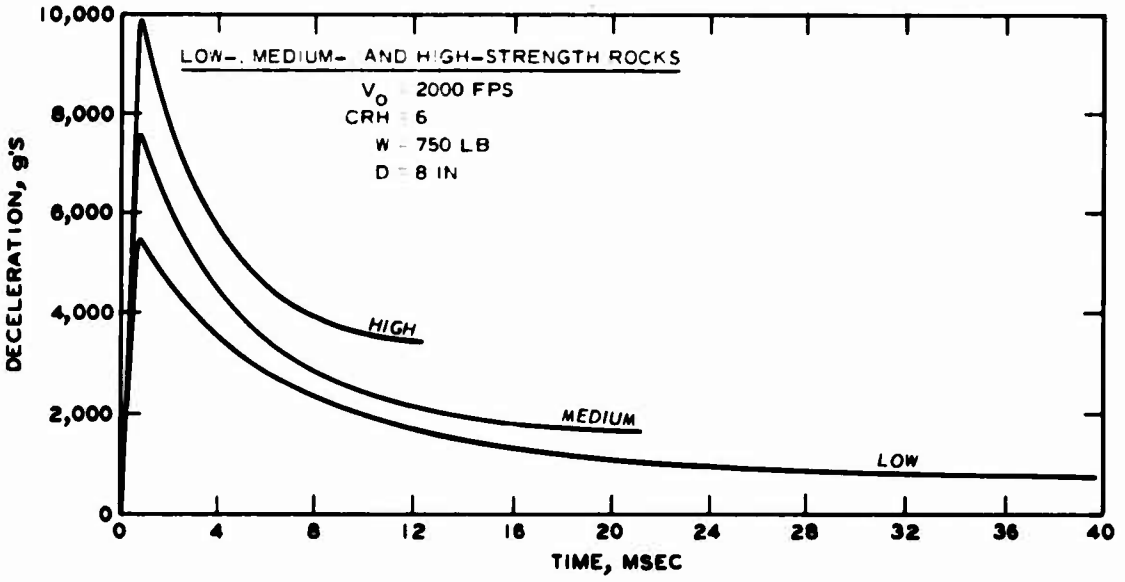

b. Case IB.

Figure 5.1 Time histories for Cases IB1 and IB.

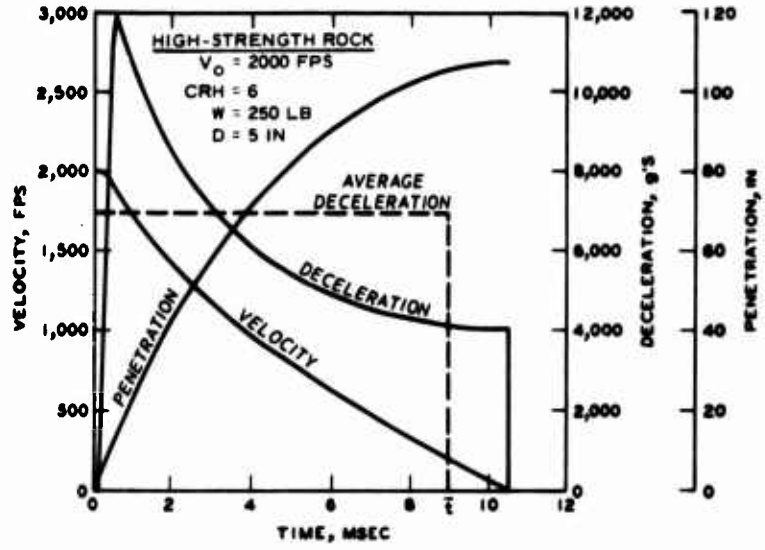

Figure 5.2 Time histories for Case IIIB3.

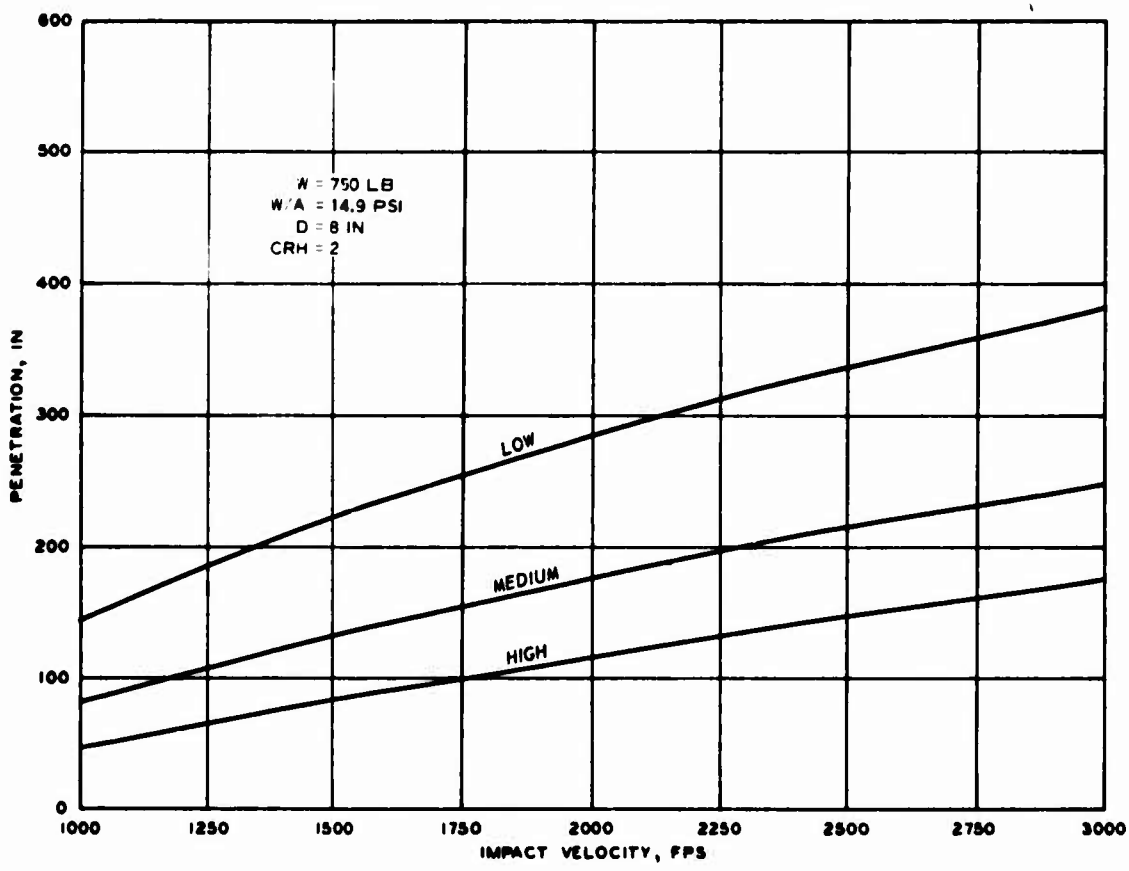

Figure 5.3 Case IA.

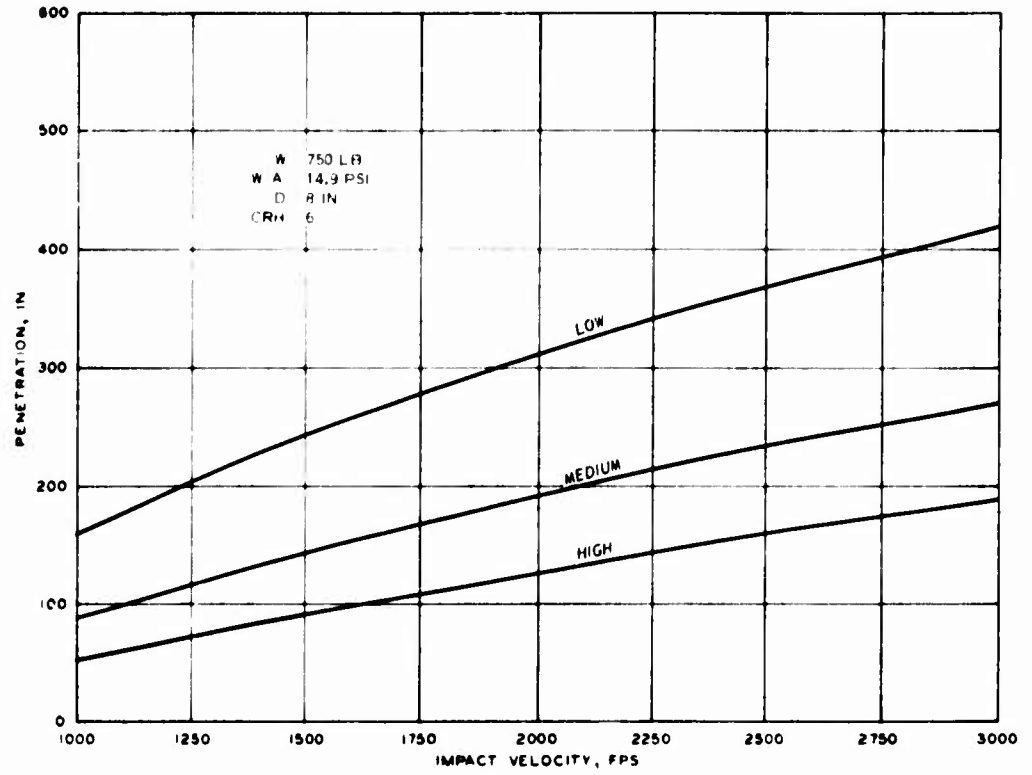

Figure 5.4 Case IB.

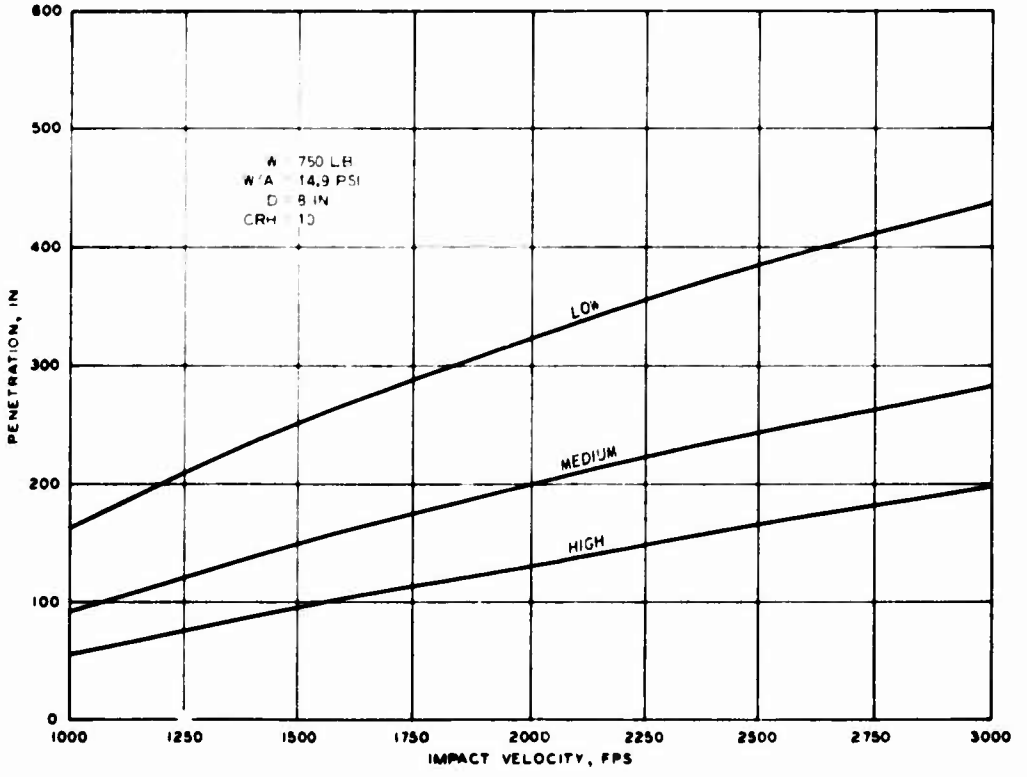

Figure 5.5 Case IC.

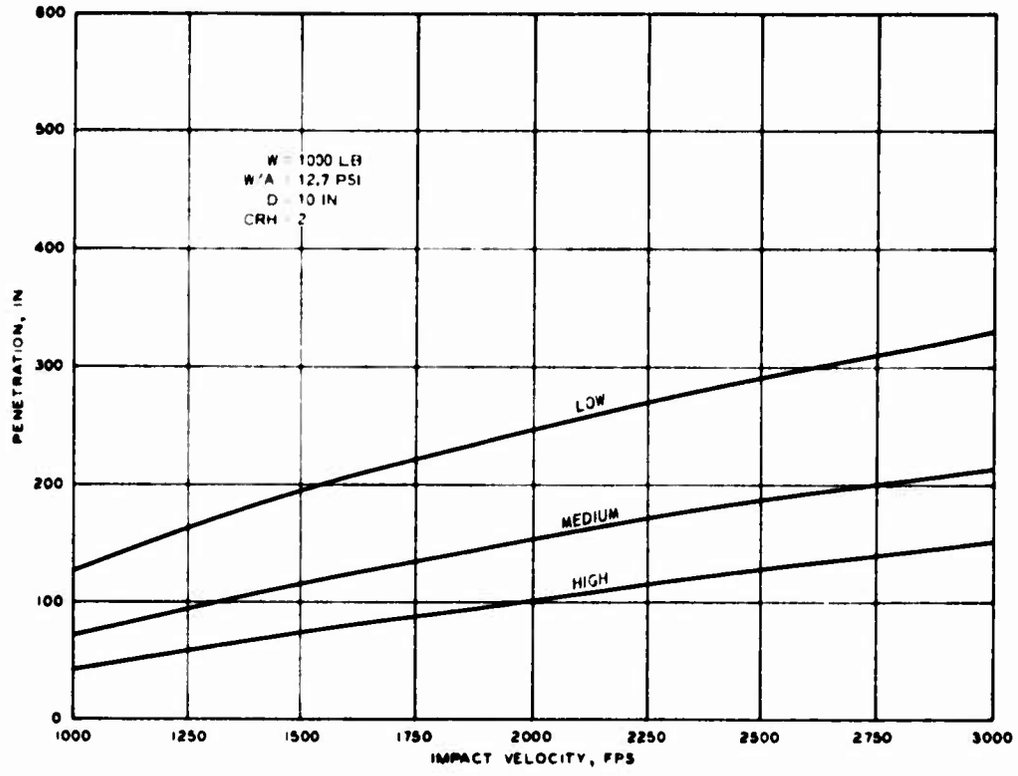

Figure 5.6 Case IIA.

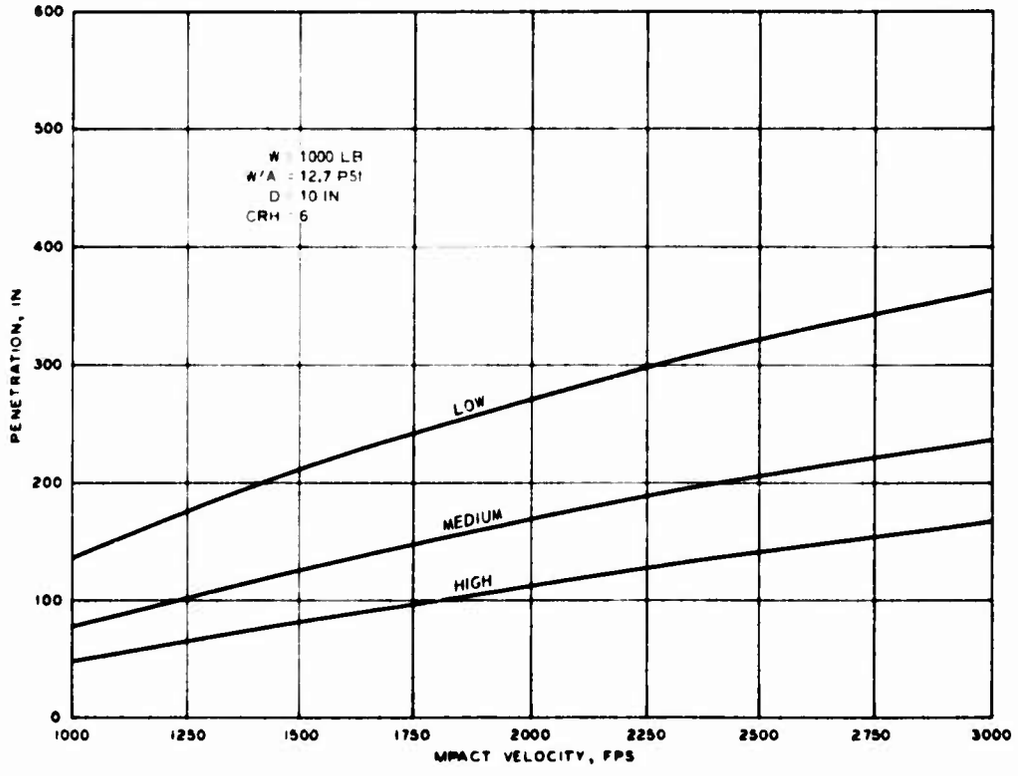

Figure 5.7 Case IIB.

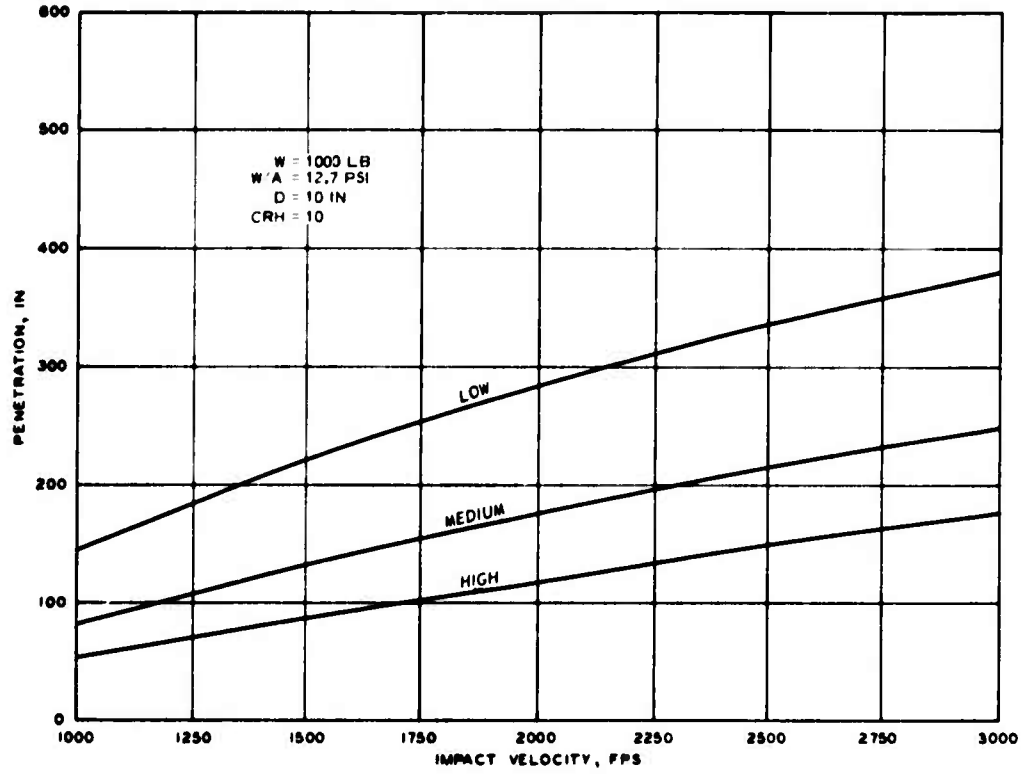

Figure 5.8 Case IIC.

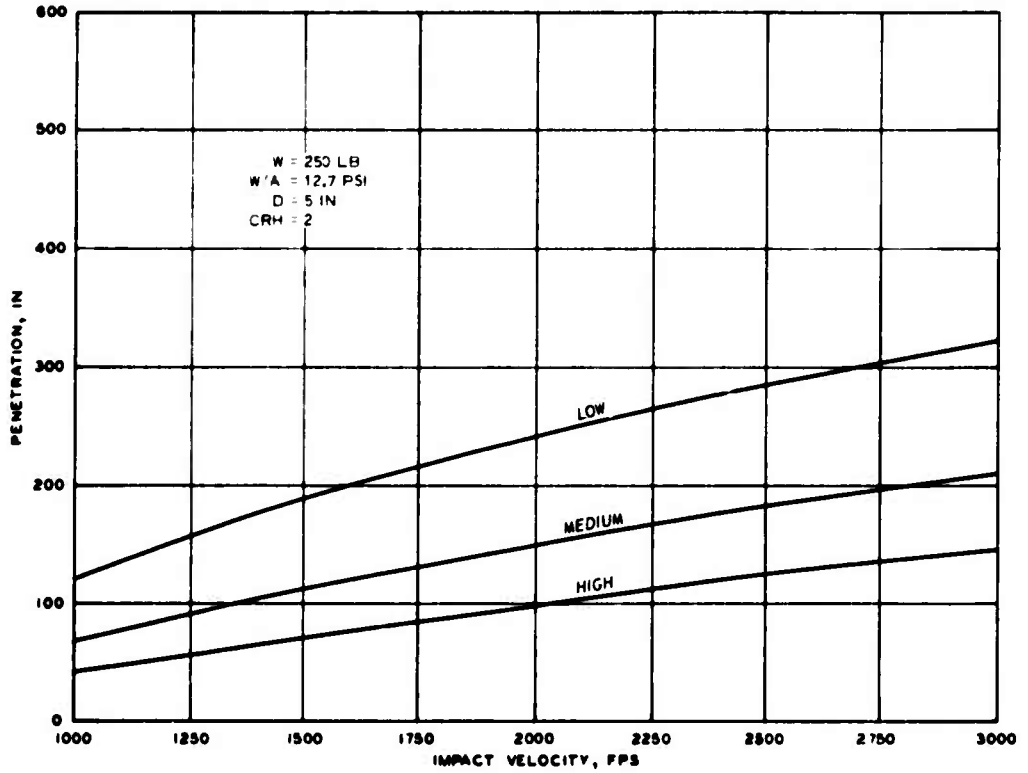

Figure 5.9 Case IIIA.

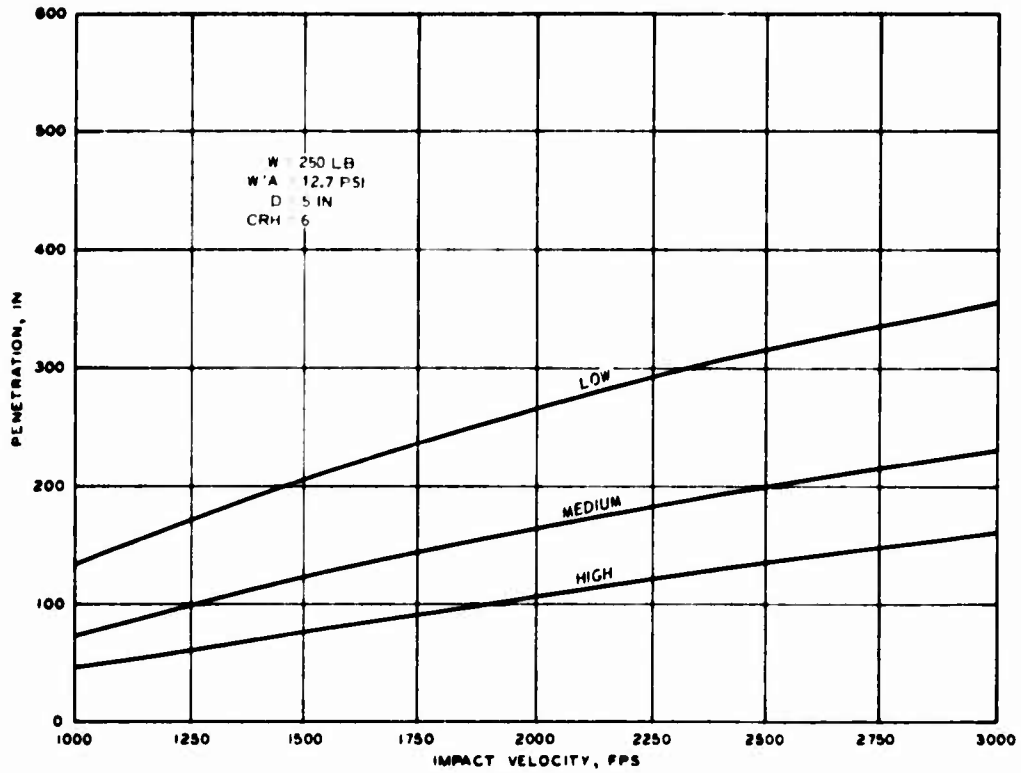

Figure 5.10 Case IIIB.

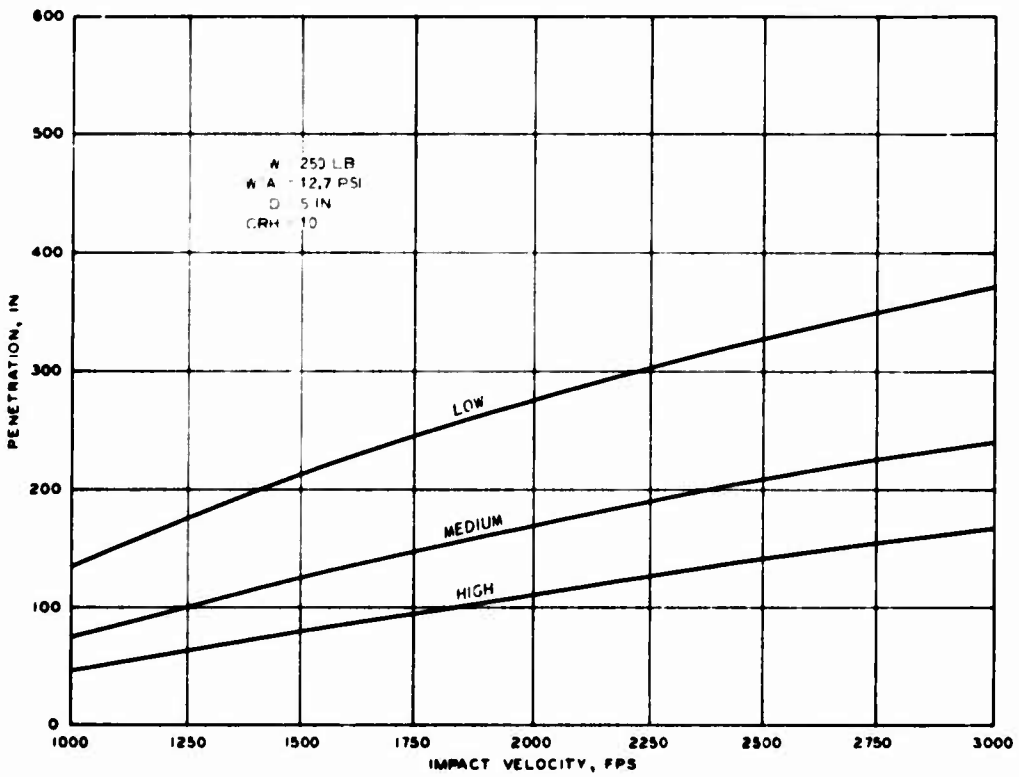

Figure 5.11 Case IIIC.

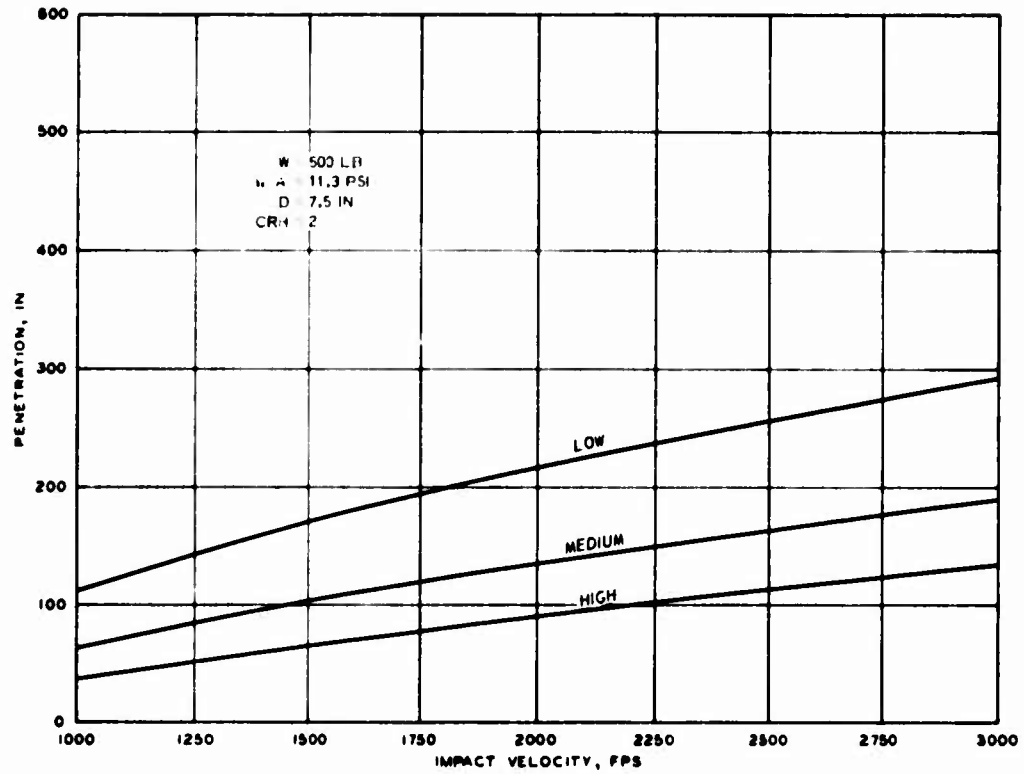

Figure 5.12 Case IVA.

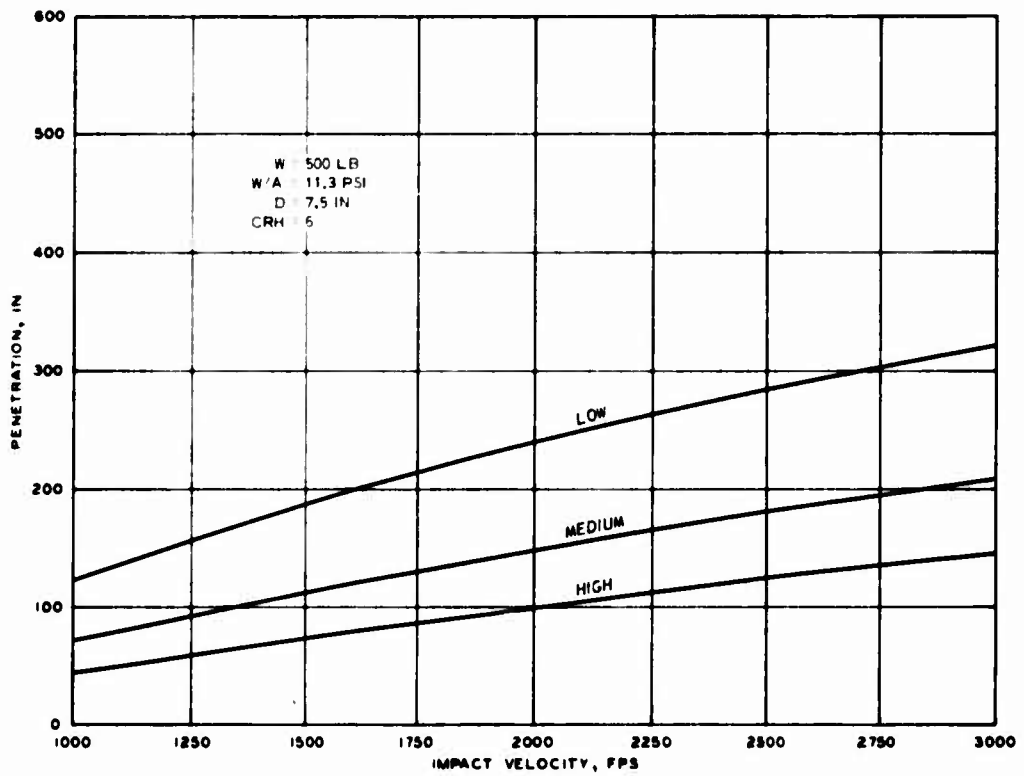

Figure 5.13 Case IVB.

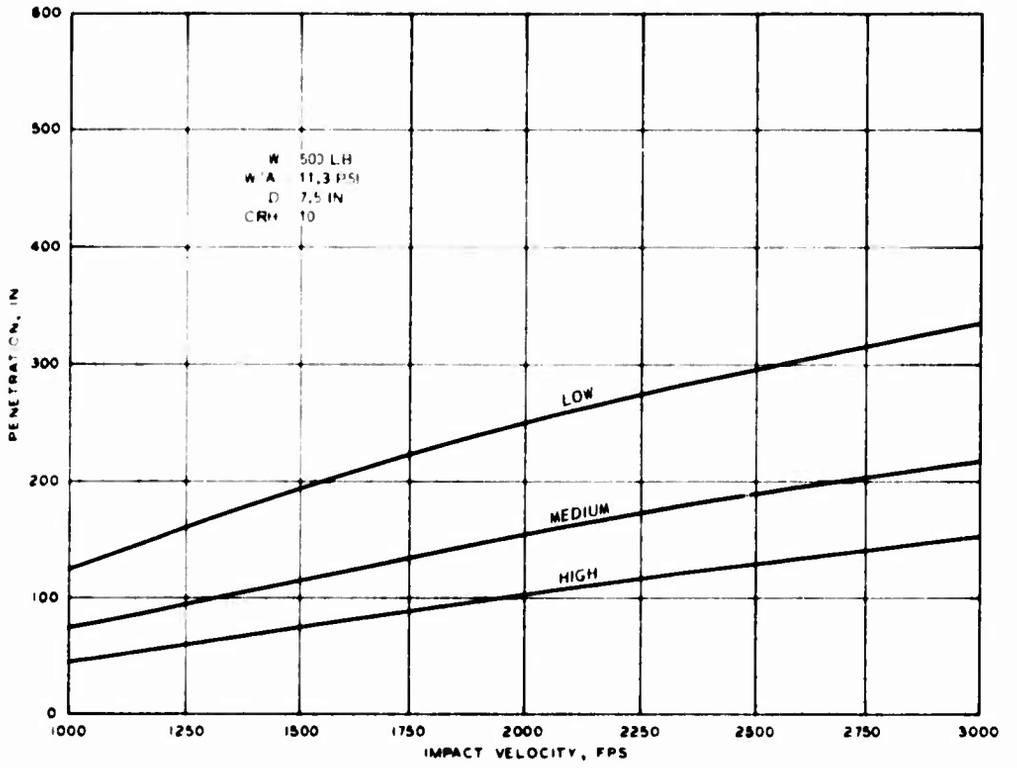

Figure 5.14 Case IVC.

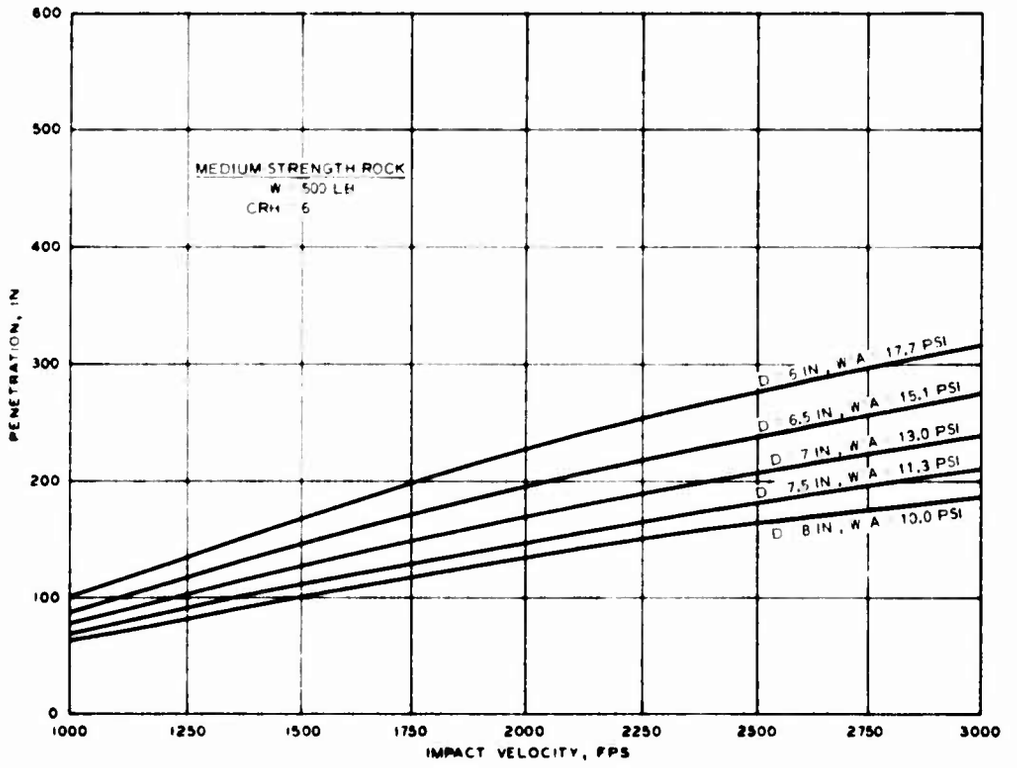

Figure 5.15 Effect of W/A on penetration versus impact velocity plots for given rock type, CRH , and weight.

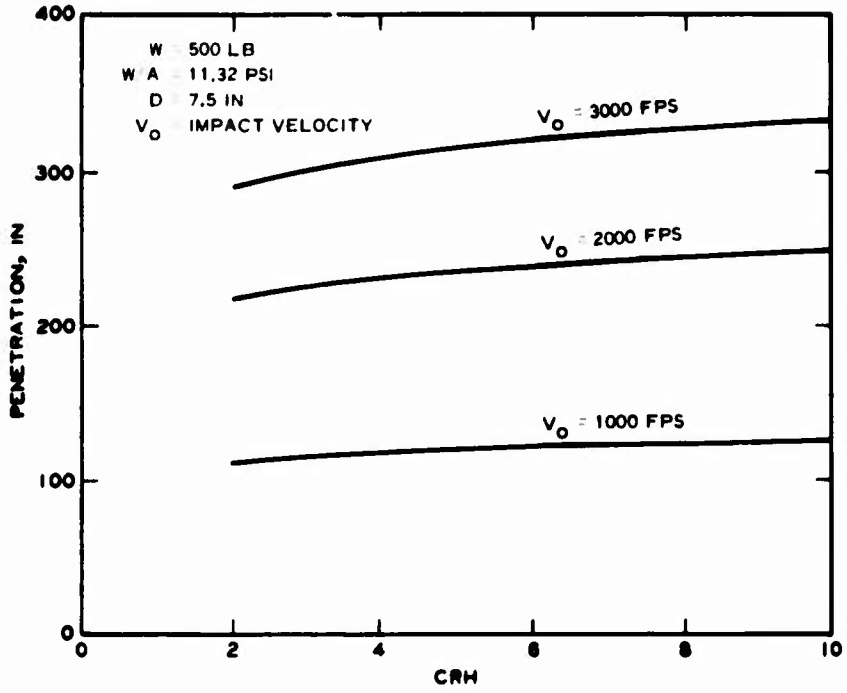

a. Low-strength rock: V_o = 1000, 2000, and 3000 fps.

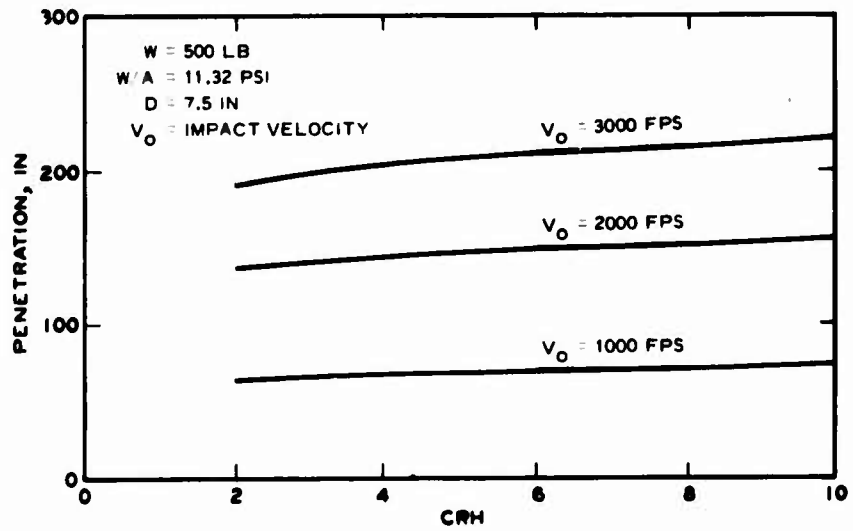

b. Medium-strength rock; V_o = 1000, 2000, and 3000 fps.

Figure 5.16 Effect of CRH on predicted penetration (sheet 1 of 2).

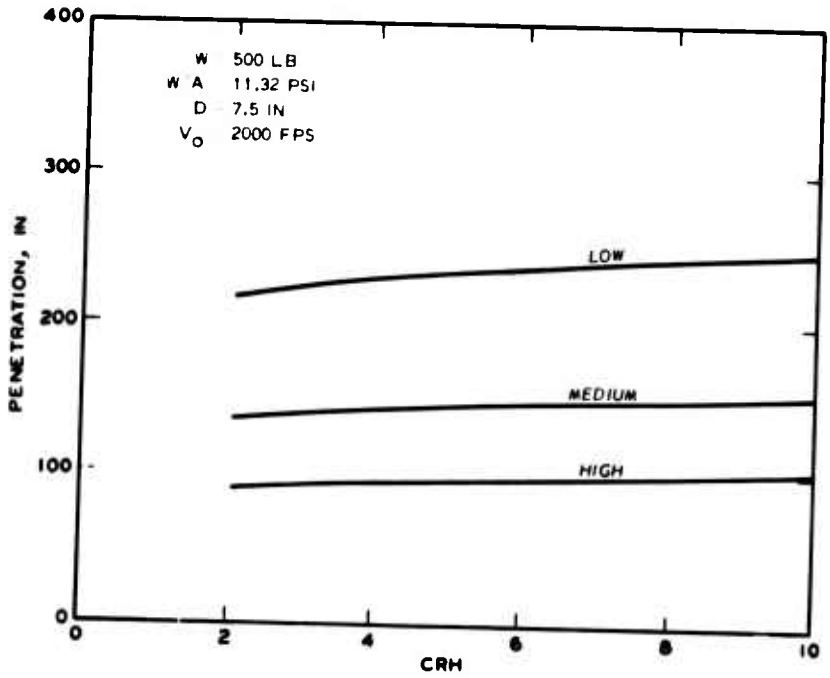

c. Low-, medium-, and high-strength rocks; V_o = 2000 fps.

Figure 5.16 (sheet 2 of 2).

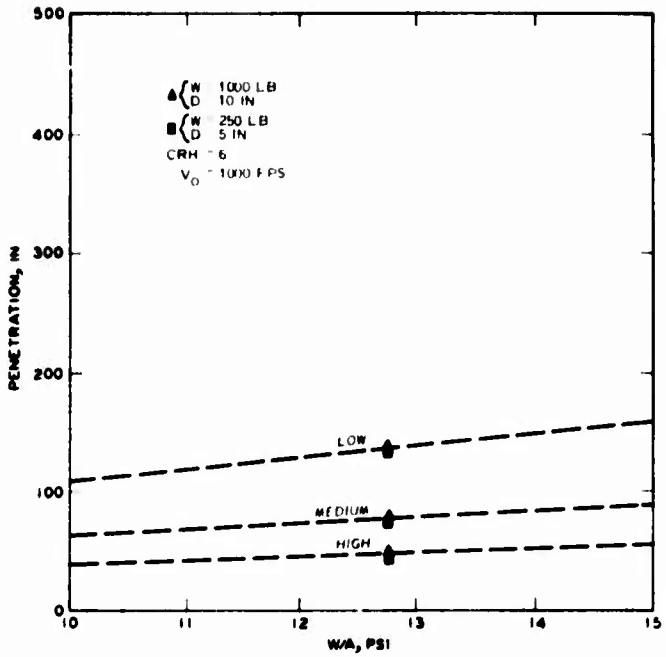

a. Low-, medium-, and high-strength rocks; V_o = 1000 fps.

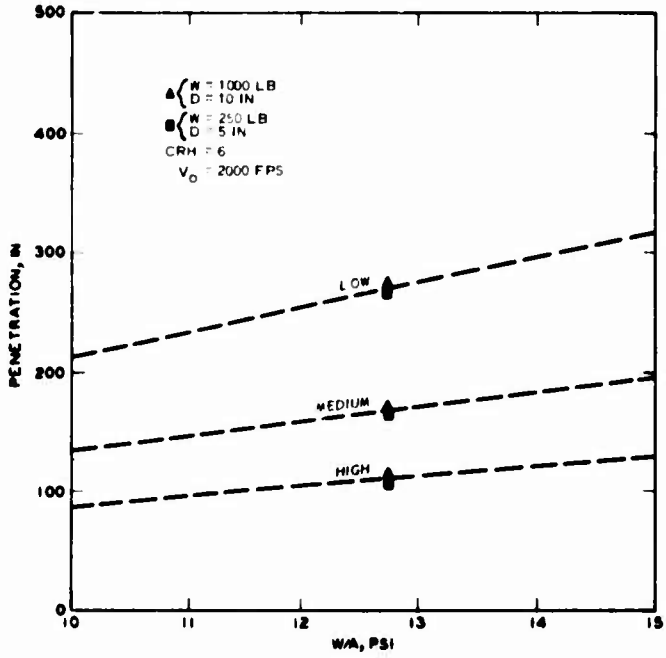

b. Low-, medium-, and high-strength rocks; V_o = 1000 fps.

Figure 5.17 Effect of W/A on predicted penetration (sheet 1 of 3).

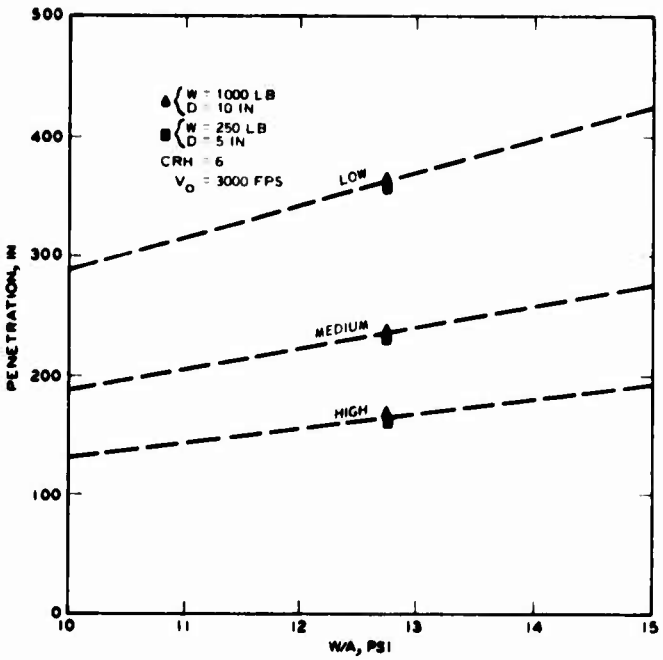

c. Low-, medium-, and high-strength rocks; V_o = 3000 fps.

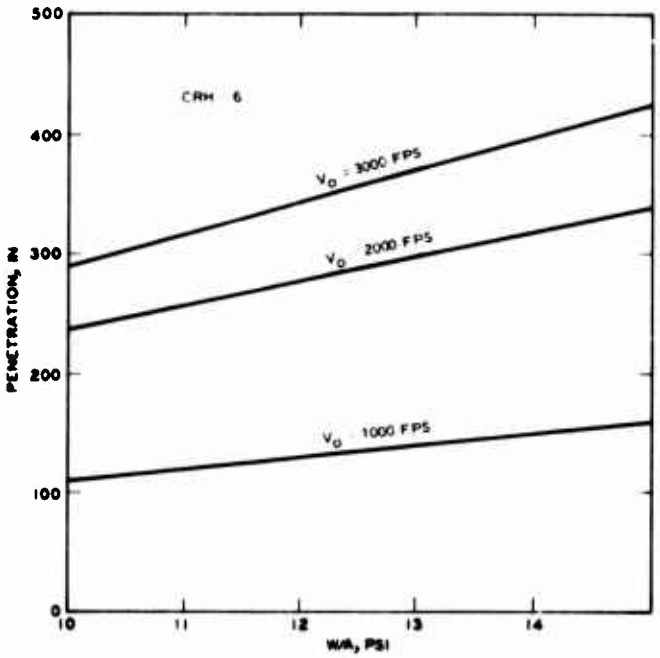

d. Low-strength rock; V_o = 1000, 2000, and 3000 fps.

Figure 5.17 (sheet 2 of 3).

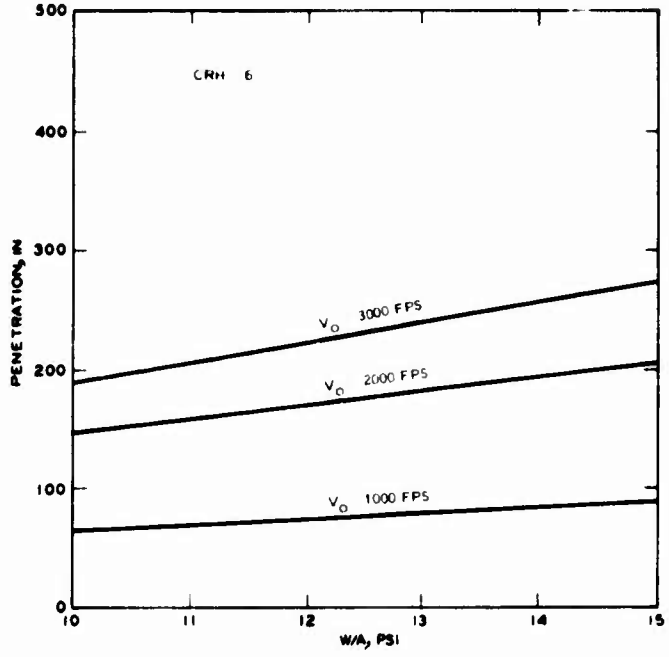

e. Medium-strength rock; V_o = 1000, 2000, and 3000 fps.

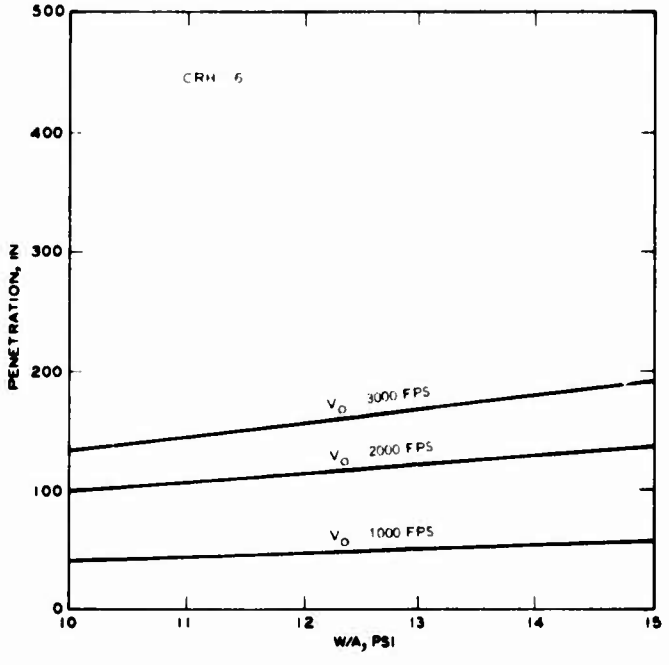

f. High-strength rock; V_o = 1000, 2000, and 3000 fps.

Figure 5.17 (sheet 3 of 3).

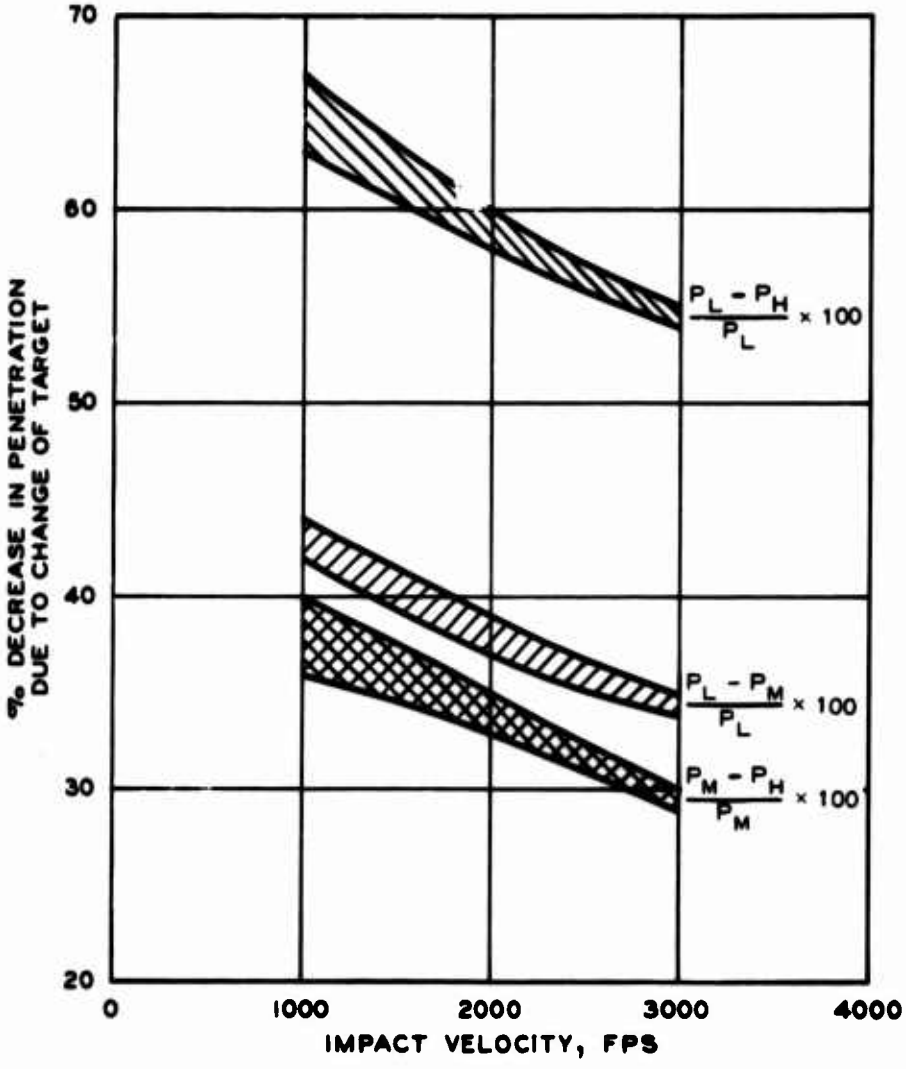

Figure 5.18 Percent decrease in penetration versus impact velocity for all cases considered in this report between the low- and high-strength rock, between the low- and medium-strength rock, and between the medium- and high-strength rock.

CHAPTER 6

SUMMARY AND CONCLUSIONS

Projectile penetration into earth media is an extremely complicated phenomenon, and the state of the art in penetration theory is such that the problem cannot be solved in all its complexity. Thompson and Bryant (Reference 39) discuss the philosophical and physical formulation of the general penetration problem, and Chapter 3 of this report presents an overview of the problems involved in characterizing rock as the target medium for penetration. Based on a theoretical penetration model discussed in Chapter 2, which requires only target material properties that can be determined from standard laboratory tests, a study of projectile penetration into rock is presented in Chapters 4 and 5.

Three rock targets are considered, with material properties chosen to be representative of general classes of rocks characterized as being low-, medium-, and high-strength. The three rock targets are characterized by only four parameters: (1) initial density, (2) locked plastic density, which is based on estimate of compressibility, (3) modulus, and (4) strength. For target sites about which only a minimum amount of information is available, it is proposed that reliable penetration depth estimates can be obtained if it is possible (on the basis of laboratory examination of cores, drillers' logs, air-photo interpretation, or geologic maps and literature) to classify the intact and in situ material according to established engineering rock classifications (Tables 3.1 and 3.2 and Figures 3.1 through 3.3, for example).

The modified Ross-Hanagud penetration theory (Chapter 2) with the WES "recipe" for selecting material properties for rock (Chapter 3) adequately predicts depth of projectile penetration into rock (Chapter 4). When the model is extended to include realistic pressure-density relations for the targets, it also appears to adequately simulate rigid body deceleration-time histories for relatively low impact velocities and low- to medium-strength rocks (Chapter 4). Therefore, the conclusions derived from parametric studies using this model (Chapters 4 and 5) have relevance for the real world problem of rock penetration.

Using the general rock properties proposed in Chapter 3, the results of five actual field penetration tests into rock (targets classified according to Tables 3.1 and 3.2) were compared with the penetration model predictions in Table 4.1, and agreement is shown to be good. A parameter study of one of the field tests resulted in the following conclusions:

1. For a given value of modulus, variation of strength within the bounds of the classification categories (low-strength "D" in this case) can produce variations in penetration for a given velocity of the order of 30-40 percent decrease in penetration for a factor of two increase in strength.

2. For a given strength, variation in modulus by a factor of 20 produces a negligible change in penetration over the velocity range 500-1900 fps.

3. For realistic values of ρ_o and ρ_p, variation of 10 percent in the estimate of ρ_p/ρ_o for the target will produce a change in the penetration depth prediction of the order of 10 percent.

Also, in Chapter 4 the penetration model is extended to treat the complete target pressure-density relation, and good agreement is obtained with motion-time histories from two finite difference code calculations of rock penetration. For these two cases, involving low- and medium-strength rock and rather low impact velocities (570 and 695 fps), inclusion of the detailed target pressure-density relation in the theoretical penetration model produces not only good penetration depth predictions but also deceleration versus time histories in general qualitative and quantitative agreement with experimental results. If this trend continues when compared with future test data from higher impact velocity field events, this will prove to be a significant advancement in the state of the art of rock penetration predictions. Also, if time histories from the penetration model are improved by use of the complete pressure-density curves, better results can be anticipated for predicting penetration into layered targets.

On the basis of the parameter study of Chapter 5, the following comments and conclusions can be made:

1. Peak deceleration increases with increasing rock strength.

2. Event duration decreases with increasing rock strength.

3. Final penetration depth decreases with increasing rock strength at a given velocity.

4. For a given rock target strength, penetration increases with increasing impact velocity, although the curves tend to flatten with increasing velocity.

5. For a given velocity and rock strength, penetration increases only slightly with projectile CRH , and the effect is greatest for higher velocities and low rock strengths. Thus, the theory suggests that for rock penetration, projectile nose shape (for ogives) can be based solely on consideration of structural integrity and stability, and not desired depth of penetration considerations.

6. The effect of sectional pressure W/A on penetration, over the range considered, is more significant than CRH .

a. Penetration increases with increasing W/A .

b. As with CRH , the effect is more significant for higher velocities and low rock strengths.

c. The information contained in Figures 5.15 and 5.17 should be of value to designers in determining practicality of achieving increased penetration depths by increased impact velocity and/or W/A .

Further work is needed in the following areas and is planned for future study under this project.

1. Effect of in situ rock condition (RQD , for example) on material properties for input to the penetration model.

2. Comparison of penetration model time histories with finite difference calculations and new experimental results of penetration into rock as they become available.

3. Comparison of constant plastic density calculations with complete hydrostat calculations of penetration into rock in order to develop better methods of estimating compressibilities in cases where the hydrostat is not known.

4. Oblique impact and consideration of angle of attack.

5. Inclusion of projectile material properties in the penetration model, if possible without greatly complicating the model.

REFERENCES

1. R. H. McNeill; "Rapid Penetration of Terrestrial Materials"; Proceedings, Conference on Rapid Penetration of Terrestrial Materials, J. L. Colp, Editor, February 1972; Texas A&M University, College Station, Texas.

2. W. J. Patterson; "Projectile Penetration of In Situ Rock"; SLA-73-0831, November 1973; Sandia Laboratories, Albuquerque, New Mexico.

3. Classified Reference.[1]

4. B. Rohani; "Fragment and Projectile Penetration Resistance of Soils; High-Velocity Fragment Penetration into Laboratory-Prepared Soil Targets"; Miscellaneous Paper S-71-12, Report 2, June 1973; U. S. Army Engineer Waterways Experiment Station, CE, Vicksburg, Mississippi.

5. J. N. Goodier; "On the Mechanics of Indentations and Cratering in Solid Targets of Strain-Hardening Metal by Impact of Hard and Soft Spheres"; Technical Report 002-64, July 1964; Stanford Research Institute, Poulter Laboratories, Menlo Park, California.

6. B. Ross and S. Hanagud; "Penetration Studies of Ice with Application to Arctic and Subarctic Warfare"; Project 7000-452, Final Report, September 1969; Stanford Research Institute, Menlo Park, California; Prepared under Contract No. 0014-64-A-0243, NR 274-008 for Submarine Arctic Warfare and Scientific Program, Naval Ordnance Laboratory, Silver Spring, Maryland, and Office of Naval Research, Washington, D. C.

7. B. Rohani; "Penetration Performance of Terminal Delivery Vehicle T-98WA into Soft and Frozen Ground; Analyses Based on Both Field Test Results and Theoretical Calculations"; Letter Report to Project Manager, Remotely Monitored Battlefield Sensor System, Army Materiel Command, Fort Monmouth, New Jersey, November 1973; U. S. Army Engineer Waterways Experiment Station, CE, Vicksburg, Mississippi.

8. B. Rohani; "Theoretical Study of Impact and Penetration of a Remotely Emplaced Antitank Mine Projectile into Earth Materials"; Miscellaneous Paper S-73-58, June 1973; U. S. Army Engineer Waterways Experiment Station, CE, Vicksburg, Mississippi.

9. B. Rohani, P. F. Hadala, and J. G. Jackson, Jr.; "Penetration of SAP and AP Bombs into a Concrete Target"; Letter Report to Defense Nuclear Agency, Subtask SB211, Work Unit 04, January 1974; U. S. Army Engineer Waterways Experiment Station, CE, Vicksburg, Mississippi.

10. B. Ross, S. Hanagud, and G. Sidhu; "Penetration Studies of Ice with Application to Arctic and Subarctic Warfare"; NWRC 7000-452-5, Final Report--Phase IV, April 1971; Stanford Research Institute, Menlo Park, California; Prepared for Submarine Arctic Warfare and Scientific

---

[1] Bibliographical material for the classified references(s) will be furnished to qualified agencies upon request.

Program, Naval Ordnance Laboratory, and Office of Naval Research.

11. G. B. Baecher; "The Size Effect in Brittle Fracture"; MS Thesis, June 1970; Massachusetts Institute of Technology, Department of Civil Engineering, Cambridge, Massachusetts.

12. M. M. Singh and P. J. Huck; "Large Scale Triaxial Tests on Rock"; Proceedings, Fourteenth Symposium on Rock Mechanics, H. R. Hardy, Jr., and R. Stefanko, Editors, June 1972, Pages 35-60; American Society of Civil Engineers, Ann Arbor, Michigan.

13. F. E. Heuze; "Sources of Errors in Rock Mechanics Field Measurements, and Related Solutions"; International Journal of Rock Mechanics and Mineral Science, 1971, Vol. 8, Pages 297-310.

14. H. H. Einstein, R. W. Bruhn, and R. C. Hirschfeld; "Mechanics of Jointed Rock"; Publication No. 268, August 1970; Department of Civil Engineering Soil Mechanics, Massachusetts Institute of Technology, Cambridge, Massachusetts.

15. J. S. Rosenblad; "Geomechanical Model Study of the Failure Modes of Jointed Rock Masses"; Technical Report MRD 1-71, January 1971; U. S. Army Engineer Division, Missouri River, St. Louis, Missouri.

16. D. R. Coates; "Classification of Rocks for Rock Mechanics"; International Journal of Rock Mechanics and Mineral Science, 1964, Vol. 1, No. 3, Page 421.

17. D. U. Deere and R. P. Miller; "Engineering Classification and Index Properties for Intact Rock"; Technical Report No. AFWL-TR-65-116, December 1966; Air Force Weapons Laboratory, Albuquerque, New Mexico.

18. D. U. Deere, A. H. Merritt, and R. F. Coon; "Engineering Classification of In-Situ Rock"; Technical Report No. AFWL-TR-67-144, January 1969; Air Force Weapons Laboratory, Albuquerque, New Mexico.

19. R. L. Geyer and J. I. Myung; "The 3-D Velocity Log; A Tool for In-Situ Determination of the Elastic Moduli of Rocks"; Proceedings, Twelfth Annual Symposium on Rock Mechanics, G. B. Clark, Editor, November 1970, Pages 71-107; University of Missouri, Rolla, Missouri.

20. D. U. Deere and others; "Design of Surface and Near-Surface Construction in Rock"; Proceedings, Eighth Symposium on Rock Mechanics, 1967, Pages 237-302; University of Minnesota, Minneapolis, Minnesota.

21. J. M. Duncan and R. E. Goodman; "Finite Element Analysis of Slopes in Jointed Rock"; Contract Report S-68-3, February 1968; U. S. Army Engineer Waterways Experiment Station, CE, Vicksburg, Mississippi; Prepared under Contract No. DACW39-67-C-0091 by College of Engineering, Office of Research Services, University of California, Berkley, California.

22. J. A. Hudson; "Estimation of the Mechanical Properties of Rock Masses"; Final Report, 11 June 1971; U. S. Bureau of Mines, Denver, Colorado.

23. J. L. Colp; "Terradynamics; A study of Projectile Penetration of Natural Earth Materials"; Report SC-DR-68-215, June 1968; Sandia Laboratories, Albuquerque, New Mexico.

24. L. Obert and W. I. Duvall; "Rock Mechanics and the Design of Structures in Rock"; 1967; John Wiley and Sons, Inc., New York, N. Y.

25. B. V. Baidyuk; "Mechanical Properties of Rocks at High Temperatures and Pressures"; Institute of Geology and Development of Mineral Resources, 1963, Moscow, USSR; Translated by J. P. Fitzsimmons, University of New Mexico.

26. S. R. Swanson and W. S. Brown; "The Mechanical Response of Pre-Fractured Rock in Compression"; Report UTEC-ME-70-037, 1970; Mechanical Engineering Department, University of Utah, Salt Lake City, Utah.

27. E. T. Brown; "The Strength of Jointed Rock Masses"; 1970; School of Mineral and Metallurgical Engineering, University of Minnesota, Minneapolis, Minnesota.

28. M. Van Thiel, Editor; "Compendium of Shock Wave Data"; UCRL-50108, June 1966; Lawrence Radiation Laboratory, Livermore, California.

29. J. Isenberg; "Nuclear Geoplosics; Part Two: Mechanical Properties of Earth Materials"; DNA 1285H2 (Formerly DASA 1285-2), November 1972; Defense Nuclear Agency, Washington, D. C.

30. R. C. Bass; "Additional Hugoniot Data for Geologic Materials"; Report No. SC-RR-66-548, October 1966; Sandia Laboratories, Albuquerque, New Mexico.

31. T. J. Ahrens, J. T. Rosenberg, and M. H. Ruderman; "Dynamic Properties of Rock; Final Report"; DASA 1868, September 1966; Stanford Research Institute, Menlo Park, California.

32. S. H. Shuster and J. Isenberg; "Equations of State for Geologic Materials"; DNA 2925Z, September 1972; Defense Nuclear Agency, Washington, D. C.

33. D. Braslau; "Partitioning of Energy in Hypervelocity Impact Against Loose Sand Targets"; Journal of Geophysical Research, 10 July 1970, Vol. 75, No. 20, Pages 3987-3999; Richmond, Virginia.

34. C. H. Johansson and P. A. Persson; "Detonics of High Explosives"; 1970; Academic Press, New York, N. Y.

35. G. E. Duvall; "Shock Waves in Solids"; Proceedings, First Conference, Shock Metamorphism of Natural Materials, B. M. French and N. M. Short, Editors, 1968, Pages 19-29; Mono Book Company, Baltimore, Maryland.

36. L. V. Al'tshuler; "Use of Shock Waves in High-Pressure Physics"; Soviet Physics Uspekhi, 1965, Vol. 8, No. 1.

37. M. H. Rice, R. G. McQueen, and J. M. Walsh; "Compression of Solids by Strong Shock Waves"; Solid State Physics: Advances in Research and Applications, F. Seitz and D. Turnbull, Editors, 1958,

Vol. 6, Page 1; Academic Press, New York, N. Y.

38. L. Thigpen; "Penetration of Projectiles into Continuous Earth Media"; Research Report SC-44-72-0204, May 1972; Sandia Corporation, Albuquerque, New Mexico.

39. L. J. Thompson and W. R. Bryant; "Projectile Penetration Theory"; Proceedings, Conference on Rapid Penetration of Terrestrial Materials, February 1972; Texas A&M University, College Station, Texas.

APPENDIX A

NOTATION

A	Deceleration
$\bar{A}$	Average deceleration
BM	Classification of low-strength rock targets
B_1	$1 - \delta^{1/3}$
B_2	$3/2 - (1 + \alpha_p)\delta^{1/3} + 1/2(\delta^{4/3})$
c_o	Initial velocity of sound
CM	Classification of medium-strength rock targets
CRH	Caliber Radius Head
D	Diameter of projectile
DM	Classification of high-strength rock targets
e_i	Volumetric strain related to the jump from zero to finite stress (elastic region) in the stress-strain curves in Figure 2.1
e_p	Volumetric strain related to the jump from the elastic to the plastic region of the uniaxial stress (i.e., unconfined compression) stress-strain curve in Figure 2.1b
E	Young's modulus of elasticity, corresponding to locked elastic region in Figure 2.1, psf = 3G
E_i	Internal energy
E_{insitu}	In situ modulus of deformation
E_{intact}	Intact modulus of deformation
E_t	Strain-hardening modulus, corresponding to locked plastic region in Figure 2.1, psf = $3G_t$
E_{t50}	Tangent modulus at 50 percent ultimate strength
EPW	Earth penetrating weapon
f	Fracture frequency
$f(\epsilon)$	Ogive nose factor
g	Acceleration of gravity
G	Elastic shear modulus
G_t	Strain-hardening shear modulus
H	High strength
K_n	Normal joint stiffness

ℓ	Projectile body length
L	Low strength
m	Projectile mass
M	Medium strength
p_s	$\frac{4}{9} E[1 - \exp(-3\beta)] - \frac{2}{3} Y \ln \delta + \frac{2}{27} \pi^2 E_t - \frac{4}{9} E_t \eta$
P	Maximum depth of penetration
P_H	Penetration into high-strength rock
P_L	Penetration into low-strength rock
P_M	Penetration into medium-strength rock
q	Material constant relating shock velocity to sound and particle velocities
R	Radius; also Schmidt hardness
RQD	Rock Quality Designation
s	Fracture spacing
$\bar{t}$	Duration
V	Velocity
V_f	In situ compressional wave velocity
V_L	Laboratory (intact) compressional wave velocity
V_o	Impact velocity
W	Weight
W/A	Sectional pressure
Y	Yield strength of target material, psf
z	Direction of penetration
α_ρ	$1 - \frac{\rho_o}{\rho_p}$
β	$\frac{Y}{2E} - \frac{e_i}{3}$
γ_a	Dry unit weight
γ_o	Grüneisen constant
δ	$1 - \frac{\rho_o}{\rho_p} \exp(-3\beta)$
Δt	Time increment

ΔV_k Incremental velocity change in the k^{th} time step as computed from Equation 2.1

Δz_k Distance penetrated during the kth time step

ε $\frac{1}{2\ CRH}$

η $\sum_{n=1}^{\infty} \frac{\delta^n}{n^2}$; also $1 - \frac{\rho_o}{\rho}$

ρ Density

ρ_o Initial density of target material, slugs/cu ft

ρ_p $\rho_o \exp(e_p)$

σ_a Uniaxial compressive strength

ϕ Limiting cone half-angle

$\phi(\varepsilon)$ $\mathrm{Tan}^{-1}\left(\frac{2\varepsilon - \varepsilon^2}{1 - \varepsilon}\right)$